SECTION 3
TRANSPORT MEANS CONCEPTS FOR STRATEGIC CARGO

3.1 Rectangular-pipe frame design for the universal container

It is proposed to manufacture the container frame of closed profiles or square pipes in order to reduce their damage under operating conditions (Fig. 3.1).

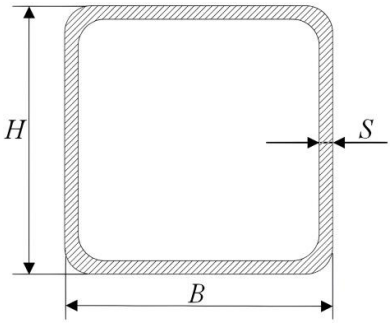

Figure 3.1 – The cross-section of a pipe:
H – the height; *B* – the width; *S* – the wall thickness

This solution was substantiated with a frame diagram shown in Fig. 3.2 [68]. The study was conducted on the example of a 24-tonne container (1CC).

The parameters of the frame pipes were determined through the corresponding calculations in Lira-CAD [1]. The frame was

considered as a rod system. The following two load diagrams of the frame were taken into account:

– the vertical load of the frame lifted by the upper corner fittings (load mode I); and

– the longitudinal load of the frame transported by rail (load mode II).

The design diagram of the frame when it is lifted by the upper corner fittings is shown in Fig. 3.3.

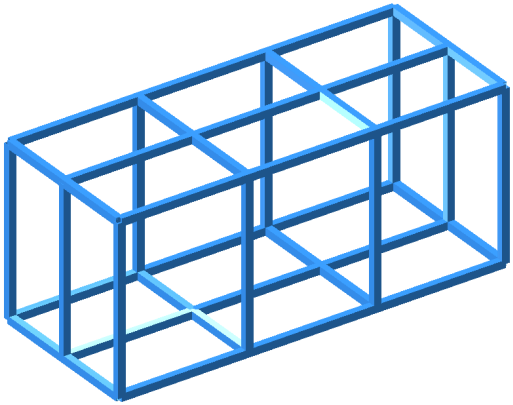

Figure 3.2 – The container frame

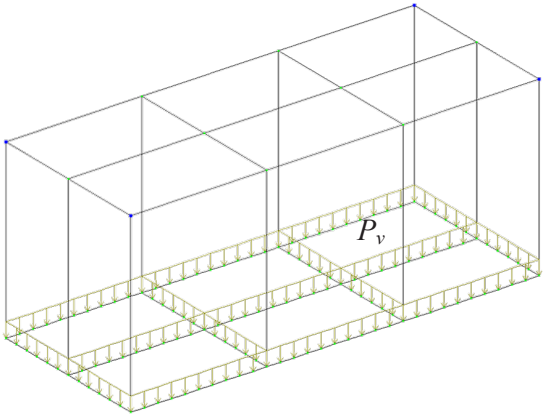

Figure 3.3 – The design diagram of the frame (load mode I)

It was taken into account that the container frame was fixed by the upper corner fittings. The vertical load P_v was transmitted to the lower part of the frame. By taking this into account, the diagrams of longitudinal forces (Fig. 3.4) and transverse forces (Fig. 3.5) acting in the frame, as well as the diagrams of bending moments (Fig. 3.6) were obtained. In Figs. 3.4–3.6, the orange colour indicates stretching, and the blue colour indicates compressing.

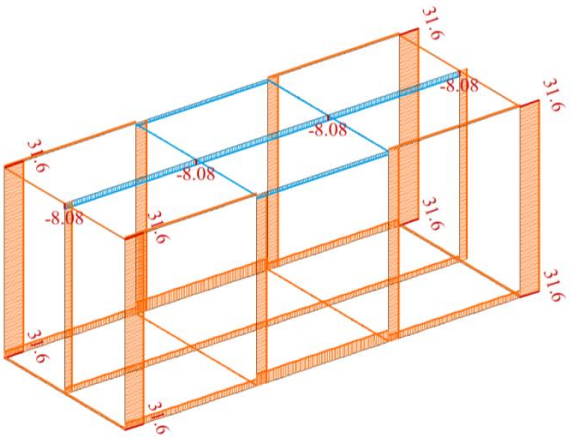

Figure 3.4 – The diagram of longitudinal forces acting in the frame (kN)

Therefore, the maximum value of the longitudinal force occurs in the vertical struts and equals 31.6 kN. This is due to the fact that they act as an intermediate adapter between the anchor point and the area of application of force to the container frame.

The maximum value of the lateral force occurs in the intermediate vertical struts. Its value is 19.6 kN.

These struts connect the bottom part of the container frame with the lower one. Therefore, in case of loading the lower part of the frame, the maximum values of this force occur here.

The maximum value of the bending moment also occurs in the intermediate vertical struts and equals 13.6 kN · m. The scheme of frame movements under the action of vertical loading is shown in Fig. 3.7.

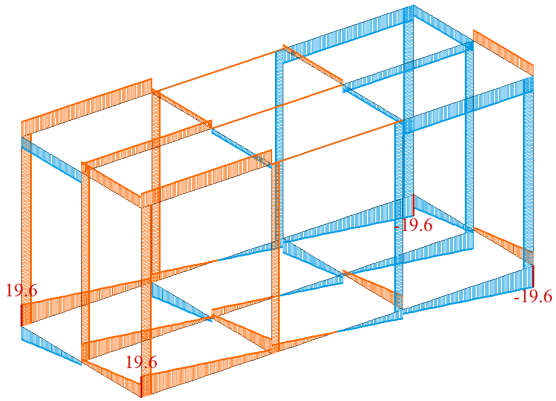

Figure 3.5 – Scheme of lateral forces acting in the frame (kN)

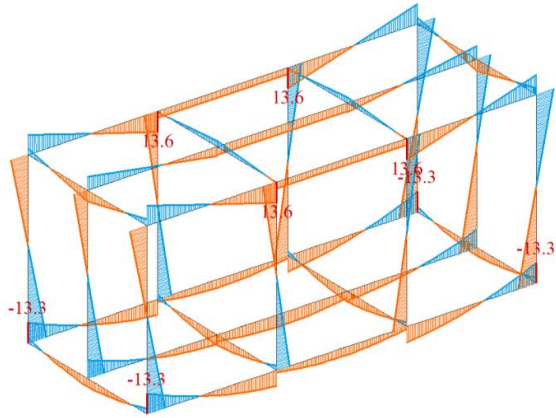

Figure 3.6 – Scheme of bending moments acting in the frame (kN · m)

At the same time, the longitudinal beams of the upper and lower parts of the frame experience the largest movements. This is due to the fact that an evenly distributed loading is applied to the beams that form the lower part of the frame.

Also, as part of the study, the calculation of the container frame under longitudinal loading was carried out, taking into account its

transportation by rail transport (on a flat wagon as a part of a train). The calculation scheme of the frame is shown in Fig. 3.8.

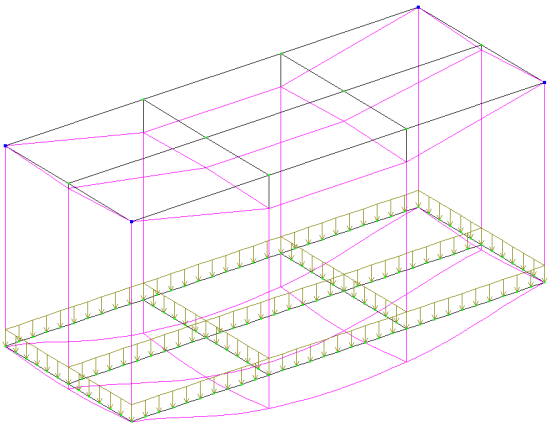

Figure 3.7 – Scheme of frame movements under the action of vertical loading

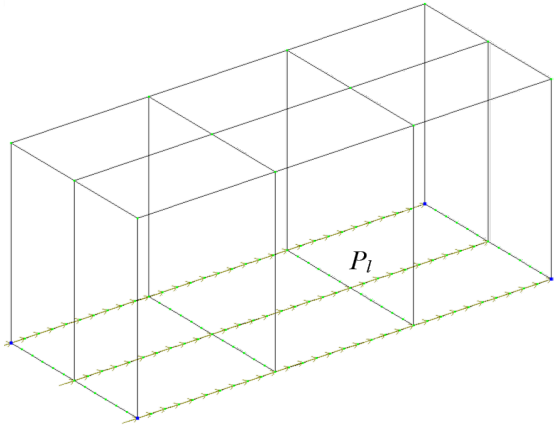

Figure 3.8 – Calculation scheme of the frame (II loading mode)

In this case, the longitudinal loading Pl was applied to the beams forming the lower part of the frame, namely to the longitudinal beams. This scheme is explained by the fact that the load on the

lower frame of the container when transported by a flat wagon is transferred from the corner fittings, which interact with the fitting stops. The movement of cargo relative to the container was not taken into account. The frame was secured in corner fittings.

To determine the amount of the longitudinal force, a mathematical model formed in the previous work of the authors [37] was used.

However, this model was further developed to determine the longitudinal loading of a container placed on a flat wagon when a longitudinal force is applied to it. In view of this, the model has the following form:

$$\begin{cases} M_{FW} \cdot \ddot{q}_1 = P - \sum_{i=1}^{n} \left(F_{FR} \cdot sign(\dot{q}_1 - \dot{q}_2) \right), \\ M_C \cdot \ddot{q}_2 = \left(F_{FR} \cdot sign(\dot{q}_1 - \dot{q}_2) \right). \end{cases} \quad (3.1)$$

here M_{FW}, M_C – inertial coefficients, which characterize, respectively, the mass of the frame of the flat wagon and the container; P – force acting on the stops of the automatic coupling device of the flat wagon; F_{FR} – frictional force between the frame of the flat wagon and the containers; q_1 and q_2 – generalized coordinates characterizing the movement of a flat wagon and a container, respectively.

The calculation was carried out under the condition that a longitudinal force of 2.5 MN is applied to the stops of the automatic coupling. It was taken into account that this force acts in the form of a "jerk" with a constant value.

It is important to note, it is necessary to take into account the value of the forces that are characteristic of their operating conditions in the case of using this model for a 1435 mm gauge car equipped with a screw tie.

The solution of the mathematical model was carried out by the method of variation of arbitrary constants, with initial conditions close to zero. Based on the calculations, it was established that the longitudinal acceleration acting on the container is about 20 m/s^2.

This value of acceleration is taken into account when constructing loading scheme of the container frame in II loading mode. The calculation results are shown in Fig. 3.9–3.11. Analyzing the data of the scheme, we can conclude that the maximum value of the longitudinal force occurs in the bottom part of the frame and equals

100 kN (Fig. 3.9). This can be explained by the fact that it was secured by the lower corner fittings. The maximum value of the lateral force was recorded in the longitudinal beams and amounted to 21.1 kN (Fig. 3.10). This is explained by the same argument as for the situation with longitudinal forces. The maximum bending moment occurs in the bottom part of the frame and is equal to 14.2 kN · m (Fig. 3.11).

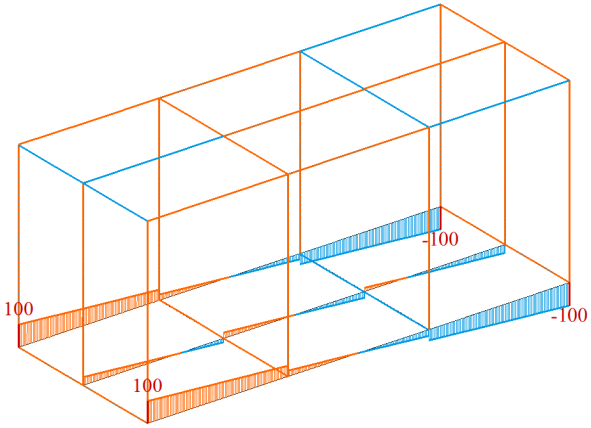

Figure 3.9 – Scheme of longitudinal forces acting in the frame (kN)

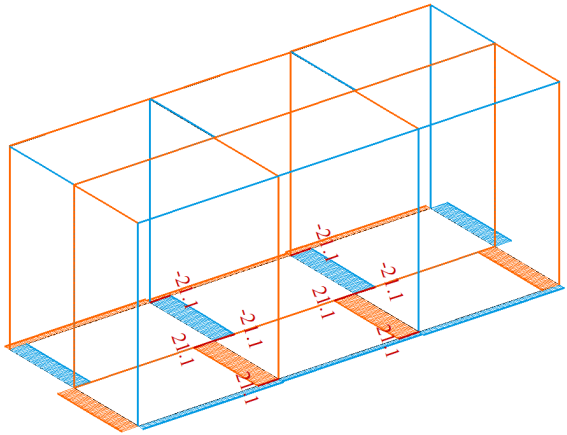

Figure 3.10 – Scheme of lateral forces acting in the frame (kN)

The scheme of frame movements in the II calculation mode is shown in Fig. 3.12.

At the same time, the lateral beams of the lower part of the frame experience maximum displacement. This circumstance is caused by the fact that it is fixed by the lower corner fittings, and the longitudinal force is applied to the lateral beams.

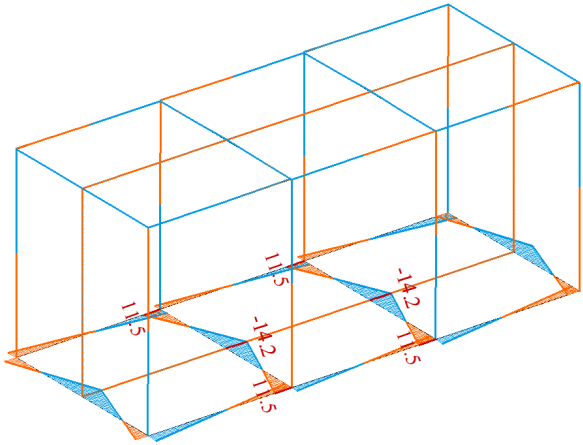

Figure 3.11 – Scheme of bending moments acting in the frame (kN · m)

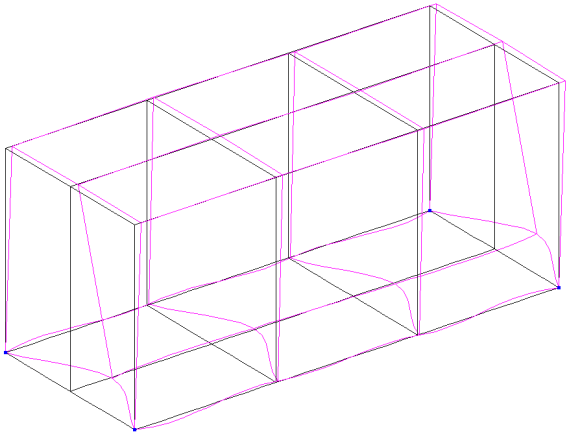

Figure 3.12 – Scheme of frame movements when a longitudinal force is applied to it

Based on the obtained results, the moment of resistance of the section of the container frame execution profile was determined. In this case, the following dependency was used:

$$W = \frac{M}{[\sigma]}, \tag{3.2}$$

here M – value of the maximum bending moment acting in the section of the frame; [σ] – allowable stresses for the material of the frame execution (steel grade 09G2S, [σ] = 210 MPa).

It should be noted that grade 09G2S steel is standard for the manufacture of containers.

The cross-sectional area of the frame execution profile was also taken into account. In this case:

$$A = \frac{F}{[\sigma]}, \tag{3.3}$$

where F – value of the longitudinal force acting in the frame.

It must be said that according to the results of the calculations, the selection of the section parameters of the frame was carried out according to formula (3.2), since here the value of the moment of resistance, from the point of view of ensuring the strength of the frame execution profile, is more important. Taking into account the conducted calculations, it was established that the profile of the frame execution is a square pipe with the following parameters: $H = B = 120$ mm, $S = 4$ mm, $W = 67{,}05$ cm^3. Based on the specified parameters, the mass of the container frame will amount to about 500 kg.

At the next stage of the research, a spatial model of the container frame was built (Fig. 3.13) and its FEM analysis was carried out in SolidWorks Simulation.

The results of the calculation of strength of the container under the II loading mode are shown in Fig. 3.14, 3.15.

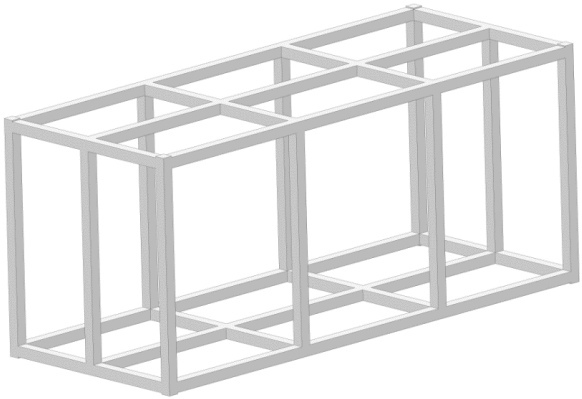

Figure 3.13 – 3-D model of the container frame

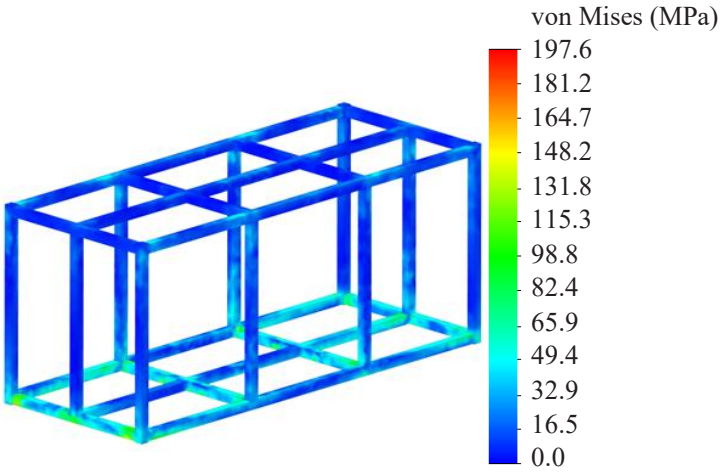

Figure 3.14 – Stressed state of the container frame

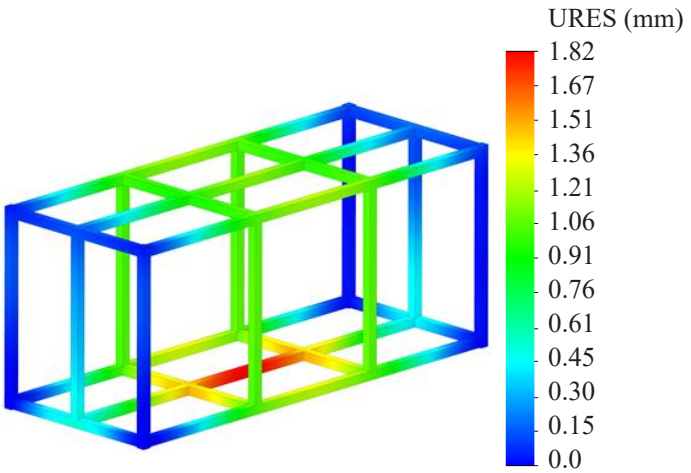

Figure 3.15 – Displacements in the nodes of the container frame

The maximum stresses occur in the lateral beam and amount to 197.6 MPa (Fig. 3.14), that is, they are lower than permissible. The maximum displacements occur in the middle part of the longitudinal beam and amount to 1.8 mm (Fig. 3.15). Therefore, the strength of the container frame under operational loadings is ensured.

3.2 Optimal parameters of the corrugations for container wall panelling

In most container types, the wall panelling is formed by corrugated sheets (Fig. 3.16 [96]).

The rational parameters of corrugations that form the panelling sheet were determined by considering them as thin-walled plates. For the end wall, these plates have a width of a = 2.438 m and a height of b = 2.591 m (Fig. 3.17). The uniformly distributed load P acts on the plate area [96]. The sheet is fixed along its perimeter,

which corresponds to the diagram of fastening the panelling sheet to the container frame.

Figure 3.16 – The universal containers:
a) 20-ft container; b) 40-ft container

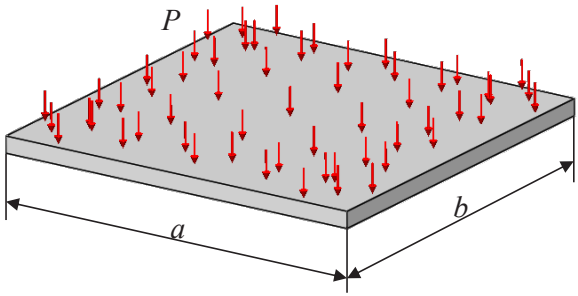

Figure 3.17 – The design model of the plate

According to the Bubnov-Galerkin method, it can be written as:

$$\sigma = P \cdot \frac{96}{\pi^4} \cdot \frac{(b^2 + \mu \cdot a^2) \cdot a^2 \cdot b^2}{\left(a^2 + b^2\right)^2 \cdot \delta^2}, \tag{3.4}$$

where μ is Poisson's ratio; δ is the plate thickness.

The resistance moment of the plate can be found by the formula:

$$W = \frac{L \cdot \delta^2}{6}, \tag{3.5}$$

where L is the length of the plate.

Herewith,

$$I = W \cdot \frac{\delta}{2}. \tag{3.6}$$

Therefore, taking into account the known permissible stresses of the plate material, the load acting on it and its geometric parameters (height and width), it was possible to determine the permissible thickness of the plate regarding the required strength.

For example, at a = 2.438 m, b = 2.591 m, μ = 0.28 and $P = P_k \cdot 0.4 \cdot g$ [96] (Fig. 3.18), where P_k is the load capacity of the container (P_k = 21.75 kN for a standard 1CC container), δ = 9.5 mm can be obtained. With this sheet thickness, the moment of inertia is I = 17.419 cm^4.

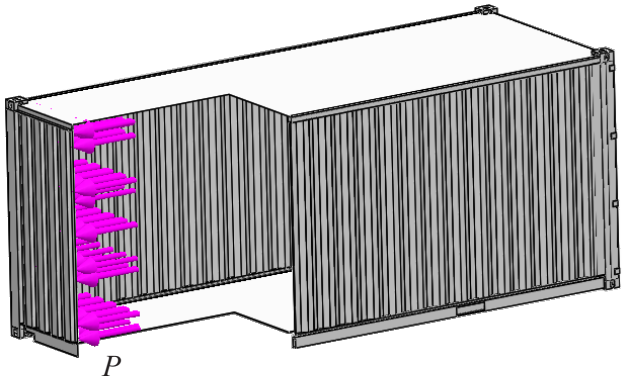

Figure 3.18 – The diagram of loads applied to the end wall of the container

A sheet with the given parameters was built in SolidWorks and its moment of inertia was determined using the built-in options (Fig. 3.19).

The moment of inertia of the cross-section was 17.42 cm^4. The weight of the sheet, provided that it was made of Steel 09G2S, was 468.08 kg.

By using the rational moment of inertia, it was possible to determine the parameters of corrugations. For the rectangular corrugation panelling (Fig. 3.20), the total moment of inertia of its cross-section was defined as the sum of the moments of inertia of the individual rods of the rectangular cross-section.

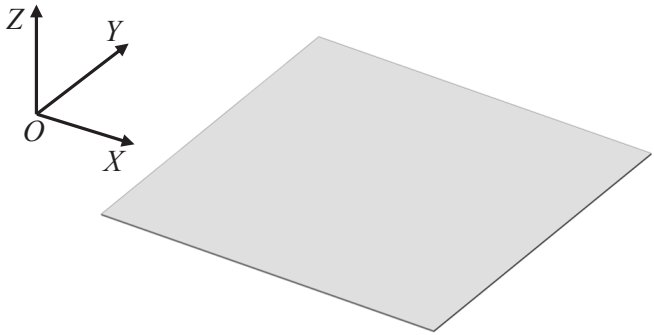

Figure 3.19 – The spatial model of the sheet

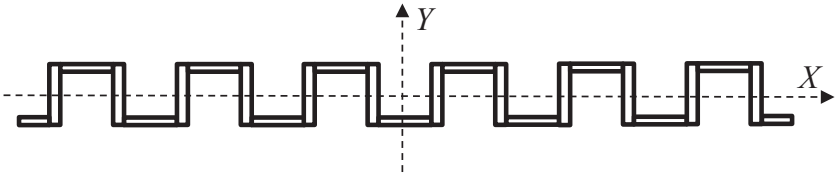

Figure 3.20 – The cross-section of a sheet formed by rectangular corrugations

For example, for a vertical rod, it can be written as [96]:

$$I = \frac{\delta \cdot h^3}{12}, \tag{3.7}$$

where h is the height of the rod.

By taking into account that the sheet length was L = 243.8 cm, the number of horizontal rods with a length of l = 8 cm was 30 pieces, and vertical ones – 31.

The parameters of the sheet, at which its minimum mass was observed, were determined with variational calculations. The objective function has the form:

$$m \rightarrow \min, \tag{3.8}$$

where m is the sheet weight.

The calculations were made with the following restrictions:

1. The length of the corrugations was 8 cm (as in a typical container sheet).

2. The moment of inertia of the sheet should be at least 17.419 cm^4.

By taking into account the calculations at the following variational parameters: δ – the sheet thickness and h – the corrugation height (Fig. 3.21), it was found that the optimal sheet in terms of the minimum material consumption was a sheet with δ = 0.1 cm and h = 1.69 cm (Fig. 3.22).

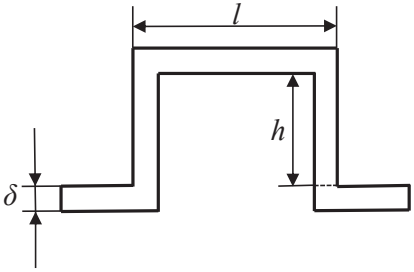

Figure 3.21 – The cross-section of corrugation

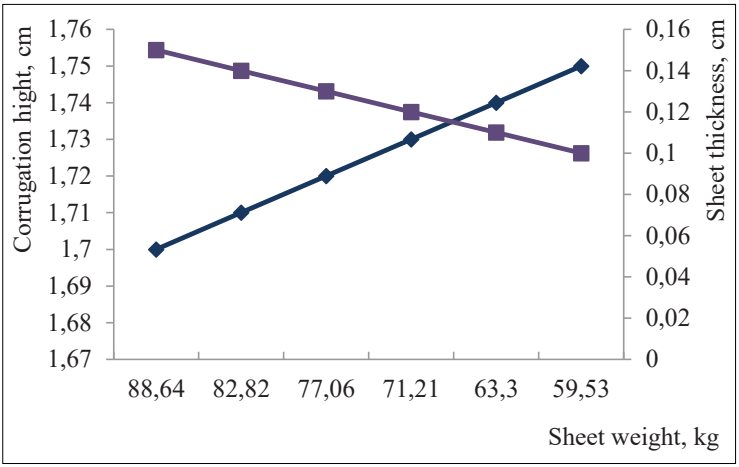

Figure 3.22 – The dependence of the weight of the end wall sheet on its parameters

The spatial model of the corrugated sheet is shown in Fig. 3.23. The weight of the sheet made of Steel 09G2C was 59.53 kg.

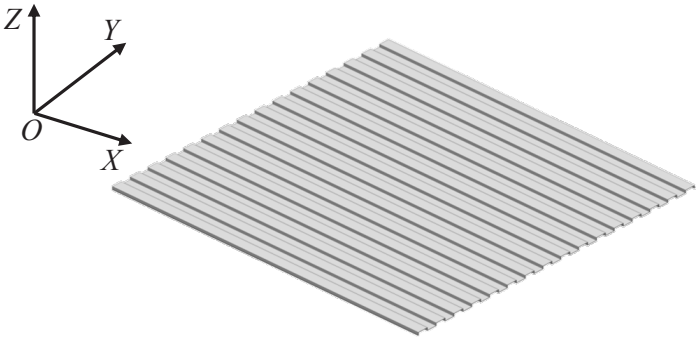

Figure 3.23 – The spatial model of a corrugated sheet for the end wall

The sidewall of the container was also calculated according to the above method. The load P, which acted on the sidewall, was taken equal to $P = P_k \cdot 0.6 \cdot g$ [96] (Fig. 3.24).

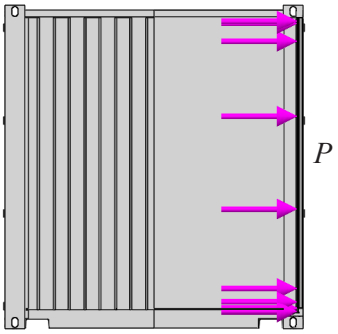

Figure 3.24 – The diagram of loads applied to the sidewall of the container

The results of the calculations showed that at $\delta = 9.25$ mm for a thin-walled sheet, the moment of inertia was $I = 39.96$ cm^4. By taking this into account, at $\delta = 0.1$ cm, $l = 8$ cm, $h = 1.7$ cm,

the moment of inertia of the corrugated sheet was $I = 39.98$ cm^4 (Fig. 3.25).

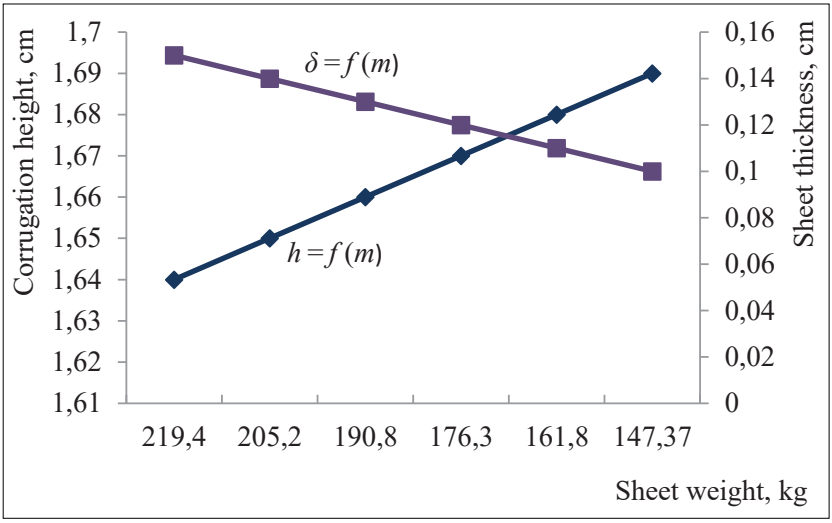

Figure 3.25 – The dependence of the weight of the sidewall sheet on its parameters

The spatial model of the corrugated sheet is shown in Fig. 3.26.

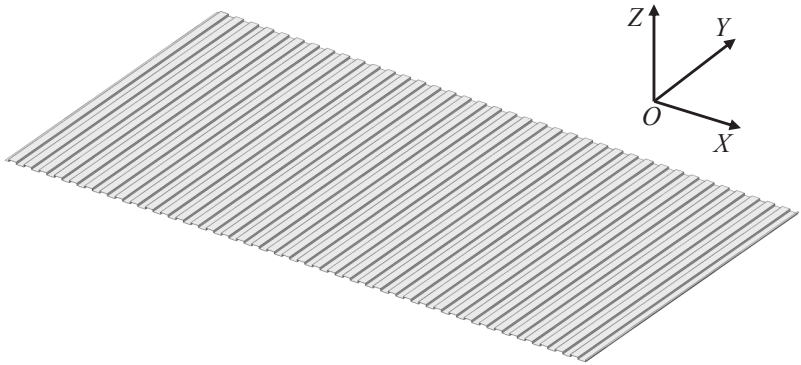

Figure 3.26 – The spatial model of the corrugated sidewall sheet

The weight of the sidewall panelling was about 147 kg. By taking into account the selected parameters of the sheets, a spatial model of the container was built (Fig. 3.27). This model was used for the strength calculation of the container in SolidWorks Simulation using the finite element method.

The finite element model of the container was built with isoparametric tetrahedra (Fig. 3.28), the optimal number of which was determined by the graphic and analytical method [83, 84].

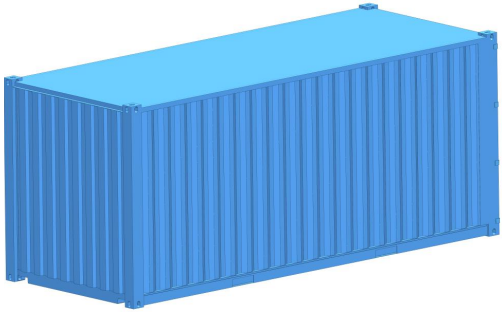

Figure 3.27 – The spatial model of the container

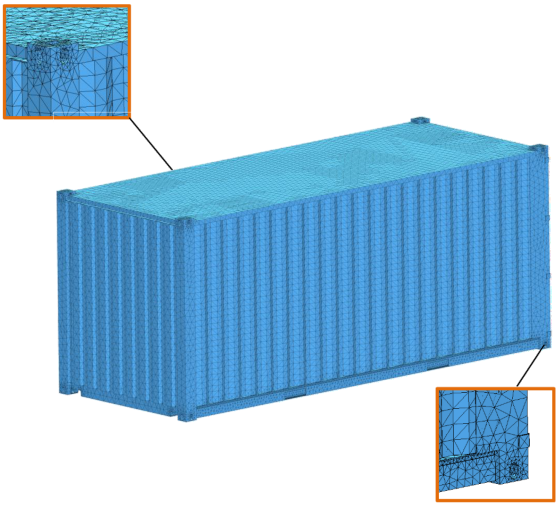

Figure 3.28 – The finite element model of the container

In the areas of rounding and conjugation of the container components, the mesh was automatically compacted. The number of nodes was 70.491, and the number of elements was 217.708. The maximum size of the element was 80 mm, and the minimum size was 16 mm.

The strength of the container was calculated for the case of its transportation by rail. As an example, the study presents the strength calculation for a container placed on the flat wagon at a shunting collision [15]. The design diagram of the container includes the vertical load P_v (Fig. 3.29), the pressure from the bulk cargo P_p (grain), as well as the longitudinal loads P_l caused by the forces of inertia arising during shunting collision.

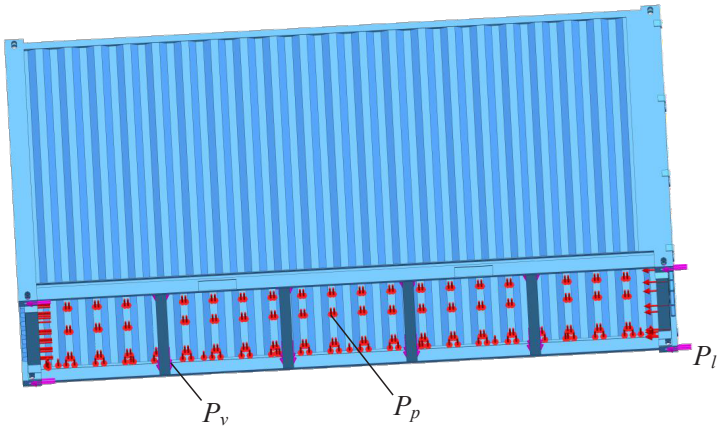

Figure 3.29 – The design model of the container

Steel 09G2S was used as the construction material. The container was fixed in the zones where it rested on the flat wagon. The calculation results are shown in Figs. 3.30, 3.31.

Based on the calculations, it can be concluded that the maximum stresses occur in the container fittings and were equal to 287 MPa (Fig. 3.30); they were lower than permissible. The maximum displacements in the container units were recorded in the end wall and were 3.5 mm (Fig. 3.31).

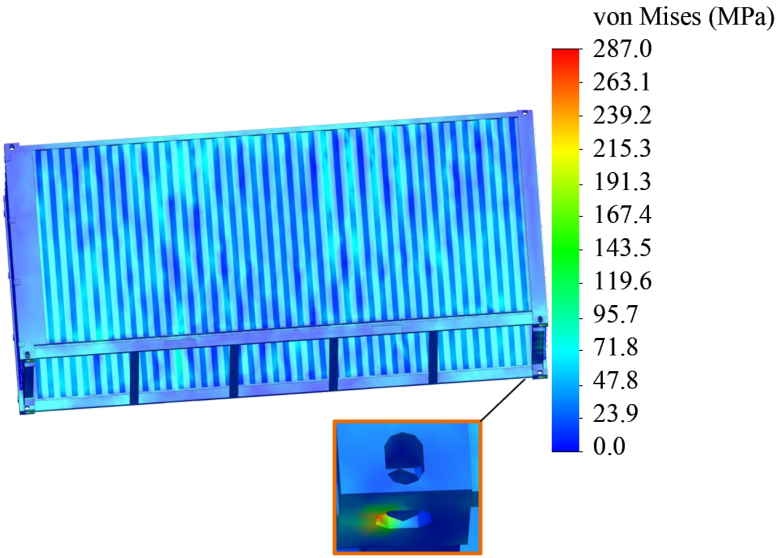

Figure 3.30 – The stress state of the container

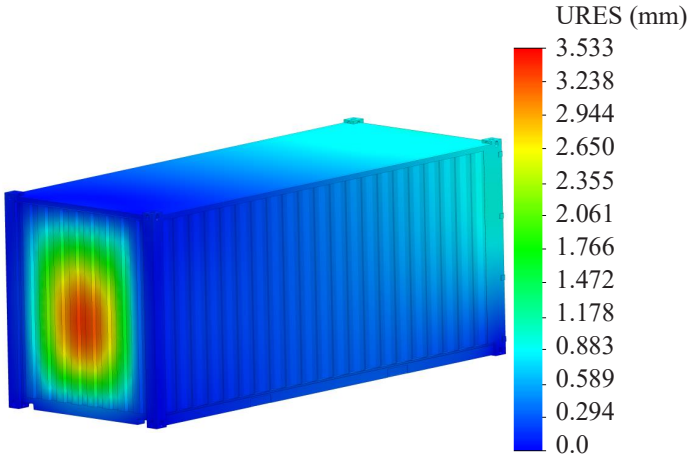

Figure 3.31 – The displacements in container units

For other design load diagrams, according to [15], the structural strength of the container was also ensured.

3.3 Strength of the sandwich panel wall container under the operating loads

3.3.1 Strength of the sandwich panel wall container under the static loads

At present, the container walls are formed by metal corrugated sheets. The thickness of sheets in the standard 1CC container is 1.6 mm. However, under operating loads panelling sheets can be damaged, which necessitates unscheduled repairs of containers.

It was proposed to introduce sandwich panels as the components of container walls to ensure their strength. The sandwich panel can be made of two metal sheets with energy-absorbing material in-between (Fig. 3.32). This solution will help to improve the strength of the container by reducing its load.

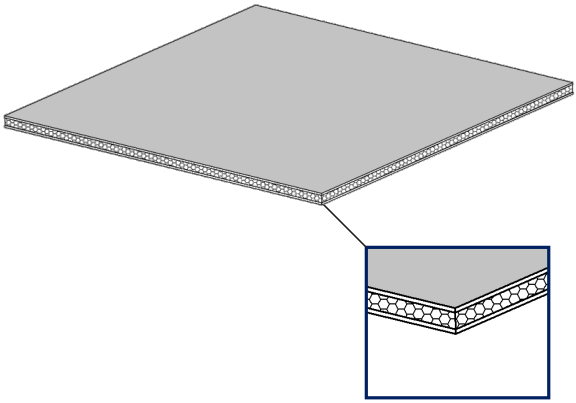

Figure 3.32 – The sandwich panel

The thickness of the sheet was calculated using the Bubnov-Galerkin method (3.4). It was taken into account that the sheet with thin walls was under the uniformly distributed load *P*.

Hence, the thickness of the sheet is:

$$\delta = \sqrt{\frac{P \cdot 96 \cdot (b^2 + \mu \cdot a^2) \cdot a^2 \cdot b^2}{\sigma \cdot \pi^4 \cdot \left(a^2 + b^2\right)^2}}. \quad (3.9)$$

After selecting the thickness of the sheet, its strength was calculated. It was assumed that the sheet was made of Steel 09G2S, which is typical for metal container structures.

The calculations included the most unfavourable load modes of transportation, i.e., shunting collision. Therefore, it was taken into account that the permissible stresses were 310.5 MPa, the sheet width was 2.438 m and the sheet height was 2.591 m [98].

The calculation was made on the example of the end wall of the container, since it perceived the greatest loads during the shunting collision of the flat wagon. Thus, it was found that the sheet thickness must be about 3 mm. The thickness of the energy-absorbing material can be taken as 33 mm according to the requirements for a standard wall (Fig. 3.33 [93]).

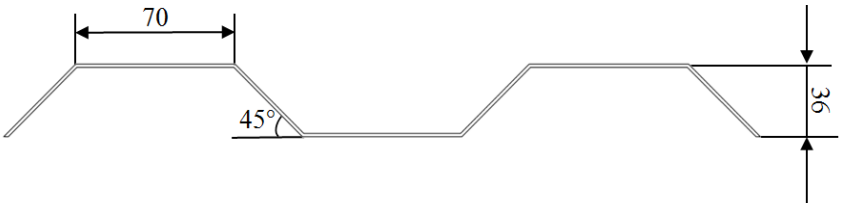

Figure 3.33 – The cross-section of a typical container panelling

The moment of resistance of the sheet can be increased by corrugations. The most rational corrugations were determined by means of spatial models of the sheets (Fig. 3.34) [7].

By using the options of SolidWorks Simulation, the moments of inertia of the cross-sections shown in Fig. 3.34, as well as their

moments of resistance, were determined (Table 3.1). The analysis of the data presented in Table 3.1 demonstrates that the most appropriate corrugations are rectangular.

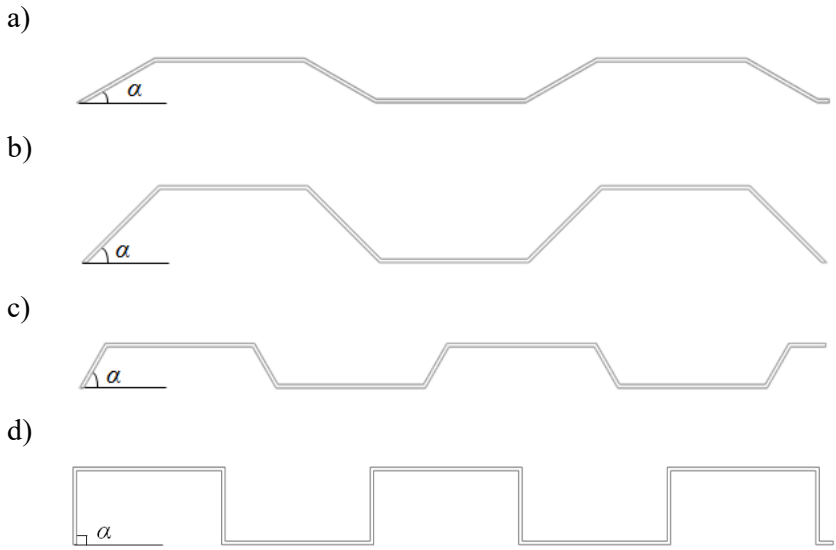

Figure 3.34 – Corrugations of panelling sheet:
a) $\alpha = 30°$; b) $\alpha = 45°$; c) $\alpha = 60°$; d) $\alpha = 90°$

Table 3.1 – The moments of inertia and cross-sectional resistance of corrugated sheets

Inclination angle of corrugations	Moment of inertia, cm^3	Moment of resistance, cm^4
30°	3.79	3.64
45°	12.52	6.95
60°	4.66	4.48
90°	19.53	10.85

By taking into account the corrugations, it is possible to reduce the sheet thickness. The thickness of the corrugated sheet can

be determined provided that its moment of inertia is not lower than that of a rectangular sheet.

The sandwich-panel corrugated sheet is shown in Fig. 3.35.

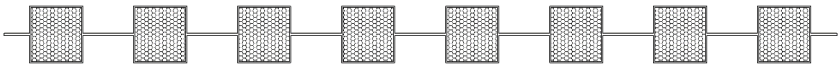

Figure 3.35 – The sandwich panel

The strength of the sandwich panel of the end wall of the container was determined with its spatial model (Fig. 3.36).

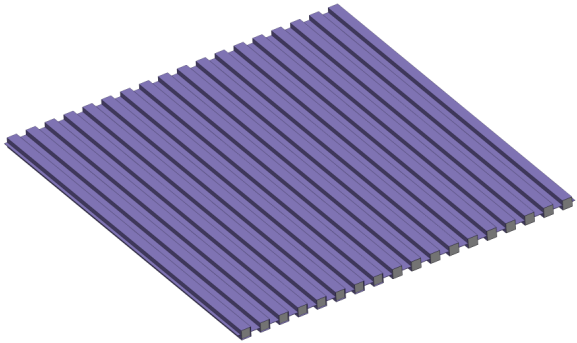

Figure 3.36 – The spatial model of a sandwich panel

The foam aluminium was used as an energy-absorbing material, which is now one of the most popular materials in mechanical engineering; it was placed between the sheets of the panel. The strength calculation was implemented using the finite element method in SolidWorks Simulation. The design diagram included the uniformly distributed force P_d on the panel (Fig. 3.37), which was equal to $0.4 \cdot P \cdot g$ [7].

The finite element model was formed by tetrahedra with four Jacobian points (Fig. 3.38). The number of finite elements of the model was determined by the graphic-analytical method. The number of nodes of the model was 16.930, and the elements – 72.027. The maximum element size was 60 mm.

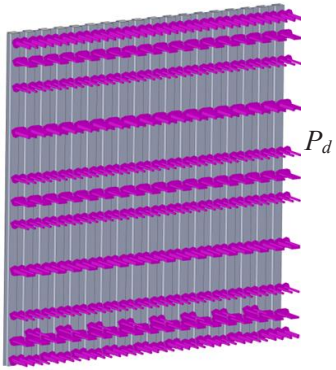

Figure 3.37 – The design diagram of the panel

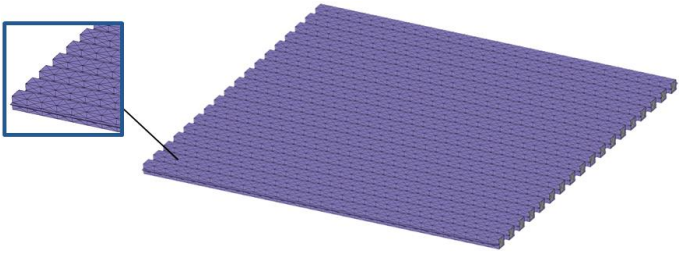

Figure 3.38 – The finite element model of the panel

The model was fixed along the perimeter. The results of the calculations are shown in Figs. 3.39 and 3.40.

Maximum stresses were recorded in the central upper and lower zones of the panel. The numerical values of stresses amounted to about 258 MPa, which was lower than permissible by 16 %. The maximum displacements occurred in the middle part of the panel and were 3.1 mm.

The next step of this study included the building of the spatial model of a container with sandwich-panel walls and their strength calculation. It was made for sandwich panels of Steel 09G2S. Thus, the thickness of the sidewall panelling was 1.6 mm, and that of the end wall was about 3.0 mm. Due to rectangular corrugations, the thickness of the end and wall sheets can be reduced to 1.0 mm.

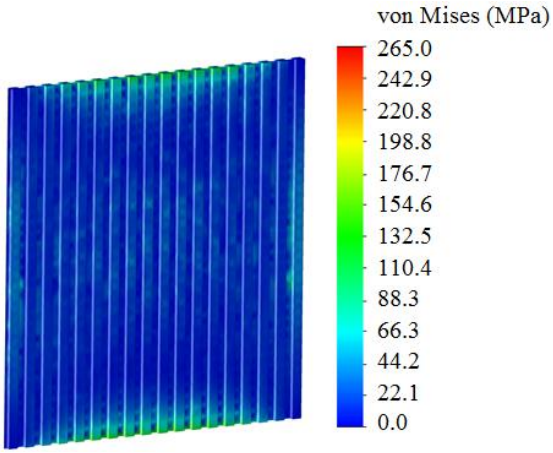

Figure 3.39 – The stress state of the sandwich panel

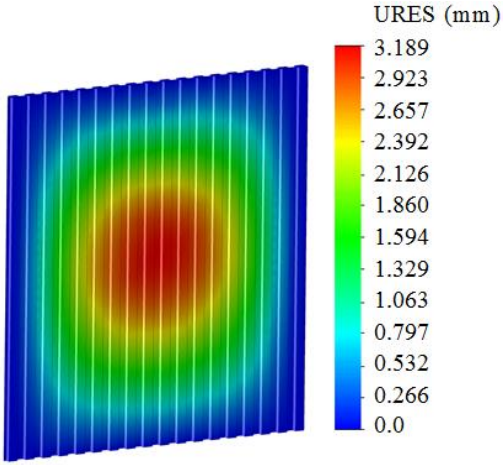

Figure 3.40 – The displacements in the sandwich panel units

The permissible stresses for the sidewall were taken equal to 210 MPa (design mode III), and the permissible stresses for the end wall – 310.5 MPa (design mode I) [15]. The strength of the load-bearing structure of a container with sandwich-panel walls

was determined by using the finite element method in SolidWorks Simulation. The Mises criterion (IV theory of strength) was used as a calculation criterion. The load diagrams of the container are shown in Fig. 3.41.

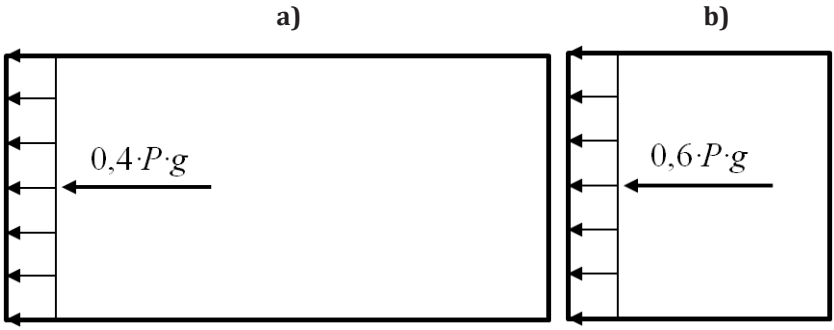

Figure 3.41 – The loads perceived by the container placed on the flat wagon:
a) longitudinal; b) transverse

The spatial model of the container was created in SolidWorks (Figure 3.42).

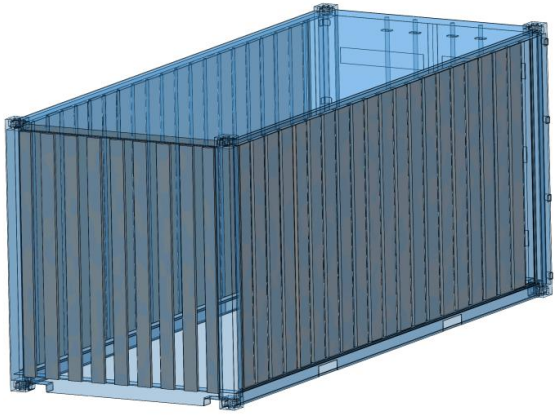

Figure 3.42 – The spatial model of the container

The transparent colour in Fig. 3.42 shows the load-bearing structure of the container, and the matte grey colour shows the filler located in the walls.

Spatial isoparametric tetrahedra were used as finite elements. The optimal number of elements was determined by the graphic and analytical method. The number of nodes is the mesh was 71.701, the number of elements – 223.937. The maximum element size was 80 mm, the minimum –16 mm. The minimum number of elements in the circle was 9, the ratio of element size increase in the mesh was 1.7. The finite-element container model is shown in Fig. 3.43.

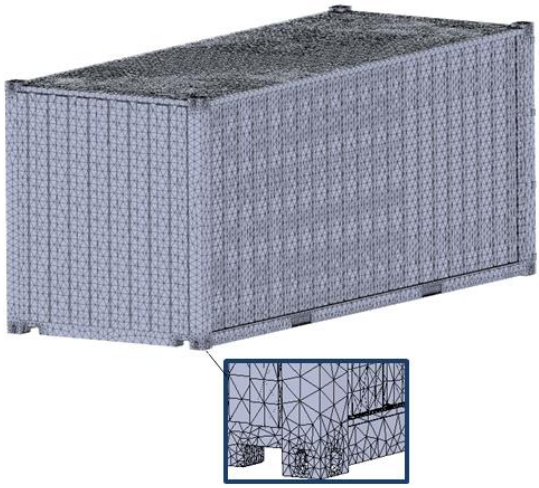

Figure 3.43 – The finite-element model of the container

In places where the container components were rounded or joined, the mesh was automatically compacted. The strength of the container under longitudinal load was determined provided that it was placed on a flat wagon.

The design diagram included the vertical load P_v on the load-bearing structure of the container, taking into account the full load capacity of the container, the longitudinal force P_l applied to the

fittings, as well as the pressure of the bulk cargo P_p (grain) on the side and end walls (Fig. 3.44). The pressure of bulk cargo was calculated according to the technique given in [15].

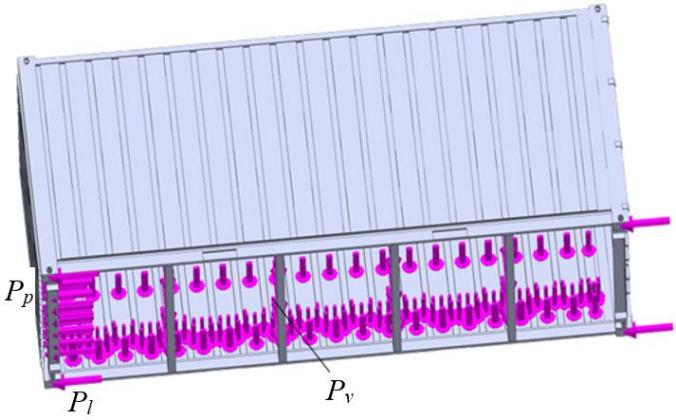

Figure 3.44 – The design model of the container

The model was fixed by the fittings. Foam aluminium was used as an energy-absorbing material [73].

The results of the calculations showed that the maximum stresses occurred in the container fittings; they were 268.3 MPa (Fig. 3.45), which was lower than permissible by 13.6 %.

In the zones of interaction of the end walls with the corner post of the container, the stresses amounted to about 215 MPa. The resulting stresses were 24 % lower than those in a typical design.

The maximum displacements were recorded in the lower part of the end wall of the container and amounted to 2.6 mm (Fig. 3.46).

The strength was also calculated with the loaded sidewall of the container in accordance with the diagram shown in Fig. 3.41, b). The calculation results are shown in Figs. 3.47 and 3.48. The maximum stresses in the container were recorded in the areas of interaction of the sidewall with the corner posts and amounted to 178 MPa (Fig. 3.47), which was 15.2 % lower than permissible. The maximum displacements were in the middle part of the

sidewall and were 3.1 mm (Fig. 3.48). Therefore, the strength of the container was ensured.

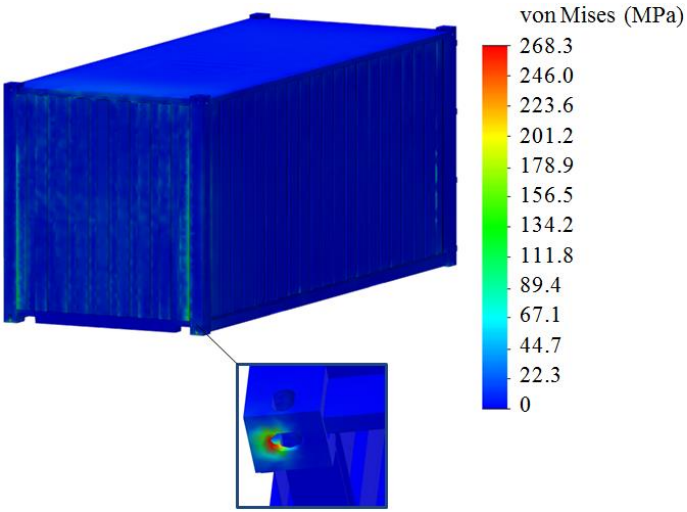

Figure 3.45 – The stress state of the container

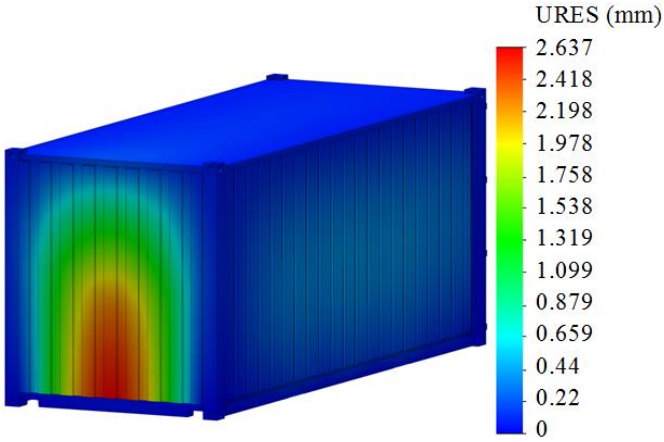

Figure 3.46 – The displacements in the container units

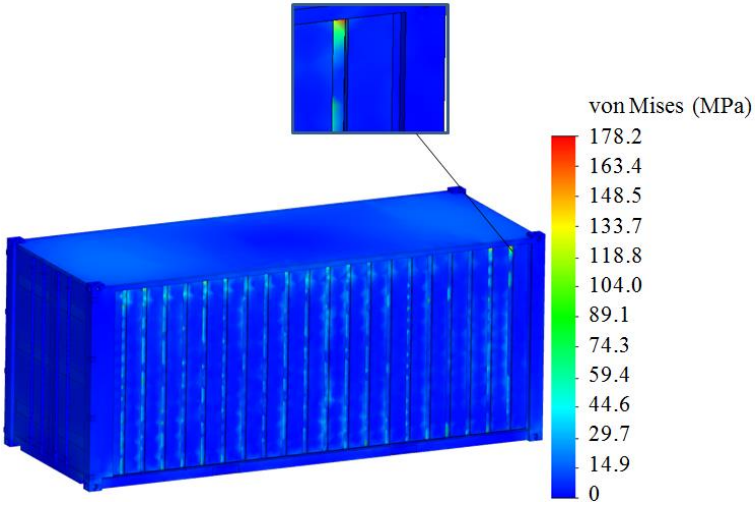

Figure 3.47 – The stress state of the container

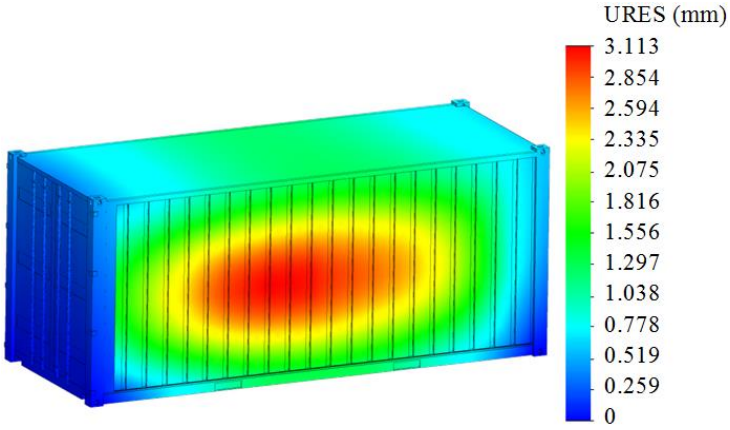

Figure 3.48 – The displacements in the container units

3.3.2 Strength of the sandwich panel wall container under the dynamic loads

The use of sandwich panels for the sidewalls of the container was substantiated by means of mathematical modelling of its dynamic load, provided that it was placed on a flat wagon during side roll oscillations [6]. The design diagram of the container placed on the flat wagon is shown in Fig. 3.49.

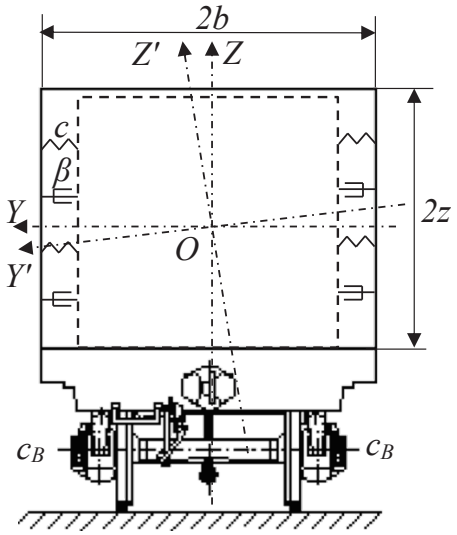

Figure 3.49 – The design diagram of the container placed on the flat wagon

The mathematical model was formed (3.10).

$$\begin{cases} I_{FW} \cdot \ddot{q}_1 + c_B \cdot b \cdot (sign(b \cdot q_1)) = F_k, \\ I_k \cdot \ddot{q}_2 - g(M_k \cdot z^2) \cdot q_2 = F_{FW} + F_B - c \cdot b^2 \cdot (q_2 - q_3) - \beta \cdot b^2 \cdot (\dot{q}_2 - \dot{q}_3), \\ I_B \cdot \ddot{q}_3 = F_k - c \cdot b^2 \cdot (q_2 - q_3) - \beta \cdot b^2 \cdot (\dot{q}_2 - \dot{q}_3), \end{cases} \quad (3.10)$$

where I_{FW} is the moment of inertia of the flat wagon; c_B is the stiffness of the springs of the spring suspension of the bogie; b is the half-width of the flat wagon frame; F_k is the moment of forces

arising between the container and the frame of the flat wagon; I_k is the moment of inertia of the container relative to the longitudinal axis; M_k is the mass of the container; z is the half-height of the container; F_{FW} is the moment of forces arising between the flat wagon and the container; F_B is the moment of forces arising between the container and the cargo; c is the stiffness of the energy-absorbing material; β is the coefficient of viscous resistance of the energy-absorbing material; I_B is the moment of inertia of the cargo; F_k is the moment of forces arising between the container and the cargo.

The mathematical model was solved in MathCad under initial conditions equal to zero. In this case, the model was reduced to the normal Cauchy form with subsequent solution using the Runge – Kutta method.

Based on the calculations, it was found that the maximum accelerations acting on the container were 1.7 m/s^2 (Fig. 3.50).

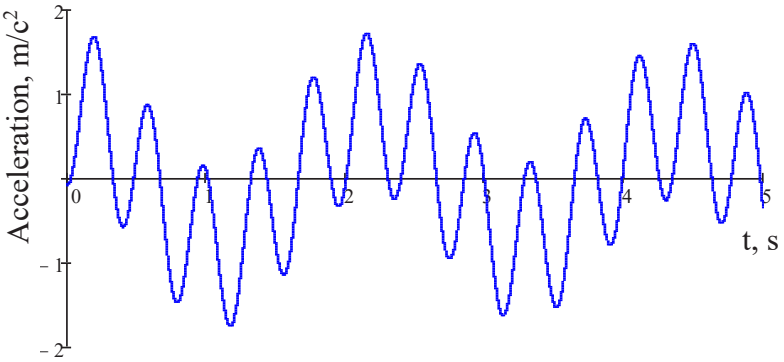

Figure 3.50 – The accelerations acting on the container

The resulting acceleration value was almost 5 % lower than that acting on a typical container. The calculation was made at a stiffness coefficient of the energy-absorbing material of 1.5 kN/m and a coefficient of viscous resistance of 2.0 kN · s/m. These parameters were determined by sequential selection when the accelerations were within the permissible values.

The formed mathematical model was verified through computer modelling of the transverse load of the container placed on the flat wagon using the finite element method in SolidWorks Simulation. For this, the spatial model of the container was built in SolidWorks (Fig. 3.51); it included structural elements rigidly interacted with each other. Strength (energy) theory IV was used as the calculation theory.

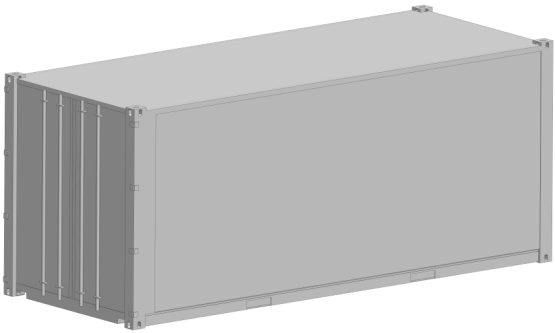

Figure 3.51 – The 1CC container with sandwich panel walls

The elastic-viscous connection in the sandwich-panels sidewalls was included as a spring-damper connection using the options of the software package.

The design diagram of the container included the vertical static load P_v and the transverse static load P_t applied to the sidewall (Fig. 3.52). The transverse load included the pressure from the load (grain) and the dynamic load applied to the wall on the tilting side of the container.

The finite-element model of the container was formed by 373.575 nodes and 1,119,509 elements (isoparametric tetrahedrons). The model was secured by the fittings. Steel 09G2S was used as a construction material. The calculation results are shown in Fig. 3.53.

The strength of the container and the safety of the cargo transported can be ensured by using a sandwich-panel floor [87]. It was assumed that each of these panels was made of two metal sheets with a layer of energy-absorbing material in-between so that to reduce the vertical dynamic loads acting on the container loaded during its transportation.

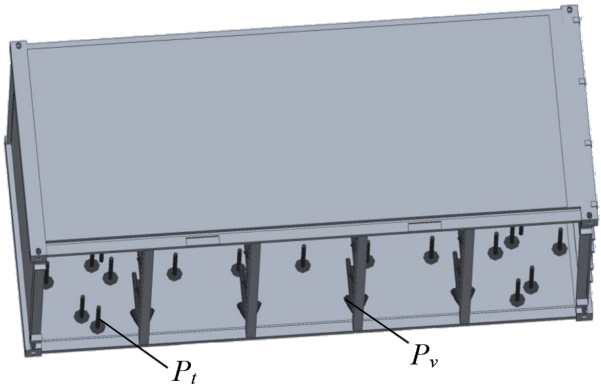

Figure 3.52 – The design diagram of the container

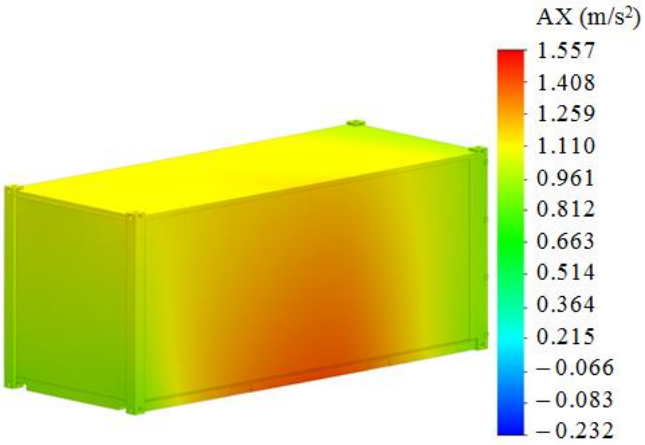

Figure 3.53 – The acceleration distribution fields acting on the container

The maximum accelerations occurred in the middle part of the sidewall and were about 1.5 m/s^2. In the end walls, the acceleration was about 0.8–0.9 m/s^2. Thus, the discrepancy between the results obtained by mathematical and computer modelling was about 8 %.

The results of determining the strength of the container when perceiving longitudinal loads are covered in [98].

3.4 Vertical load of the sandwich panel floor container transported by flat wagon

The sandwich panels were laid on the container frame formed by a set of cross bearers (Fig. 3.54).

The proposed solution was substantiated with appropriate studies. The initial stage included the determination of the thickness of the sheets that form the sandwich panel by means of the Bubnov – Galerkin method. It was taken into account that the length of one panel was l = 2.34 m, and its width was b = 1.18 m. These geometric parameters were taken based on the geometric characteristics of the standard 1 CC container. For sheets made of low-alloy Steel 09G2S, their thickness was about 6 mm, provided that strength was ensured.

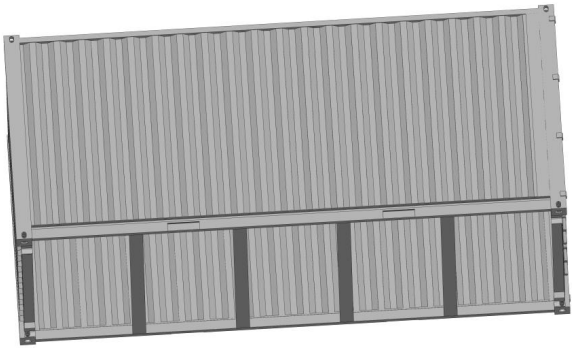

Figure 3.54 – The 1 CC container

The strength of a container with a sandwich-panel floor when perceiving vertical loads, was calculated using the finite element method in SolidWorks Simulation. Since the main load absorbed by the sandwich panel was the vertical dynamic load, it was determined by means of mathematical modelling. The calculation was made for the vertical load of the container transported by the flat wagon 13-7024.

The design diagram consisted of four bodies: the load-bearing structure of the flat wagon with four containers, two 18–100 bogies, and the cargo in the containers. Thus, the design diagram had

four degrees of freedom in the vertical plane. It was assumed that the containers had the same load at full load capacity. They were considered as attached weights relative to the flat wagon frame.

The track had elastic-dissipative characteristics [17] and reacted proportionally to both its deformations and the speed of these deformations.

The design diagram of the flat wagon loaded with containers is shown in Fig. 3.55.

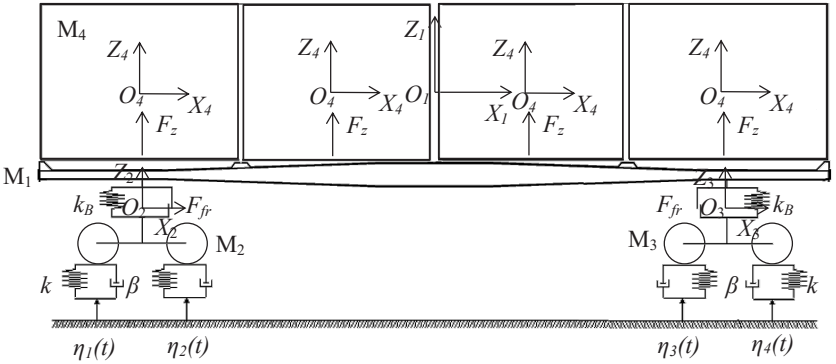

Figure 3.55 – The design diagram of the flat wagon loaded with standard 1CC containers

The mathematical model has the form:

$$\begin{cases} M_1 \cdot \ddot{q}_1 + C_{1,1} \cdot q_1 + C_{1,2} \cdot q_2 + C_{1,3} \cdot q_3 = -F_{FR} \cdot \left(sign\left(\dot{\delta}_1\right) + sign\left(\dot{\delta}_2\right)\right) - F_z, \\ M_2 \cdot \ddot{q}_2 + C_{2,1} \cdot q_1 + C_{2,2} \cdot q_2 + B_{2,2} \cdot \dot{q}_2 = F_{FR} \cdot sign\left(\dot{\delta}_1\right) + k\left(\eta_1 + \eta_2\right) + \beta\left(\dot{\eta}_1 + \dot{\eta}_2\right), \\ M_3 \cdot \ddot{q}_3 + C_{3,1} \cdot q_1 + C_{3,3} \cdot q_3 + B_{3,3} \cdot \dot{q}_3 = F_{FR} \cdot sign\left(\dot{\delta}_2\right) + k\left(\eta_3 + \eta_4\right) + \beta\left(\dot{\eta}_3 + \dot{\eta}_4\right), \\ M_4 \cdot \ddot{q}_4 = F_z - M_4 \cdot g, \end{cases} \quad (3.11)$$

where M_1 is the weight of the load-bearing structure of the flat wagon loaded with containers; M_2, M_3 are the weights of the first bogie and the second bogie, respectively; M_4 is the weight of the cargo in the container; C_{ij} is the elasticity characteristics of the elements of the oscillating system determined by the

spring suspension stiffness coefficients k_B; k is the track stiffness; B_{ij} is the dissipative coefficients; β is the damping coefficient; F_{FR} is the friction force in the spring group of the bogie; δ_i is the deformation of the spring suspension elastic elements; η_i is the track irregularity; F_z is the vertical force acting on the cargo.

In this case $q_i \sim Z_i$.

The track irregularity was described by the function presented in [17]:

$$\eta(t) = \frac{h}{2}(1 - \cos \omega t), \tag{3.12}$$

where h is the height of the irregularity; ω is the frequency of oscillations.

The system of differential equations was solved in MathCad using the Runge – Kutta stepwise iteration method. The initial conditions were close to zero.

The accelerations acting on the load-bearing structure of the flat wagon with containers were calculated in arrays $ddq_{j,i}$:

$$ddq_{j,1} = \frac{-F_{FR} \cdot \left(sign\left(\dot{\delta}_1\right) + sign\left(\dot{\delta}_2\right)\right) - F_z - C_{1,1} \cdot y_1 - C_{1,2} \cdot y_2 - C_{1,3} \cdot y_3}{M_1}, \tag{3.13}$$

$$ddq_{j,2} = \frac{F_{FR} \cdot sign\left(\dot{\delta}_1\right) + k\left(\eta_1 + \eta_2\right) + \beta\left(\dot{\eta}_1 + \dot{\eta}_2\right) - C_{2,1} \cdot y_1 - C_{2,2} \cdot y_2 - B_{2,2} \cdot \dot{y}_2}{M_2}, \tag{3.14}$$

$$ddq_{j,3} = \frac{F_{FR} \cdot sign\left(\dot{\delta}_2\right) + k\left(\eta_3 + \eta_4\right) + \beta\left(\dot{\eta}_3 + \dot{\eta}_4\right) - C_{3,1} \cdot y_1 - C_{3,3} \cdot y_3 - B_{3,3} \cdot \dot{y}_3}{M_3}, \tag{3.15}$$

$$ddq_{j,4} = \frac{F_z - M_4 \cdot g}{M_4}, \tag{3.16}$$

where $y_1 = q_1$, $y_2 = q_2$, $y_3 = q_3$.

Based on the calculations, the accelerations acting on the load-bearing structure of the flat wagon with containers were obtained (Fig. 3.56).

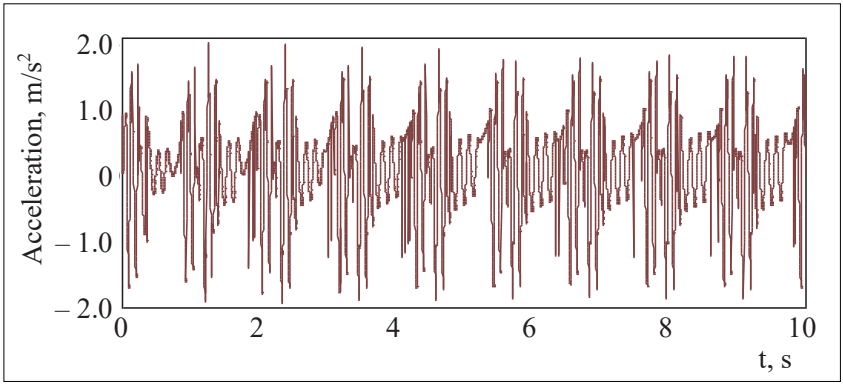

Figure 3.56 – The accelerations acting on the load-bearing structure of the flat wagon with containers

Consequently, the accelerations acting on the container were about 2 m/s^2. The resulting acceleration value was 5.7 %, which was lower than that acting on a typical container.

The determined acceleration value was taken into account when calculating the strength of the container. The spatial model of the container was built in SolidWorks according to its album of drawings (Fig. 3.57). Foam aluminium was used as an energy-absorbing material.

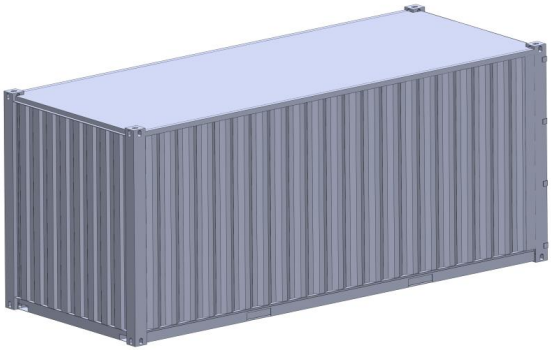

Figure 3.57 – The spatial model of the container

The container was secured by corner fittings. The finite element model was built with tetrahedra. The optimal number of finite elements of the model was determined graphically and analytically. The number of elements of the model was 201.800 with a maximum size of 100 mm and a minimum size of 20 mm. The model was formed with 62.175 nodes. The structural material was Steel 09G2S.

The design diagram included the own weight, as well as the weight of the cargo (Fig. 3.58).

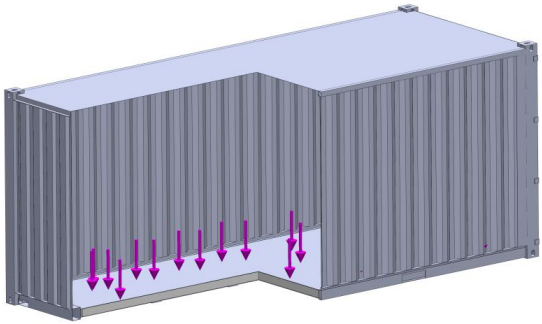

Figure 3.58 – The design model of the container

The finite element model of the container is shown in Fig. 3.59.

Figure 3.59 – The finite element model of the container

The results of the calculations showed that the maximum stresses in the container were in its sidewalls (Fig. 3.60) and amounted to 118.4 MPa (Fig. 3.61); they were lower than permissible (210 MPa) for this steel grade.

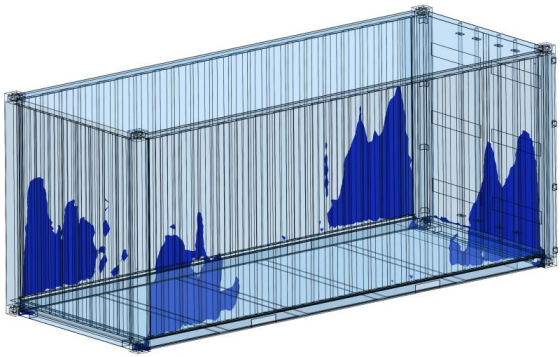

Figure 3.60 – The most loaded areas of the container

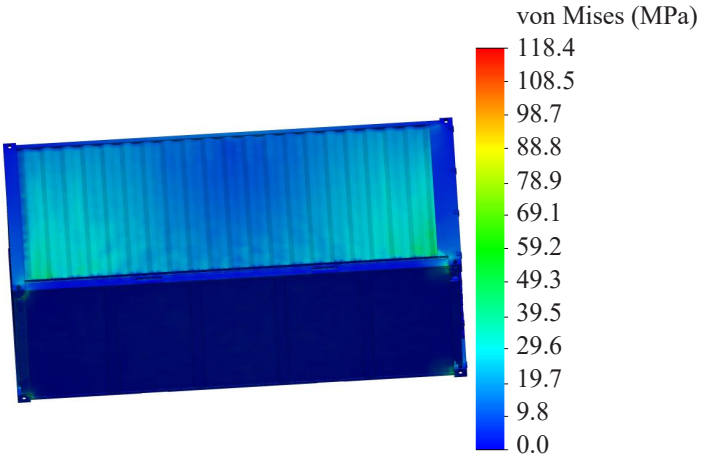

Figure 3.61 – The stress state of the container

The maximum displacements occurred in the bottom sheet of the sandwich panel located in the centre of the floor and were 1.13 mm (Fig. 3.62, 3.63).

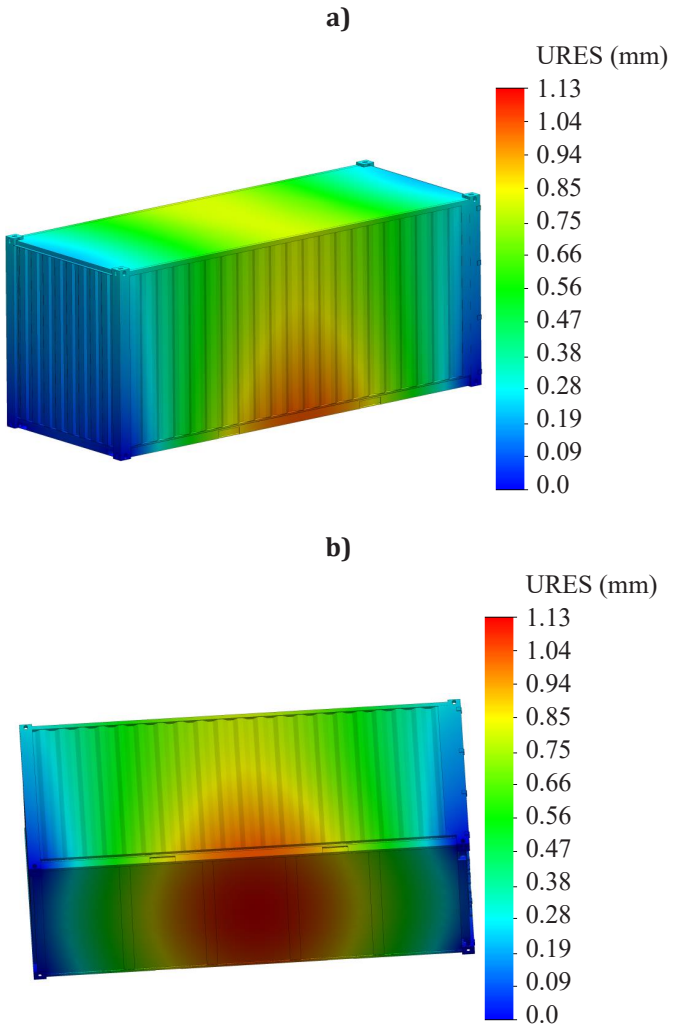

Figure 3.62 – The displacements in the container units
a) side view; b) bottom view

The displacements along the length of the container floor were determined using the probing function in SolidWorks Simulation.

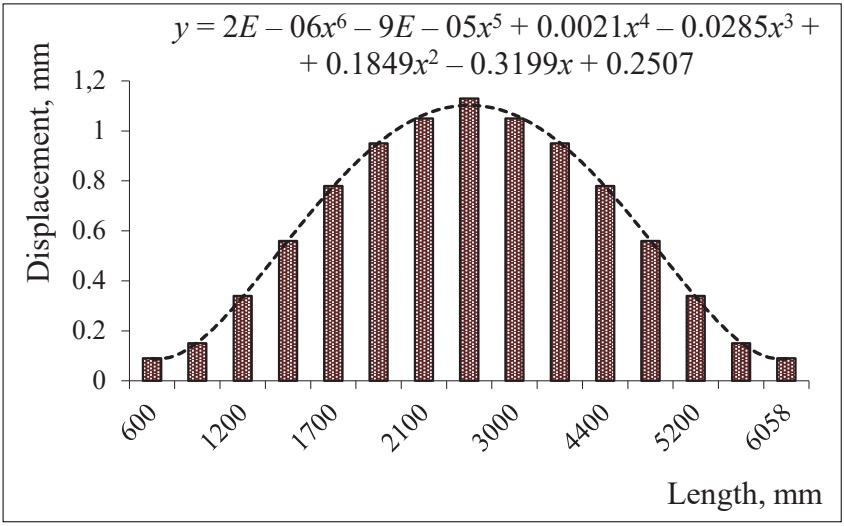

Figure 3.63 – The distribution of maximum displacements by lower sheets of the container floor

The study included also a strength test for the container floor. The load diagram of the container floor when the test equipment moved relative to it is shown in Fig. 3.64. It was taken into account that the wheels of the equipment were placed in the centre of the floor.

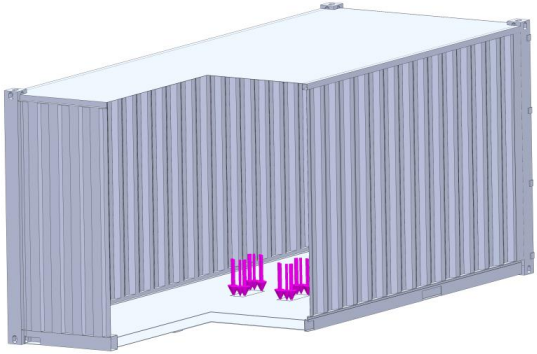

Figure 3.64 – The load diagram of the container floor when loading/unloading equipment moves on the floor

The container was fastened by the corner fittings. Thus, the maximum stresses were in the interaction zone of the upper sheet of the central sandwich panel with the longitudinal beam and were 84.3 MPa (Fig. 3.65), which was much lower than permissible.

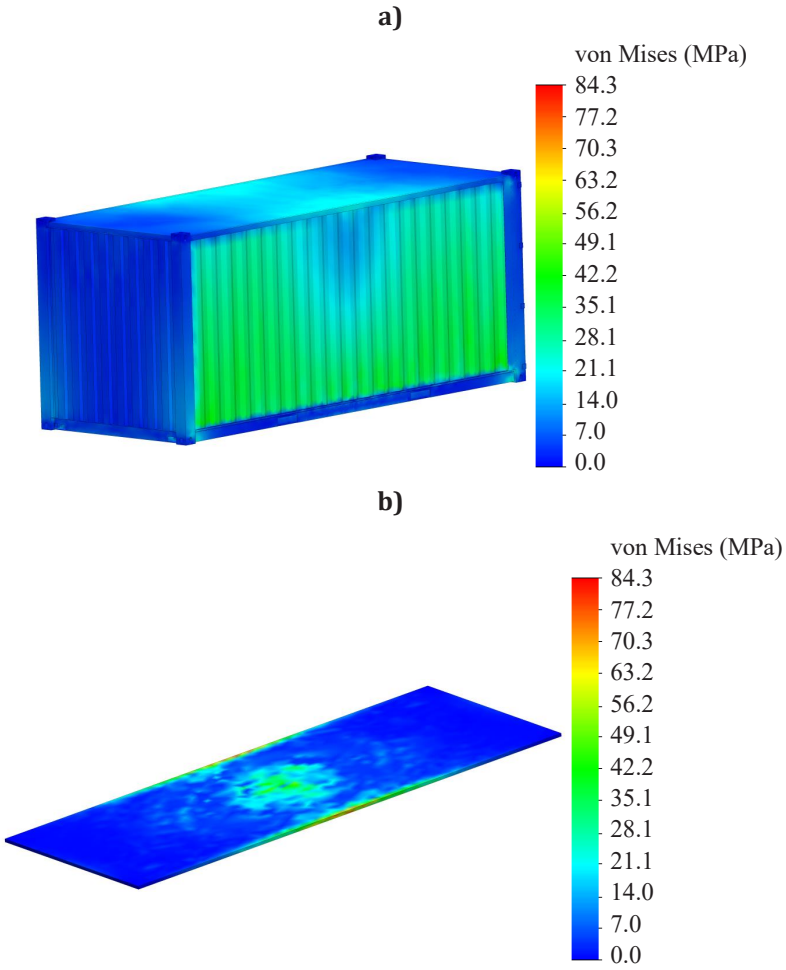

Figure 3.65 – The stress state of the container when loading/unloading equipment moves on the floor: a) container; b) floor

The maximum displacements were in the middle sandwich panel, which formed the floor of the container, and were less than 1 mm (Figs. 3.66 and 3.67).

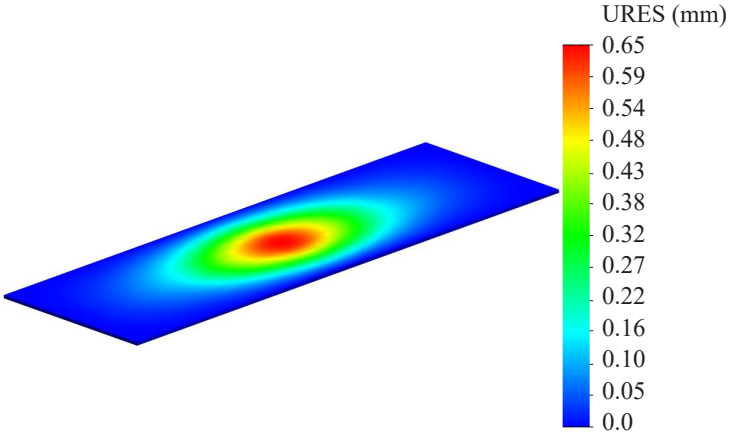

Figure 3.66 – The displacements in the floor of the container when loaded with loading/unloading equipment

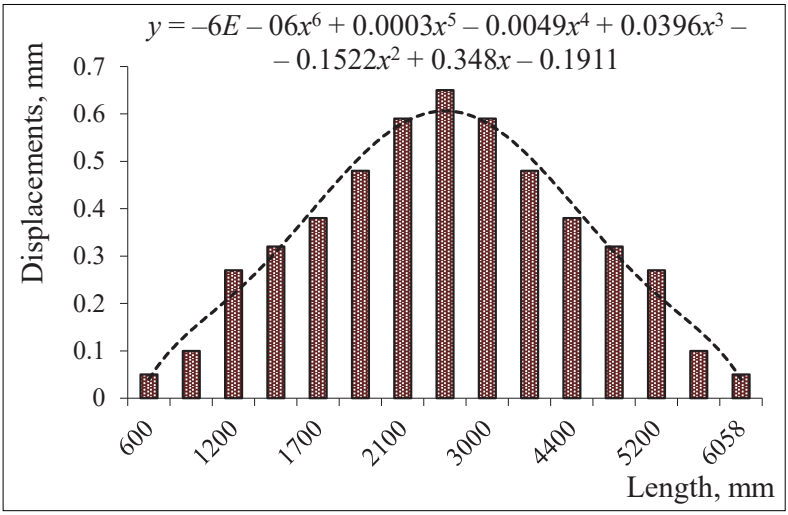

Figure 3.67 – The maximum displacement distribution by lower sheets of the container floor

This displacement field distribution can be explained by the diagram of fixation of the sandwich panels and their load. Thus, the strength of the container floor at a given load mode was also ensured.

3.5 Dynamic load of the sandwich panel wall container transported by train ferry

The possibility of transporting a sandwich panel container by train ferry was checked by means of the appropriate calculations at the most unfavourable train ferry oscillations, i.e., the roll oscillations (similar to lateral oscillation in wagon dynamics).

The design diagram of the container on the flat wagon fixed on the train ferry deck is shown in Fig. 3.68 [95].

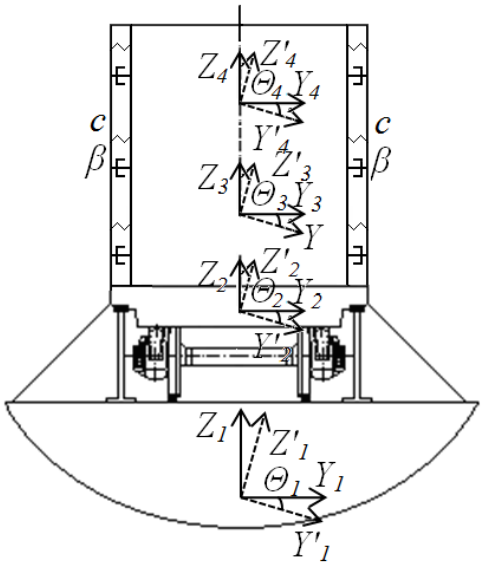

Figure 3.68 – The design diagram of the container on the flat wagon

The system was assumed to have four degrees of freedom, characterized by angular displacements around the longitudinal axis of train ferry, flat wagon, container and cargo, respectively. In the calculations, the cargo was considered as conditional at the full load capacity of the container. The energy-absorbing material in the container walls was modelled by an elastic-viscous connection with a viscous resistance coefficient of 20 kN·s/m and a stiffness coefficient of 15 kN/m. These parameters were determined based on the author's previous research.

The mathematical model did not include the frictional forces between the components of the system, such as centre plate/centre bowl, stop/jack/bolster beam, cargo/container, etc.

The mathematical model has the form:

$$\begin{cases} I_{RF} \cdot \ddot{q}_1 + \left(\Lambda_\theta \cdot \dfrac{B}{2} \right) \dot{q}_1 = P(t), \\ I_{FW}^{\theta} \cdot \ddot{q}_2 = p'_{FW} \cdot \dfrac{h_{FW}}{2} + M_{FW}^{D} + M_{FW}^{C}, \\ I_{C}^{\theta} \cdot \ddot{q}_3 = p'_{C} \cdot \dfrac{h_C}{2} + M_{C}^{FW} + M_{C}^{L} \\ I_{L}^{\theta} \cdot \ddot{q}_4 = -\beta \cdot h_C \cdot \dot{q}_3 - c \cdot h_C \cdot q_3 + M_{L}^{C}, \end{cases} \tag{3.17}$$

$$P(t) = p'_{RF} \cdot \frac{h}{2} + \Lambda_\theta \cdot \frac{B}{2} \cdot \dot{F}(t), \tag{3.18}$$

where I_{RF} is the moment of inertia of the train ferry; Λ_θ is the coefficient of resistance to oscillation; B is the width of the train ferry; h is the board height; p'_{RF} is the wind load on the surface projection; $P(t)$ is the law of perturbing force (sea wave); $I_{FW}{}^{\theta}$ is the moment of inertia of the flat wagon; h_{FW} is the height of the side surface of the flat wagon; p'_{FW} is the wind load on the side surface of the flat wagon; M_{FW}^{D} is the moment of forces arising between the flat wagon and the deck of the train ferry; M_{FW}^{C} is the moment of forces arising between the flat wagon and containers; I_{C}^{θ} is the moment of inertia; h_C is the height of the side surface of the container; p'_C is the wind load on the side surface of the flat wagon;

M_C^{FW} is the moment of forces arising between the flat wagon and the train ferry deck; M_C^L is the moment of forces arising between the cargo and containers; I_L^θ is the moment of inertia of the cargo in the container; M_L^C is the moment of forces arising between the cargo and the container; β is the coefficient of viscous resistance of energy-absorbing material; c is the stiffness of energy-absorbing material.

The movement of the wave was described by the trochoid. System of differential equations (3.18) was solved in MathCad. The system of second-order differential equations was reduced to a system of first-order differential equations, followed by the use of standard algorithms for solving the system using the rkfixed Mathcad function.

The generalized accelerations were calculated in the array $ddq_{j,i}$:

$$ddq_{j,1} = \frac{p'_{RF} \cdot \frac{h}{2} + \Lambda_\theta \cdot \frac{B}{2} \cdot \dot{F}(t) - \left(\Lambda_\theta \cdot \frac{B}{2} \right) \dot{y}_1}{\left(\frac{D}{12 \cdot g} (B^2 + 4 z_g{}^2) \right)}, \tag{3.19}$$

$$ddq_{j,2} = \frac{p'_{FW} \cdot \frac{h_{FW}}{2} + M_{FW}^D + M_{FW}^C}{I_{FW}^\theta}, \tag{3.20}$$

$$ddq_{j,3} = \frac{p'_C \cdot \frac{h_C}{2} + M_C^{FW} + M_C^L}{I_C^\theta}, \tag{3.21}$$

$$ddq_{j,4} = \frac{-\beta \cdot h_C \cdot \dot{q}_3 - c \cdot h_C \cdot q_3 + M_L^C}{I_B^\theta}. \tag{3.22}$$

Based on the calculations, it was found that the highest values of accelerations occurred at the course angles of the wave relative to the hull of the train ferry $\chi = 60°$ and $\chi = 120°$. Here, the maximum acceleration of the container relative to the regular place on the deck was about 2.3 m/s^2 (Fig. 3.69). The numerical value of acceleration is indicated without the free-fall acceleration.

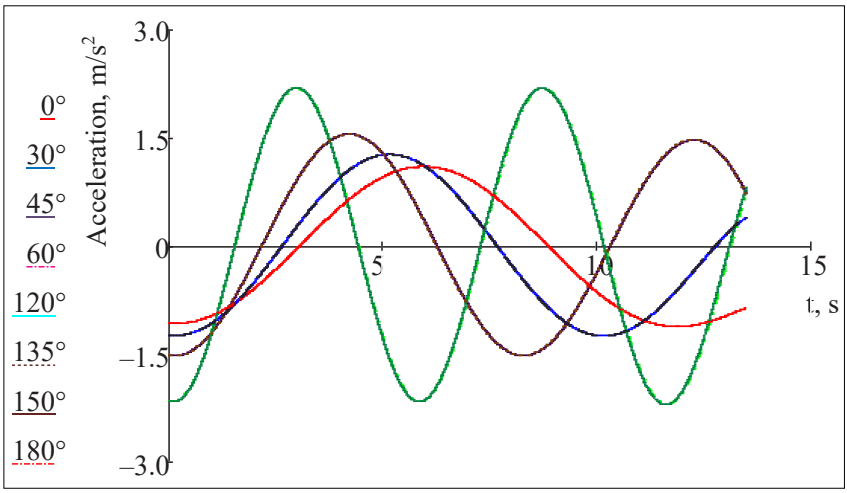

Figure 3.69 – The accelerations acting on the container transported by train ferry

The total acceleration was determined by the formula:

$$\ddot{\theta}_{tot} = \ddot{\theta}_{rp} + g \cdot \sin\theta, \tag{3.23}$$

where $\ddot{\theta}_{rp}$ is the acceleration acting relative to the regular place of the flat wagon loaded with containers on the deck; g is the free-fall acceleration; θ is the train ferry roll angle.

Taking into account the hydrometeorological characteristics of the sea and the surface projection of the train ferry, a roll angle of $\theta = 12.2°$ was obtained. The roll angle was calculated for the static wind action on the surface projection of the train ferry. The calculation was made for a train ferry of the Plevna Heroes class when it moved on the Black Sea. With this in mind, the total amount of acceleration acting on the container was 4.4 m/s^2 (0.45 g). The resulting acceleration value was 4.3 % lower than that acting on a container of a typical design. The accelerations were also calculated for other roll angles of the train ferry (Figure 3.70).

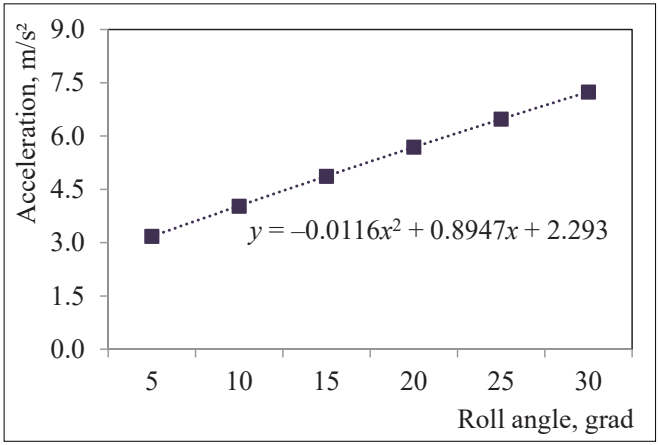

Figure 3.70 – The dependence of accelerations acting on the container on the roll angle of the train ferry

The mathematical model was verified according to the Fisher criterion. The obtained accelerations were taken into account to determine the stability of the container on the flat wagon. The calculation was carried out according to the technique given in the author's previous publication [45]. The calculation results are shown in Fig. 3.71.

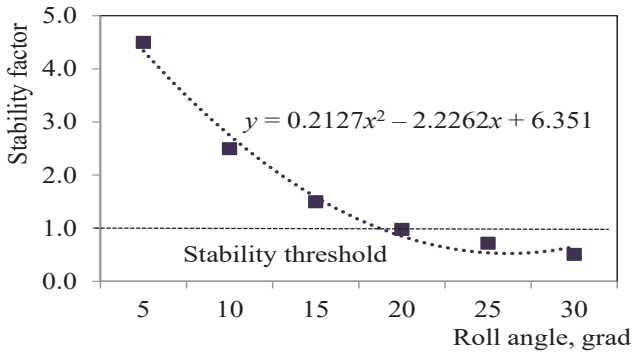

Figure 3.71 – The dependence of the stability factor of the container on the roll angle

An analysis of the dependence shown in Fig. 3.71 shows that the stability of the container is ensued at roll angles up to 17°.

3.6 Load of the hopper container concept under the operating modes

3.6.1 Analysis of the stress state of the hopper container transported by rail

A hopper-type container design was proposed for the higher efficiency of freight transportation (Fig. 3.72). The special feature of this container is that its end walls are placed at an angle for self-unloading of bulk cargo through the discharge doors that form its floor. The load-bearing structure of the container is represented by a frame with upper and bottom rails, corner and intermediate poles, slope poles, main longitudinal and intermediate beams. The container is equipped with lower and upper corner fittings with standard dimensions for securing it to the vehicle and for loading/unloading operations.

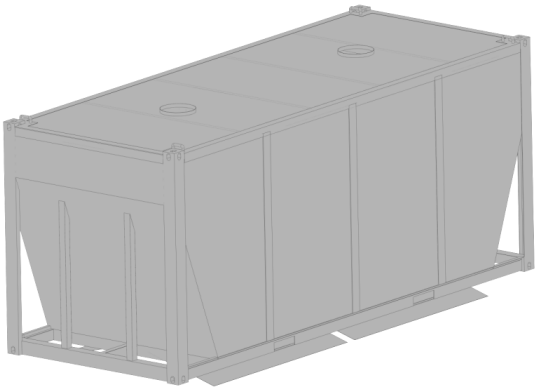

Figure 3.72 – The hopper container

The load of the container under the most unfavourable operating modes, namely the shunting collision of the flat wagon loaded with containers, was determined with mathematical modelling. The studies were carried out in a plane coordinate. The design diagram of the flat wagon with containers is shown in Fig. 3.73.

The first stage of the study included no displacements of the container relative to the flat wagon frame at shunting collision [45]. That is, the container was considered as a mass attached to the flat wagon frame. It was also taken into account that a longitudinal load of 3.5 MN acted on the rear stop of the automatic coupling of the flat wagon.

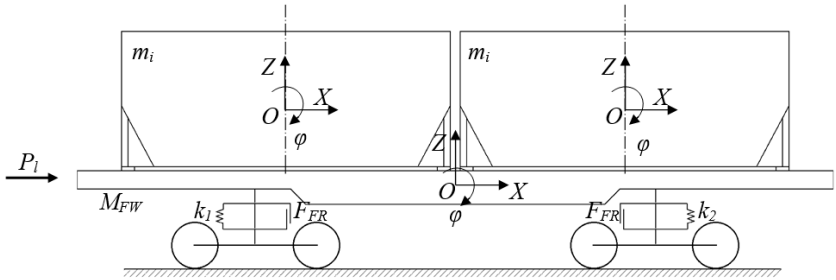

Figure 3.73 – The design diagram of the flat wagon loaded with containers

Thus, the motion equation of the design model is as follows:

$$M'_{FW} \cdot \ddot{x} + M_{FW} \cdot h \cdot \ddot{\varphi} = P_l, \tag{3.24}$$

$$\begin{aligned} &I_{FW} \cdot \ddot{\varphi} + M_{FW} \cdot h \cdot \ddot{x} - g \cdot \varphi \cdot M_{FW} \cdot h = \\ &= l \cdot F_{FR}(sign\dot{\Delta}_1 - sign\dot{\Delta}_2) + l(k_1 \cdot \Delta_1 - k_2 \cdot \Delta_2), \end{aligned} \tag{3.25}$$

$$M_{FW} \cdot \ddot{z} = k_1 \cdot \Delta_1 + k_2 \cdot \Delta_2 - F_{FR}, (sign\dot{\Delta}_1 + sign\dot{\Delta}_2,) \tag{3.26}$$

$$m_i \cdot \ddot{x} + (m_i \cdot z_{ci}) \cdot \ddot{\varphi} = 0, \tag{3.27}$$

$$I_i \cdot \ddot{\varphi} + (m_i \cdot z_{ci}) \cdot \ddot{x} - g(m_i \cdot z_{ci}) \cdot \varphi = 0, \tag{3.28}$$

$$m_i \cdot \ddot{z} = 0, \tag{3.29}$$

where

$$\Delta_1 = z - l \cdot \varphi; \;\; \Delta_1 = z + l \cdot \varphi,$$

where M'_{FW} is the weight of the flat wagon; M_{FW} is the mass of the load-bearing structure of the flat wagon; I_{FW} is the moment of inertia of the flat wagon relative to the longitudinal axis; P_l is the longitudinal impact force in the automatic coupling; l is half of the base of the flat wagon; F_{FR} is the dry friction force in the spring assembly; k_1, k_2 are the stiffness of springs in the suspension ,of flat wagon bogies; m_i is the container weight; z_{ci} is the height of the container's centre of gravity; I_i is the moment of inertia of the i-th container; x, φ, z are the coordinates that determine the longitudinal, angular relative to the transverse axis, and vertical displacement of the flat wagon, respectively.

The calculations included the technical characteristics of the flat wagon model 13-401M on bogies 18-100.

Equations of motion (3.25)–(3.30) were solved using the Runge-Kutta method. The starting conditions were set to zero. Based on the calculations, it was found that the maximum acceleration acting on the container in the longitudinal direction was 36.7 m/s^2. This acceleration value was taken for the strength calculation of the container.

The strength of the container was studied by means of its spatial model built in SolidWorks using the finite element method in SolidWorks Simulation and the Mises criterion.

The finite element model was formed by isoparametric tetrahedra. The number of nodes was 37.163 and the number of elements was 113.342. The maximum size of the element was 120 mm, the minimum size was 24 mm.

The first stage of the study included the strength calculation of the container placed on the flat wagon during shunting collision.

The design model of the container included also the vertical load P_v (Fig. 3.74) and the pressure of the bulk cargo (coal) P_p to the inner surface of the container. The longitudinal load P_l was applied

to the fitting stops, which included the acceleration obtained by design model (3.25)–(3.30).

The model was secured by the fittings. Steel 09G2S with elastic isotropic properties was used for the container.

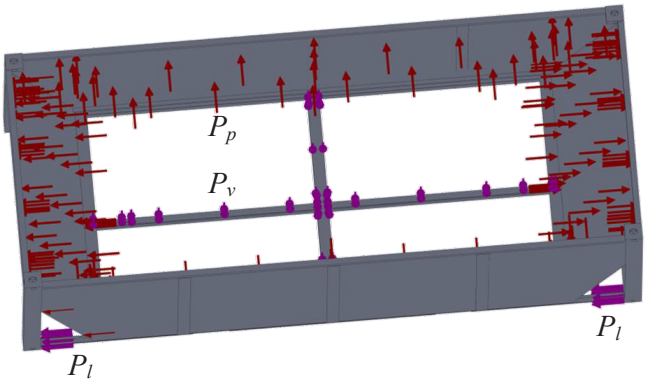

Figure 3.74 – The design diagram of the container

The results of the calculations are shown in Fig. 3.75. The maximum equivalent stresses were recorded in the areas of interaction of the bottom cord with the container. Their numerical value was 315.1 MPa, that is, they did not exceed the permissible values [15]. The distribution of maximum equivalent stresses over the length of the bottom rail is shown in Fig. 3.76. The graphical dependence was constructed with the symmetrical longitudinal load on the front and rear fittings of the container. Figure 3.76 shows that the end parts of the rails were the most loaded. In its middle part, the maximum equivalent stresses were about 190 MPa.

The study included also the determination of the load of the proposed container design during stacking. It was taken into account that the stack had seven containers [16]. Thus, the design diagram included the following loads: vertical static P_v, bulk cargo pressure P_p, and vertical load P_l acting on the upper fittings (Fig. 3.77).

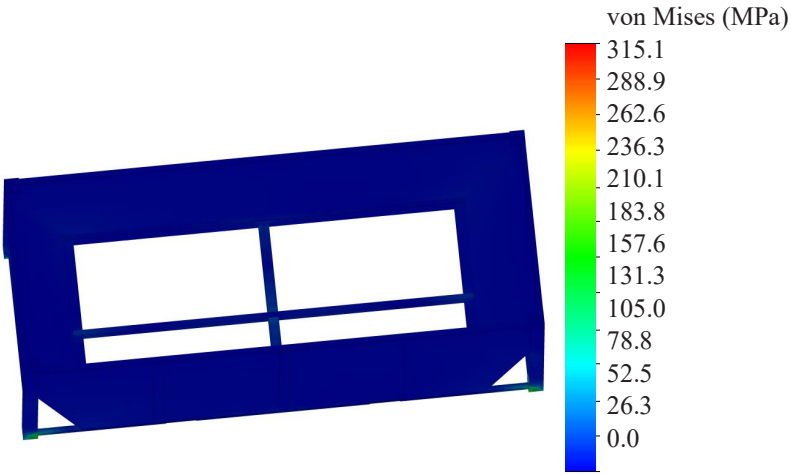

Figure 3.75 – The stress state of the container

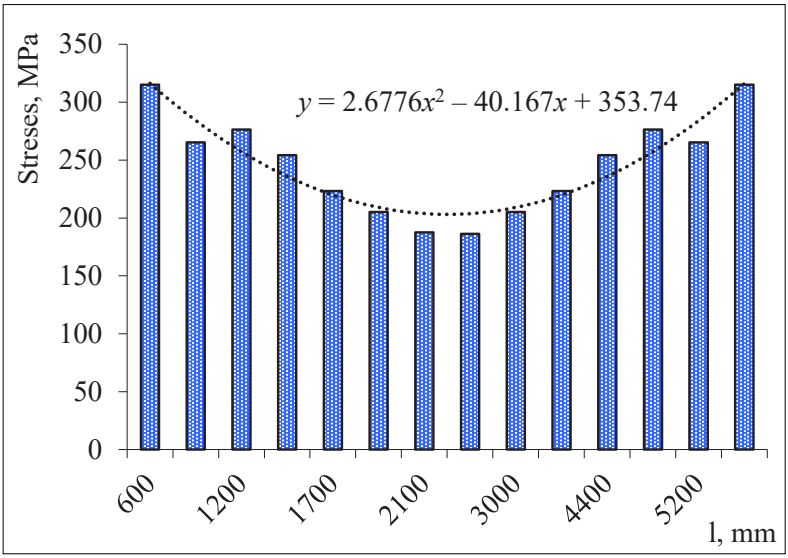

Figure 3.76 – The distribution of maximum equivalent stresses along the bottom rail

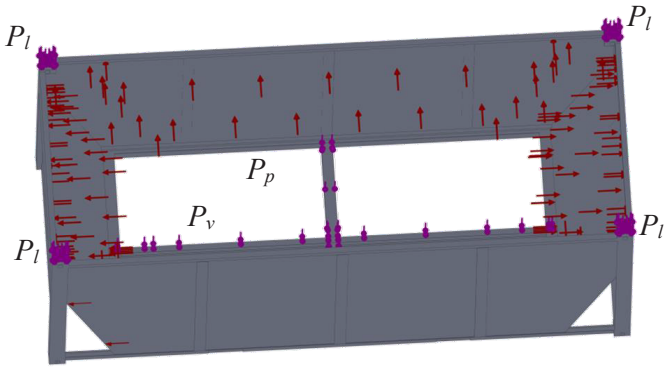

Figure 3.77 – The design diagram of the container

The model was secured by the lower fittings; the maximum equivalent stresses were in the corner posts of the container and were 245.3 MPa (Figure 3.78), which was lower than permissible [15].

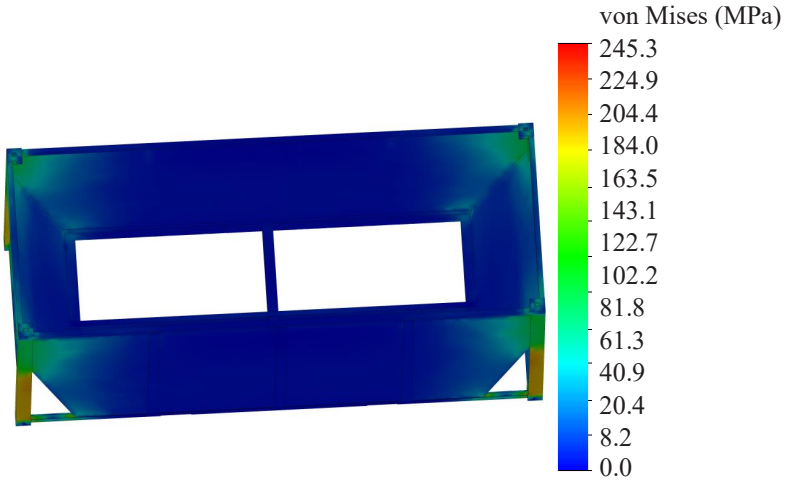

Figure 3.78 – The stress state of the container

The distribution of the maximum equivalent stresses over the height of the corner post is shown in Fig. 3.79. The middle part of the post was the most loaded.

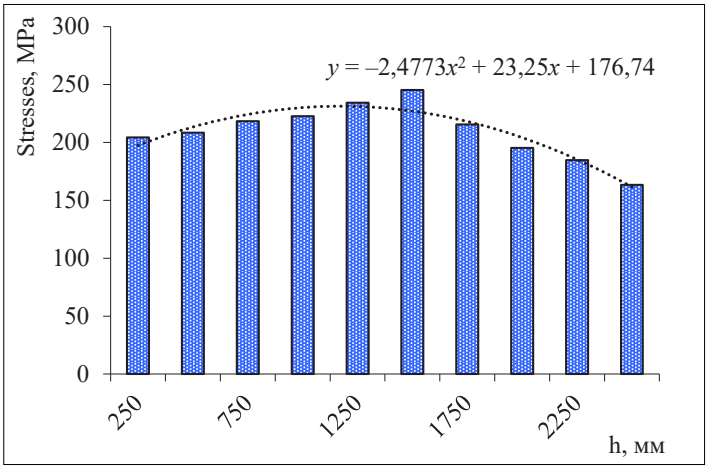

Figure 3.79 – The distribution of maximum equivalent stresses along the height of the corner post

For the goods that need protection from atmospheric precipitation, it was proposed to equip the container with a detachable roof (Fig. 3.80) [97].

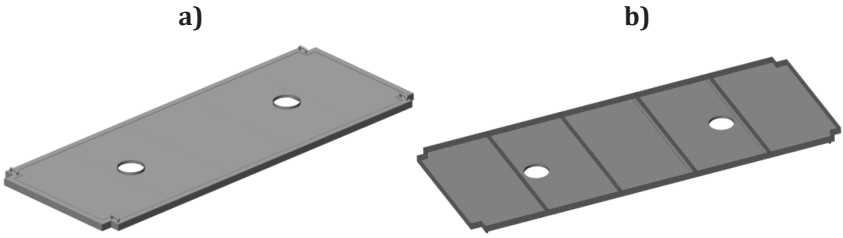

Figure 3.80 – The detachable roof:
a) top view; b) bottom view

The roof must take into account the geometric characteristics of the container. The roof consisted of a frame (Fig. 3.81) and panelling. The roof frame was formed by corners interacting with each other by welding.

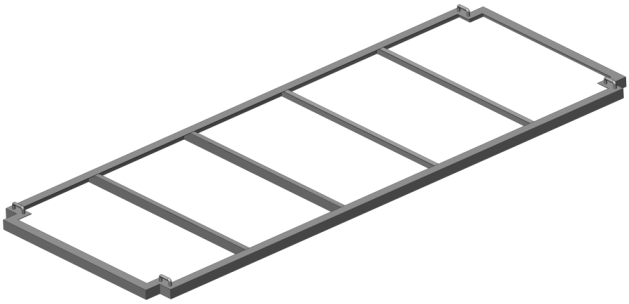

Figure 3.81 – The roof frame

The thickness of the roof panelling was assumed to be equal to the thickness of the container wall panelling. The container was equipped with upper discharge doors on the roof so that to ensure the safety of the container while unloading the cargo. These upper doors must be open in order to eliminate the vacuum in the middle of the container when pouring the cargo. The upper doors were located over the geometric centre of the covers of the discharge doors. Their diameter was identical to the diameter of the covers of the loading doors of the box wagon. The weight of the roof was about 300 kg.

The strength of the roof under operating loads was also calculated. The design diagram of the roof included also the longitudinal load P_l from the fitting stops (Fig. 3.82). Thus, the roof works for compression. The calculations included also the force of gravity using the options of the software package.

The roof was secured in the areas of its interaction with the top rail of the container.

Isoparametric tetrahedra were used in the FEM. The model had 109.553 nodes and 327.338 elements. The structural material for the roof was Steel 09G2S.

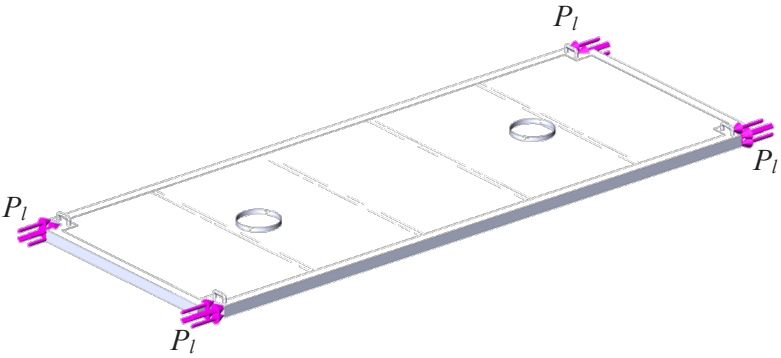

Figure 3.82 – The design diagram of a detachable roof

Based on the calculations, it was found that the maximum equivalent stresses occurred in the areas of interaction of the roof with the upper fittings and were 50.2 MPa, which was much lower than permissible [15] (Fig. 3.83).

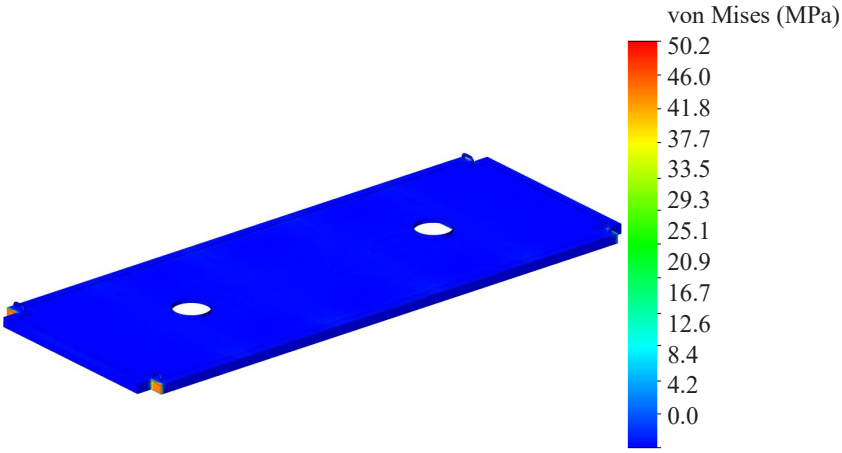

Figure 3.83 – The stress state of the roof

3.6.2 Analysis of the load of the hopper-type container transported by train ferry

In order to assess the possibility of transporting the hopper container by sea, the loads on it were studied. The study included the transportation of the container on a train ferry as part of a combined train.

The stresses in the load-bearing structure of the container were determined using the finite element method, implemented in SolidWorks Simulation. The Mises criterion was used as the calculation criterion. The design diagram of the container is shown in Fig. 3.84. The following was included in the calculation: the vertical load P_v and the pressure force of bulk cargo P_p. Grain was taken as one of the most common types of bulk cargo transported in containers. The design model included also the reactions P_f that occurred in the container fittings towards the action of dynamic load during a roll. These reactions were applied to the fitting stops on the side where the container tilted.

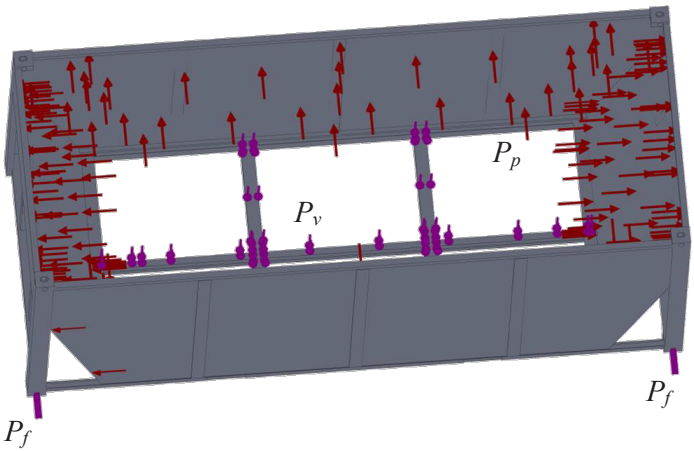

Figure 3.84 – The design diagram of the container

The pressure forces were determined using the Coulomb method [36]:

$$p = G\frac{\sin(\vartheta-\rho)}{\sin(\vartheta+\psi-\rho)}, \tag{3.30}$$

where G is the weight of the prism displacement of the cargo; ϑ is the angle of inclination of the slope plane to the horizontal line; ρ is the angle of internal friction (for a perfect medium it is equal to carg); δ is the angle of friction between the cargo and the wall.

Importantly, the maximum pressure corresponds to the direction of the sliding area. The maximum pressure can be determined using the technique proposed by V. V. Sinelnikov [36], according to which, it is necessary to replace the variable ϑ, the inclination angle of the sliding plane in the maximum pressure condition $\left(\frac{dp}{d\vartheta}=0\right)$, with some variable x (in this case, the angle $\alpha = 0$), which, in general, cannot be determined analytically. By taking it into account, the formula for determining the pressure forces of bulk cargo is:

$$p = \gamma h\frac{\cos^2(\rho-\alpha)}{\left[1+\sqrt{\frac{\sin\rho\sin(\rho-\alpha)}{\cos\alpha}}\right]^2\cos\alpha}, \tag{3.31}$$

where γ is the bulk weight of the cargo, kN/m^3; h is the container height, m.

The design diagram of the container is shown in Fig. 3.85. With angular displacement of the container relative to the longitudinal axis, the dynamic load was also taken into account, since it caused an additional force effect on the cargo and the container walls. Therefore, the following formula was used to determine the pressure forces of the bulk cargo on the container walls:

$$p = \gamma h\frac{\cos^2(\rho-\alpha)}{\left[1+\sqrt{\frac{\sin\rho\sin(\rho-\alpha)}{\cos\alpha}}\right]^2\cos\alpha}+F_a, \tag{3.32}$$

where F_a is the additional pressure caused by the dynamic load on the bulk cargo.

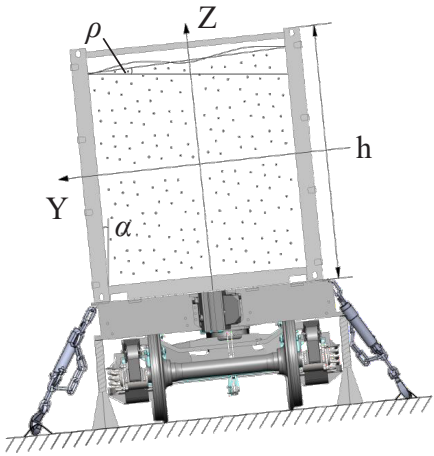

Figure 3.85 – The design diagram for determining the pressure forces of bulk cargo on the container walls

The value of the dynamic load acting on the container with the bulk cargo was determined by the technique given in [45]. For the container which did not move relative to the flat wagon frame, the acceleration acting on it was 0.25 g. The calculation included a roll angle of the train ferry of 12.2° caused by the static effect of wind on the surface projection. As far as the value F_a was 4.26 kPa, the total pressure of the bulk cargo was 11.6 kPa.

Isoparametric tetrahedra were used for the finite element model of the container. The number of elements was 112.714, and the number of nodes was 37.005. The maximum size of the element was 120 mm, the minimum size was 24 mm. The container was secured in the areas of its interaction with the flat wagon. The construction material was low-alloy Steel 09G2S. The calculation results are shown in Fig. 3.86.

Thus, the strength of the container transported by sea as part of a combined train was ensured.

The study included also the determination of the container stability equilibrium at the typical diagram of interaction with the flat wagon transported by sea. The design diagram of the container is shown in Fig. 3.88. The results of the calculations are shown in Fig. 3.89.

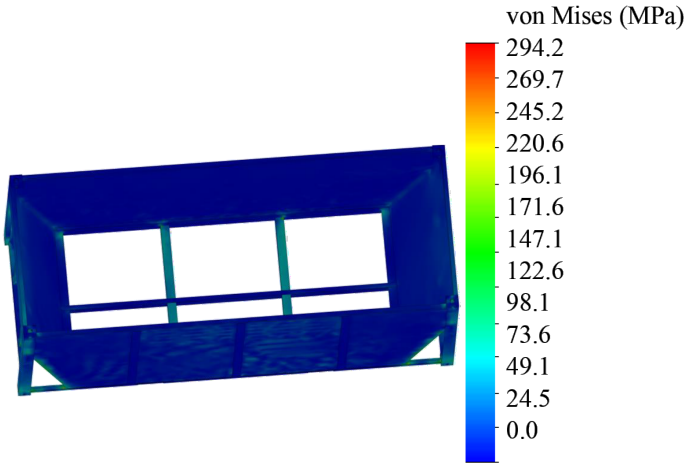

Figure 3.86 – The stress state of the container

equivalent stresses in the container were recorded in its bottom rail and amounted to 294.2 MPa, which is lower than permissible [15] (Fig. 3.87).

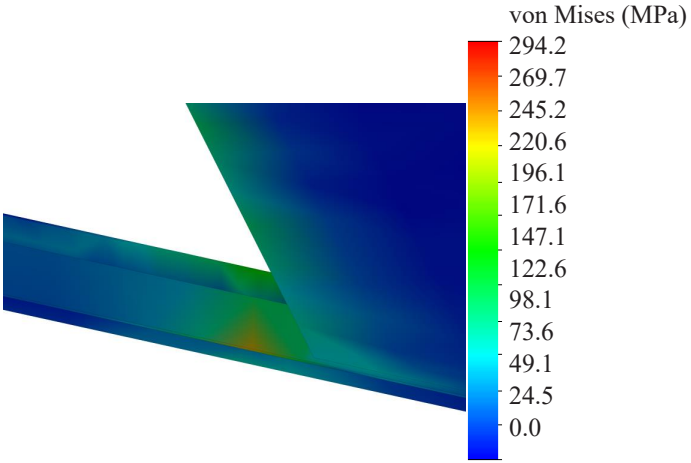

Figure 3.87 – The maximum equivalent stresses in the container

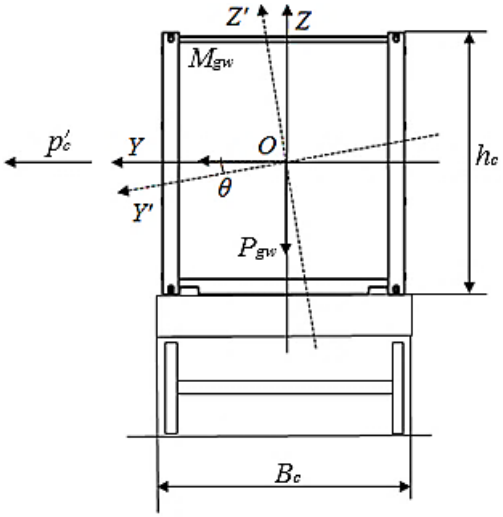

Figure 3.88 – The design diagram for determining the container stability

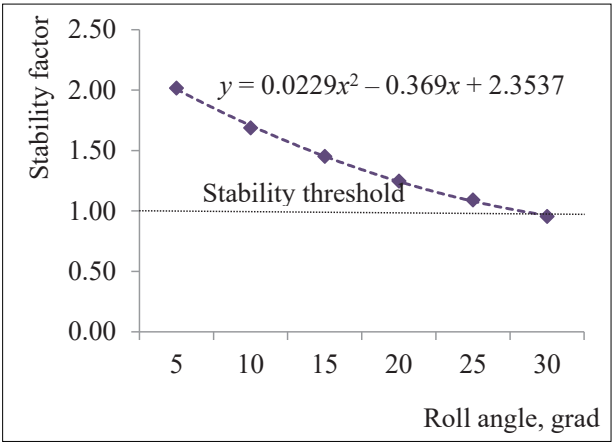

Figure 3.89 – The dependence of the stability factor of the container on the roll angle

Thus, the stability of the container at the typical diagram of interaction with the flat wagon, was ensured at roll angles up to 26°.

3.6.3 Vertical dynamics of the flat wagon with hopper-type containers and their elastic interaction

The vertical accelerations acting on the load-bearing structure of the flat wagon loaded with hopper containers were determined using mathematical model (3.34) [66, 67]. The calculation was based on the flat wagon model 13-7024 built at Kryukovsky Railway Car Building Works (Kremenchug, Ukraine), a long wheel-base flat wagon which can simultaneously transport four 1 CC containers or two 1AA containers.

The design diagram of the flat wagon loaded with containers is shown in Fig. 3.90. The mechanical system under study consisted of four bodies: a load-bearing structure, two running gears, and containers, i.e., it had four degrees of freedom. The containers were considered as attached masses that interacted with the flat wagon frame through elastic connections. It was assumed that the containers had the same load. The stiffness of the connection between the containers and the frame was calculated according to the technique given in [45]. It was also taken into account that the flat wagon moved along an elastic track.

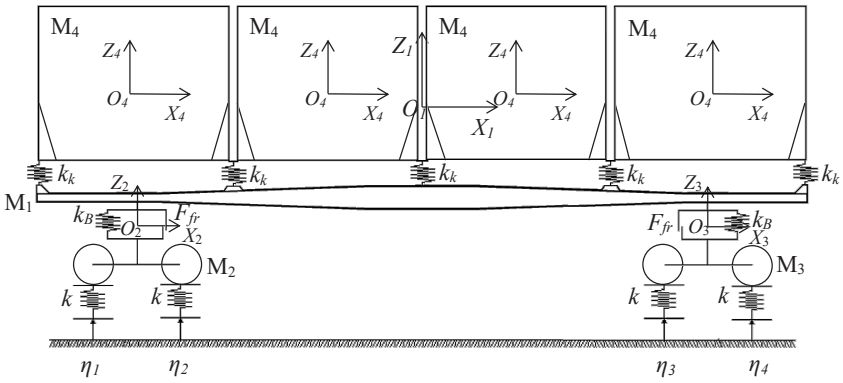

Figure 3.90 – The design diagram of the flat wagon loaded with hopper-type containers

The system of differential equations of motion has the form:

$$\begin{cases} M_1 \cdot \ddot{q}_1 + C_{1,1} \cdot q_1 + C_{1,2} \cdot q_2 + C_{1,3} \cdot q_3 = -F_{fr} \cdot \left(sign\left(\dot{\delta}_1\right) + sign\left(\dot{\delta}_2\right)\right) - \sum_{i=1}^{4} F_z, \\ M_2 \cdot \ddot{q}_2 + C_{2,1} \cdot q_1 + C_{2,2} \cdot q_2 = F_{fr} \cdot sign\left(\dot{\delta}_1\right) + k\left(\eta_1 + \eta_2\right), \\ M_3 \cdot \ddot{q}_3 + C_{3,1} \cdot q_1 + C_{3,3} \cdot q_3 = F_{fr} \cdot sign\left(\dot{\delta}_2\right) + k\left(\eta_3 + \eta_4\right), \\ M_4 \cdot \ddot{q}_4 = F_z - M_4 \cdot g, \end{cases} \quad (3.33)$$

$$F_z = -k_k \left(q_1 - q_4\right),$$

where M_1 is the weight of the bearing structure of the flat wagon; M_2, M_3 are the weight of the first and second bogies, respectively; C_{ij} is the elasticity characteristics of the elements of the oscillating system, determined by the stiffness coefficients of the spring suspension k_B; k are the track stiffness, k_k is the stiffness of the connection between the load-bearing structure of the flat wagon and the containers; F_{fr} is the frictional force in the bogie's spring group; δ_i is the deformations of elastic elements of spring suspension; η_i is the track irregularity.

The mathematical model was solved using the Runge-Kutta method at initial conditions equal to zero.

The generalized accelerations were calculated in the array $ddq_{j,i}$:

$$ddq_{j,1} = \frac{-F_{fr} \cdot \left(sign\left(\dot{\delta}_1\right) + sign\left(\dot{\delta}_2\right)\right) - C_{1,1} \cdot y_1 - C_{1,2} \cdot y_2 - C_{1,3} \cdot y_3 - \sum_{i=1}^{4} F_z}{M_1}, \quad (3.34)$$

$$ddq_{j,2} = \frac{F_{fr} \cdot sign\left(\dot{\delta}_1\right) + k\left(\eta_1 + \eta_2\right) - C_{2,1} \cdot y_1 - C_{2,2} \cdot y_2}{M_2}, \quad (3.35)$$

$$ddq_{j,3} = \frac{F_{fr} \cdot sign\left(\dot{\delta}_2\right) + k\left(\eta_3 + \eta_4\right) - C_{3,1} \cdot y_1 - C_{3,3} \cdot y_3}{M_3}. \quad (3.36)$$

$$ddq_{j,4} = \frac{F_z - M_4 \cdot g}{M_4}. \quad (3.37)$$

The input parameters to the mathematical model were the technical characteristics of the flat wagon, bogies (model 18-100), track, as well as containers. The calculation was carried out for a speed of the flat wagon of 90 km/h. The results of the calculations are shown in Figs. 3.91–3.93.

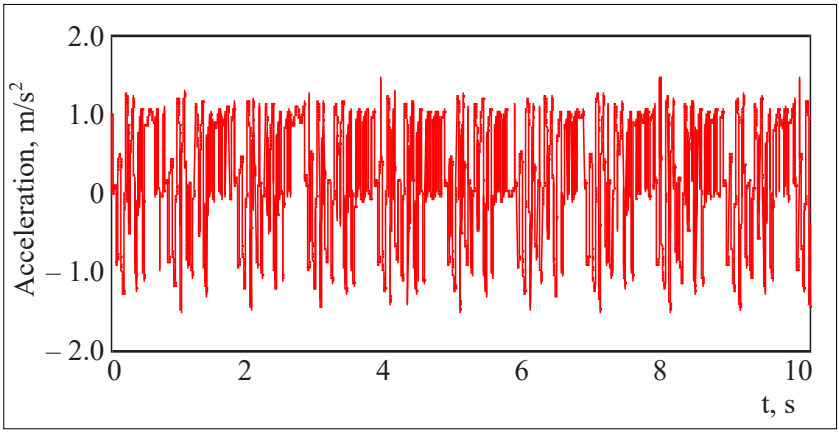

Figure 3.91 – The acceleration acting in the centre of mass of the bearing structure of the flat wagon

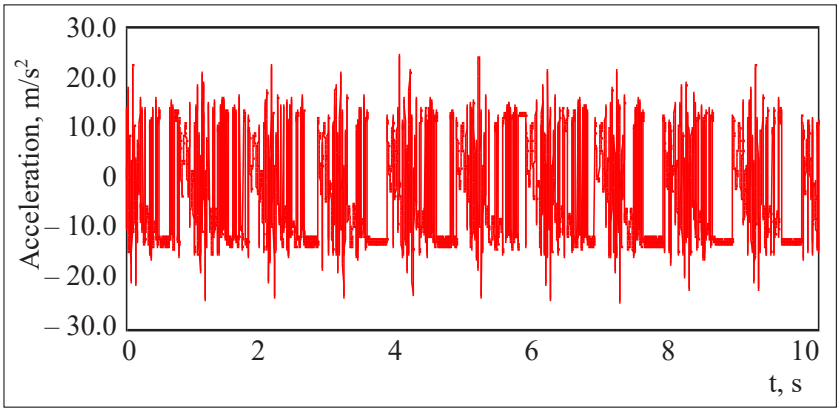

Figure 3.92 – The acceleration to the bogies

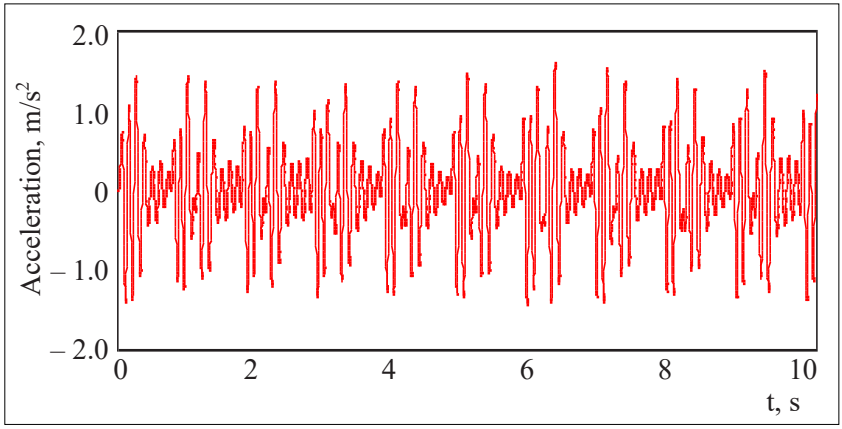

Figure 3.93 – The acceleration to the containers

The maximum acceleration acting in the centre of mass of the bearing structure of the flat wagon was 1.51 m/s^2 (Fig. 3.91); it did not exceed the permissible value [15].

The acceleration of the bogies was 24.5 m/s^2 (Fig. 3.92). The acceleration acting on the containers was 1.6 m/s^2 (Fig. 3.93). The forces arising in the spring suspension were equal to 68.1 kN. The vertical dynamics coefficient was 0.12. The movement of the flat wagon was assessed as excellent [15].

The accelerations acting on the load-bearing structure of the flat wagon loaded with hopper containers were also determined by computer modelling. The spatial model of the load-bearing structure of the flat wagon was built in SolidWorks (Fig. 3.94).

It was taken into account that the flat wagon was loaded with four hopper containers (Fig. 3.95).

The accelerations and their distribution fields were determined using the finite element method implemented in SolidWorks Simulation. Tetrahedra were used as finite elements. The optimal number of tetrahedrons was calculated using the graphic and analytical method. The number of elements in the mesh was 152.961 and nodes – 52.569; the maximum element size was 140 mm, the minimum – 28 mm.

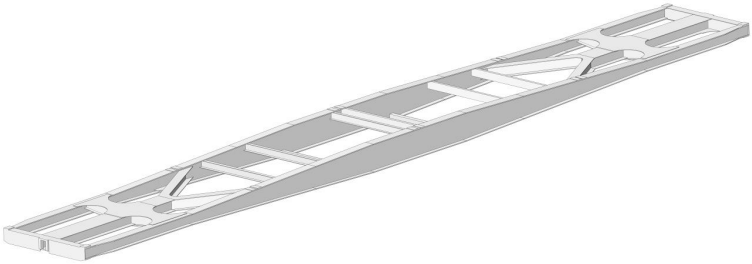

Figure 3.94 – The spatial model of the load-bearing structure of the flat wagon

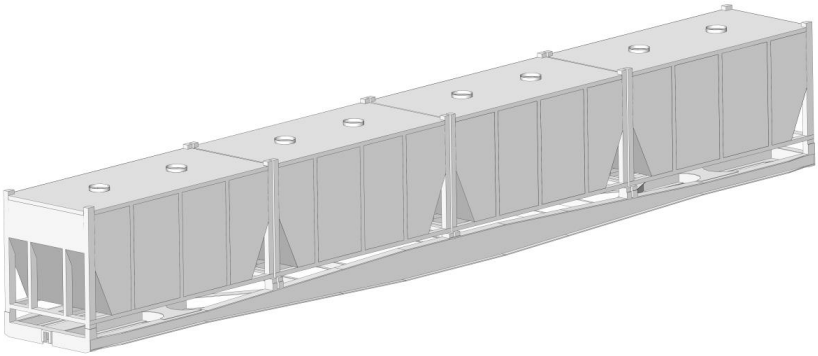

Figure 3.95 – The hopper containers on the flat wagon

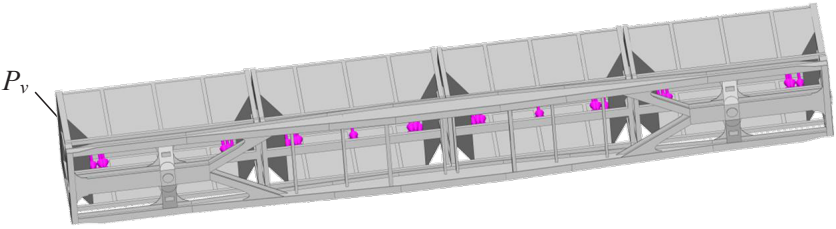

Figure 3.96 – The design diagram of the load-bearing structure of the flat wagon loaded with containers

The model was secured by the centre plates. The design diagram included the vertical load P_v caused by the weight of the cargo on the container frame (Fig. 3.96). The calculation included a conditional load using the full load capacity of containers.

Steel 09G2S was used as the material of the load-bearing structure of the flat wagon and containers. The calculation results are shown in Fig. 3.97.

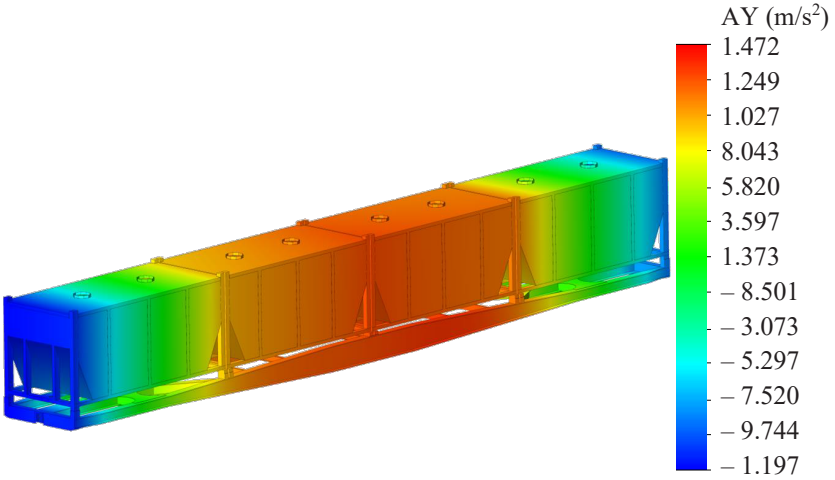

Figure 3.97 – The accelerations acting on the load-bearing structure of the flat wagon loaded with containers

The maximum acceleration was concentrated in the middle part of the bearing structure of the flat wagon and was 1.47 m/s^2. The obtained value of vertical acceleration corresponded to the excellent course of the wagon [15]. The acceleration decreases in the end parts of the load-bearing structure and increased again in its end parts (Fig. 3.98) as the load-bearing structure was secured by the centre plates.

According to the design diagram shown in Fig. 3.96, variational calculations were carried out and the accelerations acting on the load-bearing structure of the flat wagon at different loads of the containers were determined. The results of the calculations are given

in Table 3.2. The calculations included the equal load of each of the four containers. Table 3.2 shows also the results of mathematical modelling of the vertical load of the flat wagon with containers, which were obtained by means of mathematical modelling.

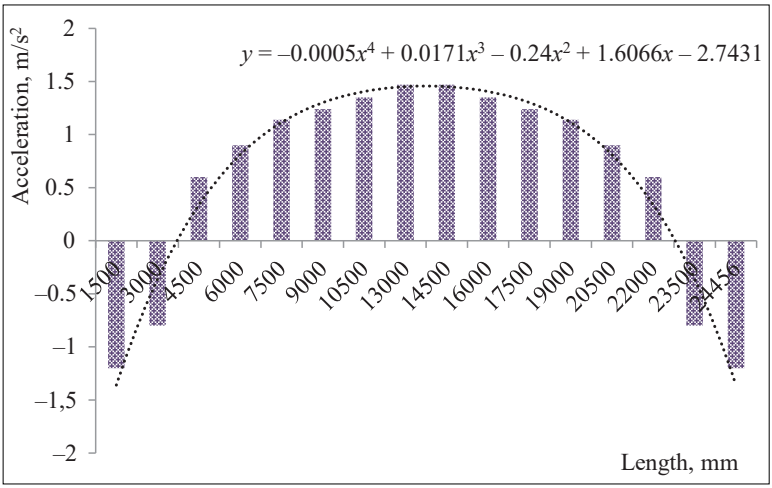

Figure 3.98 – The acceleration distribution by the length of the flat wagon frame

Table 3.2 – The accelerations on the load-bearing structure of the flat wagon

Container weight, t	Acceleration, m/s²	
	Mathematical model	Computer model
24	1.28	1.47
22	1.42	1.59
20	1.54	1.72
18	1.67	1.84
16	1.73	1.96
14	1.87	2.08
12	2.1	2.21

The built model was verified with the F-criterion.

$$F_c = \frac{S_{ad}^2}{S_y^2}, \tag{3.38}$$

where S_{ad}^2 is the variance of adequacy; S_y^2 is the error mean square.

The variance of adequacy was determined using the formula

$$S_{ad}^2 = \frac{\sum_{i=1}^{n} \left(y_i - y_i^p \right)}{f_i}, \tag{3.39}$$

where y_i^p is the calculation value obtained by modelling; f_i is the number of degrees of freedom.

$$f_i = N - q, \tag{3.40}$$

where N is the number of experiments in the planning matrix; q is the number of equation coefficients.

The error mean square was determined by the formula:

$$S_y^2 = \frac{1}{N} \sum_{i=1}^{n} S_i^2, \tag{3.41}$$

where S_i^2 is the variance in each row where the parallel experiments were conducted.

The optimal number of experiments was determined using Student's t-test:

$$n = \frac{t^2 \cdot \sigma^2}{\delta^2}, \tag{3.42}$$

where t was calculated by the ratio $\Phi(t) = \gamma/2$; $\Phi(t)$ is the Laplace function, tabular value; σ is the root mean square deviation of the random variable under study, which is known a priori, even before experimental measurements; δ^2 is the absolute measurement error.

It was found, that the number of experiments was sufficient. The calculations took the model as linear, which characterized the change in accelerations in the load-bearing structure of the flat wagon depending on its load (Fig. 3.99).

Here, the regression equation has the form:

$$y = b_0 + b_1 x_1, \tag{3.43}$$

where b_0 and b_1 are unknown coefficients.

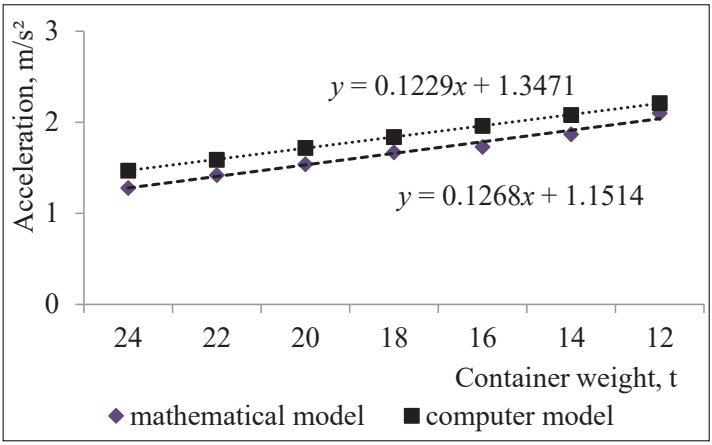

Figure 3.99 – The dependence of accelerations of the bearing structure of the flat wagon on the container weight

Thus, the number of degrees of freedom of the model was equal to $f_1 = 5$. With the error mean square $S_y^2 = 0.05$ and the variance of adequacy $S_{ad}^2 = 0.07$, the calculated value of the criterion was $F_c = 1.45$, which is less than the tabular value of the criterion $F_t = 3.87$. So, with the significance level $p = 0.05$, the hypothesis of the adequacy of the developed model was not denied.

3.7 Load of the detachable module for long cargo transported by rail

The efficiency of the transportation process can be increased by introducing a detachable module for long cargoes (Fig. 3.100) [39, 69]. A special feature of the detachable module is its framed design. The cargo area is represented by a frame which consisted of main longitudinal beams 1, main cross bearers 2 and a row of intermediate cross bearers 3. End superstructures 4 on the detachable module can prevent moving the cargo in the longitudinal plane. These superstructures are formed by a set of cross bearers and vertical beams.

The detachable module is also equipped with side poles 5 to keep the cargo from transverse displacements. In this case, the corner posts interact with the first pole on the console side through inclined belts 6. Fitting stops 7 are provided for fastening the detachable module on vehicles in the corner parts. As an example, Fig. 3.101 shows a detachable module placed on the flat wagon, as one of the most common vehicles for transporting detachable transport means in international traffic.

This module can also be used as a device for fastening containers in open wagons. The relevant studies of the load on the detachable module are presented in [41–43, 55–60, 89]. This solution can significantly increase the economic effect. For example, when 1CC containers were transported in open wagons, the economic effect amounted to UAH 88,028,000, and with 1AA containers, it was UAH 49,376,000.

In this case, the spatial stiffness of the vertical posts in the transverse direction can be ensured by the lashing devises used to keep the cargo from tipping over. One of them for 1.520 mm-gauge lines is chains attached to the upper parts of the poles located one opposite the other.

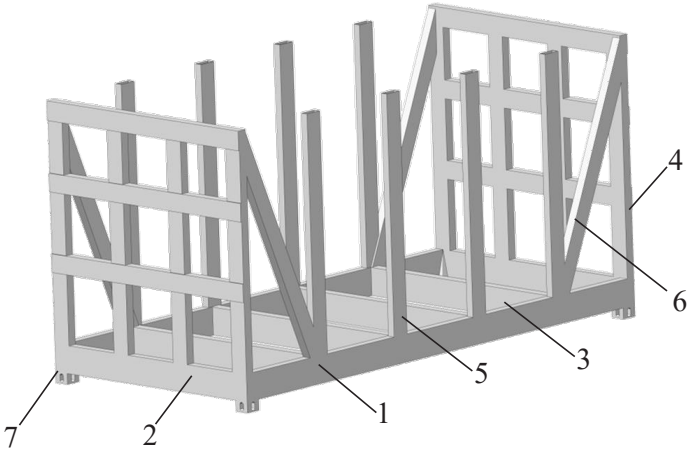

Figure 3.100 – The detachable module

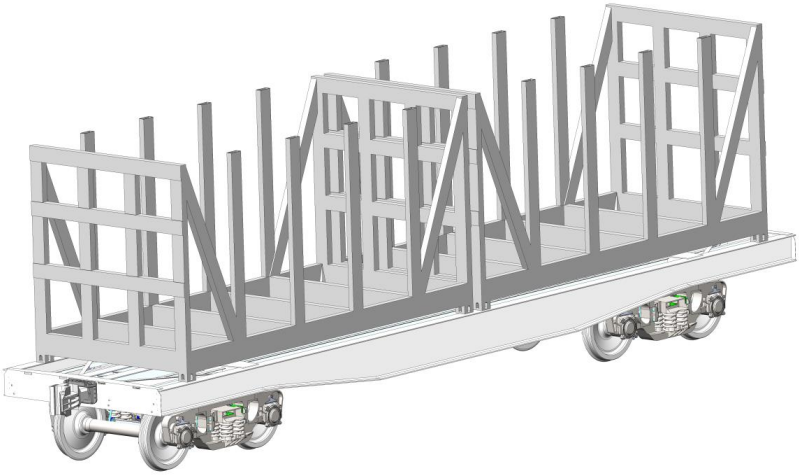

Figure 3.101 – The detachable modules on the flat wagons

The profiles of the detachable module were selected based on the moment of resistance at a known value of the maximum bending moments acting in its sections. In this case, the classical dependence of the resistance of materials was used:

$$W = \frac{M}{[\sigma]}, \tag{3.44}$$

where M is the bending moment; [σ] is the permissible stresses.

Thus, the detachable module was taken as a rod system on four supports (Fig. 3.102). The calculation was carried out in LIRA–CAD [1].

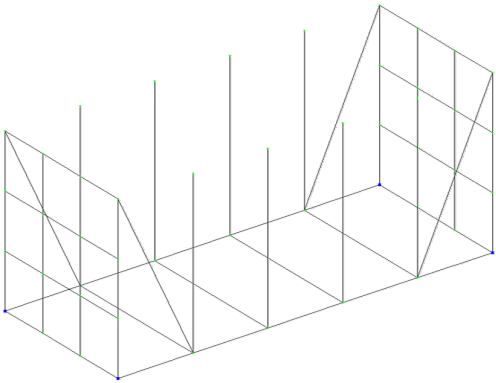

Figure 3.102 – The rod model of the detachable module

The geometric parameters of the detachable module were assumed to be identical to those of 1CC containers. The design diagram included the most unfavourable load modes for the detachable module, i.e., perception of longitudinal loads (mode I) and transverse loads (mode II). That is, the asymmetrical load of the detachable module under operating conditions was taken into account.

The design diagram of the detachable module for mode I included the most unfavourable load, i.e., the shunting collision of the flat wagon [69], when the longitudinal load P_l acted on the end support of the detachable module (Fig. 3.103). The vertical load P_v was applied to the cargo area of the detachable module, caused by its own weight, as well as the cargo in it. The load P_p was applied to the side poles caused by the cargo pressure. The forces P'_l were applied to the front fittings facing the engine.

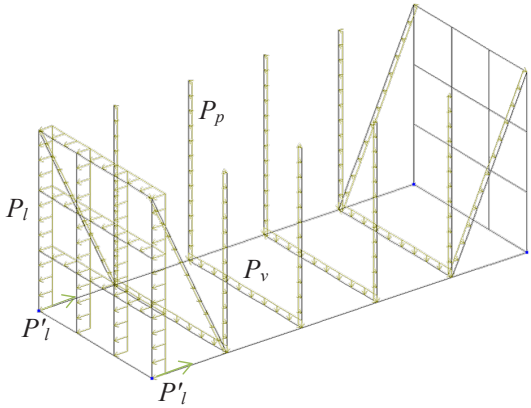

Figure 3.103 – The design diagram of a detachable module at mode I

The longitudinal load acting on the detachable module was determined by a mathematical modelling of its load. Mathematical model (3.103) was formed, which characterized the longitudinal load of the detachable module placed on the flat wagon. It was taken into account that a longitudinal force of 3.5 MN acted on the rear stop of the flat wagon [15]. The potential frictional forces between the horizontal surfaces of the fitting stops of the flat wagon and the fittings of the detachable module were also taken into account [69] (Fig. 3.104). The flat wagon model 13-401 on bogies 18-100 was used as a prototype. Although flat wagons are universal, they can be used as specialized ones, provided fitting stops are mounted in them.

The model included a rigid connection between the fitting stop and the fitting.

The mathematical model has the form:

$$\begin{cases} M_w \cdot \ddot{q}_1 = P_l - \sum_{i=1}^{n} \left(f_{fr} \cdot sign(\dot{q}_1 - \dot{q}_2) + C(q_1 - q_2) \right), \\ M_{dm} \cdot \ddot{q}_2 = \left(f_{fr} \cdot sign(\dot{q}_1 - \dot{q}_2) + C \cdot (q_1 - q_2) \right), \end{cases} \quad (3.45)$$

where M_w is the gross weight of the flat wagon; P_l is the longitudinal force acting on the automatic coupling; n is the number

of detachable modules placed on the flat wagon; f_{fr} is the friction force between fitting stops and fittings; M_{dm} is the weight of the detachable module; C is the stiffness of the connection between the fitting and the fitting stop; q_1, q_2 are the coordinates corresponding to the movement of the flat wagon and the detachable module, respectively, relative to the longitudinal axis.

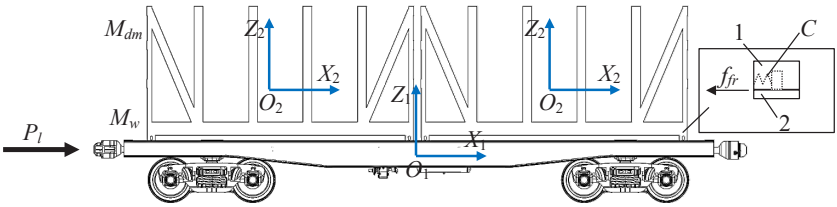

Figure 3.104 – The design diagram of the flat wagon with detachable modules:
1 – fitting; 2 – fitting stop

Mathematical model (3.108) was solved using the Runge-Kutta method implemented by MathCad under initial conditions close to zero.

Thus, the generalized acceleration acting on the detachable module was determined in the array $ddq_{j,i}$:

$$ddq_{j,1} = \frac{P_l - \sum_{i=1}^{n}\left(f_{fr} \cdot sign(y_3 - y_4) + C(y_1 - y_2)\right)}{M_w}, \quad (3.46)$$

$$ddq_{j,2} = \frac{\left(f_{fr} \cdot sign(y_3 - y_4) + C \cdot (y_1 - y_2)\right)}{M_{dm}}, \quad (3.47)$$

where $y_1 = q_1; y_2 = q_2; y_3 = \dot{q}_1; y_4 = \dot{q}_2$.

It was found that the acceleration acting on the detachable module was about 37 m/s^2 (Fig. 3.105).

This acceleration, as a component of the dynamic load, was taken into account when calculating the detachable module at mode I.

The results of the calculation in accordance with the diagram shown in Fig. 3.105 made it possible to obtain the distribution of internal factors in the detachable module components. Fig. 3.106 shows the bending moments (relative to the vertical axis) occurring in the detachable module. The blue colour indicates the negative moments, and the orange colour shows the positive ones.

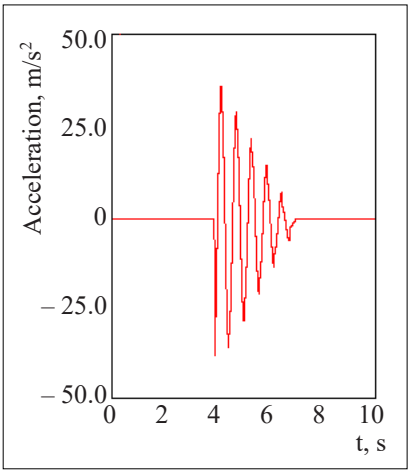

Figure 3.105 – The longitudinal accelerations acting on the detachable module

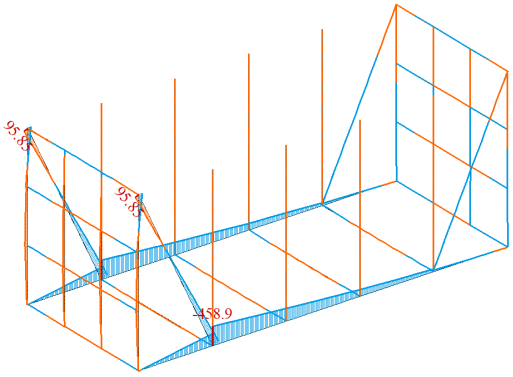

Figure 3.106 – The distribution of bending moments in the detachable module at mode I (kN · m)

Therefore, the maximum bending moments were observed in the zones of interaction of inclined belts with cross bearers and were 458.9 kN · m.

By using the options of the software in which the calculation was carried out, the diagram of displacements of the components of the detachable module in this design mode was also obtained (Fig. 3.107). Here, the largest displacements were for the end support located on the side of the longitudinal load.

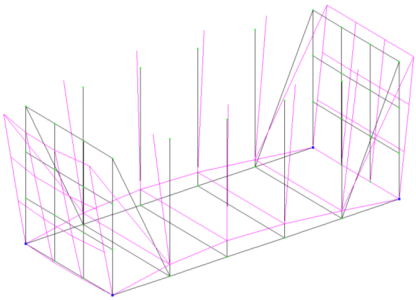

Figure 3.107 – The diagram of displacements of the detachable module components at design mode I (scale 50:1)

The subsequent stage of the study included the determination of the bending moments in the detachable module for mode II. The design diagram of the detachable module is shown in Fig. 3.108.

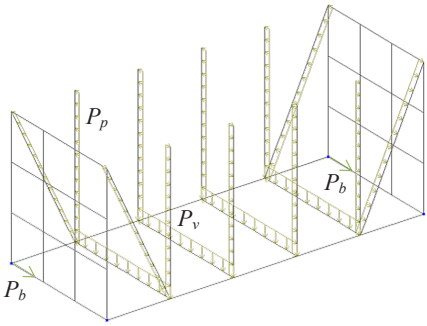

Figure 3.108 – The design diagram of a detachable module at mode II

It was taken into account that the vertical load P_v acted on the cargo area of the detachable module, and the load P_p was applied to the side poles. In that case, the load P_p, together with the pressure from the cargo, also included the load caused by the lateral inertia forces.

This load was determined by the formula from [69]:

$$P_p = \frac{(F' + W')}{L_p}, \tag{3.48}$$

where F' is the transverse load caused by the centrifugal force; W' is the wind load; L_p is the height of the pole.

The centrifugal force was determined according to the known formula [15]:

$$P_c = \frac{P_{gw} \cdot V^2}{g \cdot R}, \tag{3.49}$$

where P_{gw} is the gross weight of the detachable module; V is the speed of the flat wagon on which the detachable module is located; R is the curve radius.

Based on the calculations, the distribution of bending moments in the detachable module was obtained when it perceived the lateral loads. Fig. 3.109 shows the bending moments (relative to the vertical axis) arrising in the detachable module.

The maximum values of bending moments were in the areas of interaction of the side poles with cross bearers; they amounted to 10.91 kN · m.

The diagram of displacements of the detachable module components at design mode II is shown in Fig. 3.110.

Here, the maximum displacements were on the middle side poles on the side where the detachable module tilted.

According to the calculated bending moments, the profiles of the detachable module were selected. The most technologically rational profiles of the detachable module were taken into account – a channel and a rectangular pipe (Fig. 3.111) [69].

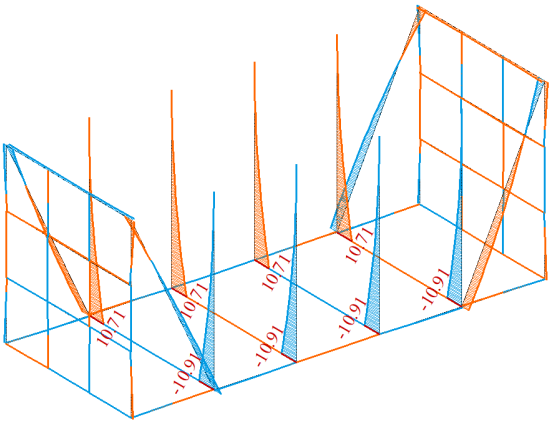

Figure 3.109 – The distribution of bending moments in the detachable module at mode II (kN · m)

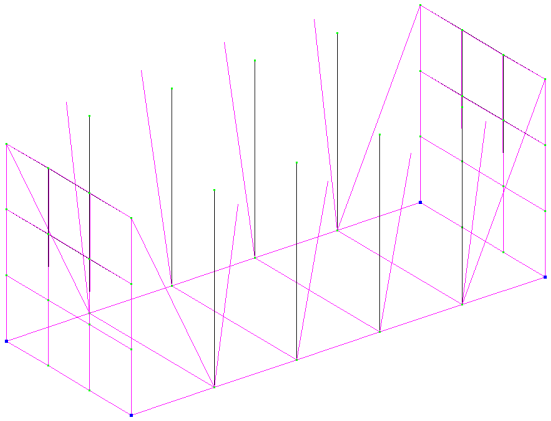

Figure 3.110 – The diagram of displacements of the detachable module components at design mode II (scale 50:1)

For example, for a cargo area with a calculated moment of resistance $W = 277.8$ cm^3, it is rational to use these profiles with the parameters given in Table 3.3.

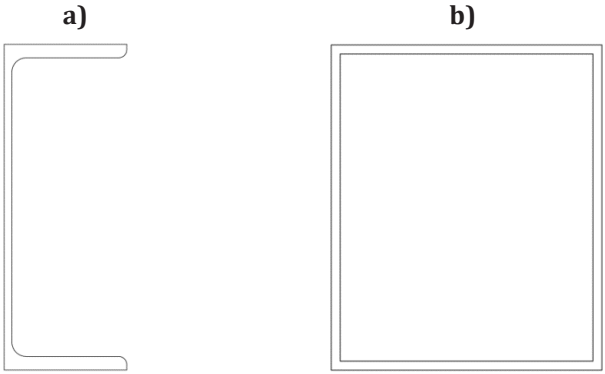

Figure 3.111 – The profile options for the detachable module:
a) channel; b) rectangular pipe

Table 3.3 – The main parameters of the cargo area profiles of the detachable module

Profile	Moment of resistance, cm^3	Mass of 1 m, kg
Channel No. 27	310.0	27.7
Rectangular pipe 180 × 150	286.98	45.97

Therefore, the channel profile is the most appropriate for the detachable module. Importantly, this profile is also one of the most common profiles used for modular vehicles.

The resistance moment of the cross-section could be increased by using an additional vertical sheet (Fig. 3.112). This solution was substantiated by the fact that vehicles, in particular, rail vehicles, must have a structural safety margin. The minimum safety factor according to [15] must be 1.3. Therefore, to ensure an appropriate safety margin, it was necessary to use a 4-mm-thick sheet. Here, the moment of resistance of the cross-section was 360 cm^3 with a mass of 1m 35.6 kg.

The parameters of the profiles of the end superstructures and vertical poles were selected by the same way; that was channel No.20, reinforced with a 3.5-mm thick sheet.

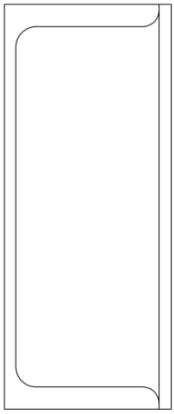

Figure 3.112 – The channel bar covered with a vertical sheet

By taking into account the selected profile of the frame of the detachable module, its spatial model was built and the strength calculation was carried out in SolidWorks Simulation. The finite element model (Fig. 3.113) was built with spatial tetrahedra, the number of which was calculated graphically and analytically.

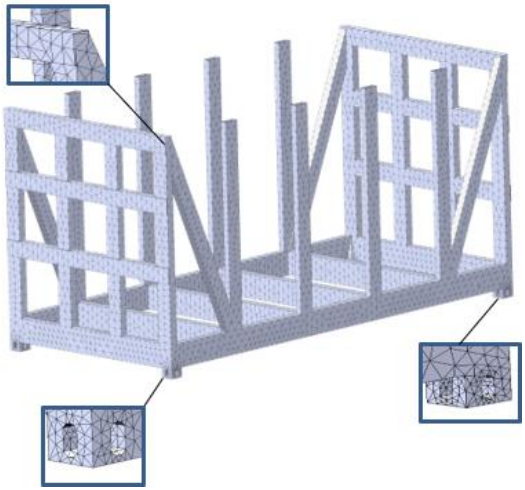

Figure 3.113 – The finite element model of the detachable module

Thus, the model had 150.474 elements with a maximum size of 100 mm and a minimum size of 20 mm, as well as 55.221 nodes. The mesh was automatically compacted in the zones of rounding and jointing of the individual elements.

The design diagrams of the detachable module are shown in Fig. 3.119. The forces are marked the same way as those shown in Figs 3.108 and 3.113, respectively.

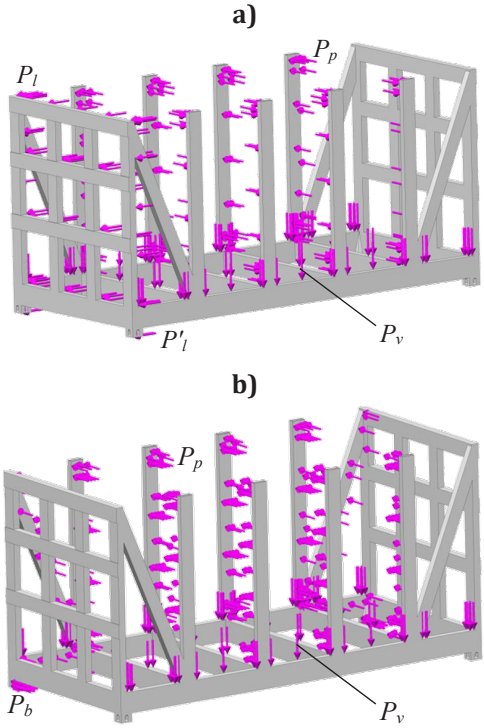

Figure 3.114 – The design diagrams of the detachable module: a) mode I; b) mode II

The fitting stops of the detachable module had connections simulated its interaction with the fitting stops of the flat wagon. The construction material of the detachable module was low-alloy Steel 09G2S, as the most common for manufacturing transport means [15].

The results of the calculation of the detachable module are shown in Figs. 3.120 and 3.121. The analysis of the obtained results shows that the maximum stresses in the detachable module at mode I occurred in the cross bearers, where they interacted with the fittings and were 286.5 MPa (Fig. 3.115, a). The resulting stresses were lower than permissible by 7.7 %. The stresses equal to 310.5 MPa were taken as permissible [15].

At mode II, the maximum stresses were in the main longitudinal beam on the side at which the detachable module tilted and amounted to 292.4 MPa (Fig. 3.115, b). These stresses were concentrated in the areas of interaction of the main longitudinal beam with the fitting stops. These stresses did not exceed the permissible ones and were 5.8 % lower.

The maximum displacements in the detachable module in mode I were in the upper belt of the end superstructure and amounted to 4.1 mm (Fig. 3.116, a). This distribution of displacement fields can be explained the interaction of the superstructure on all sides with the components of the detachable module, while its upper part is free.

At mode II, the maximum displacements were recorded in the central poles on the tilted side of the detachable module. These displacements were 6.2 mm (Fig. 3.116, b). They were explained by the fixation of the vertical pole from below, while its upper end was free.

The obtained displacement fields were consistent with the diagrams shown in Figs. 3.103 and 3.108.

The safe operation of the detachable module was verified using its modal analysis by means of the built-in options of SolidWorks Simulation. The results of the calculation made it possible to determine the frequencies and shapes of the natural oscillations of the detachable module (Fig. 3.117).

In Fig. 3.117, the transparent colour shows the static shape of the detachable module, and the matte colour shows its deformations. For better visualization, the scale of deformations was increased by 15 times.

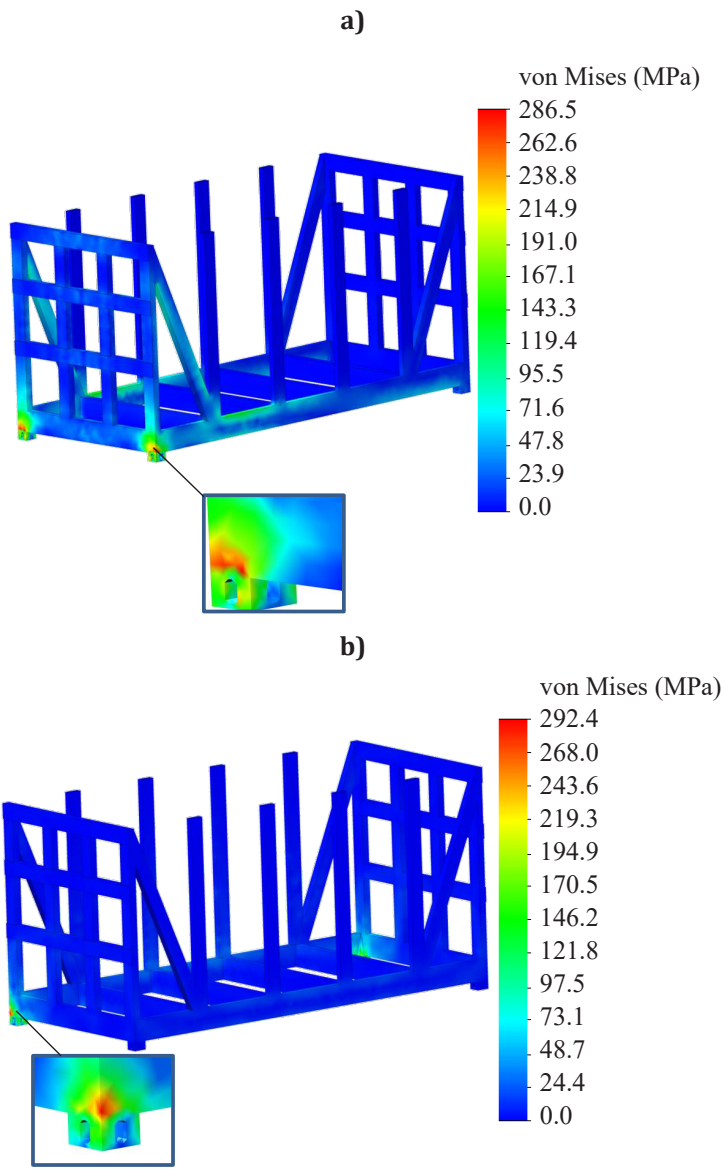

Figure 3.115 – The stress state of the detachable module:
a) mode I; b) mode II

a)

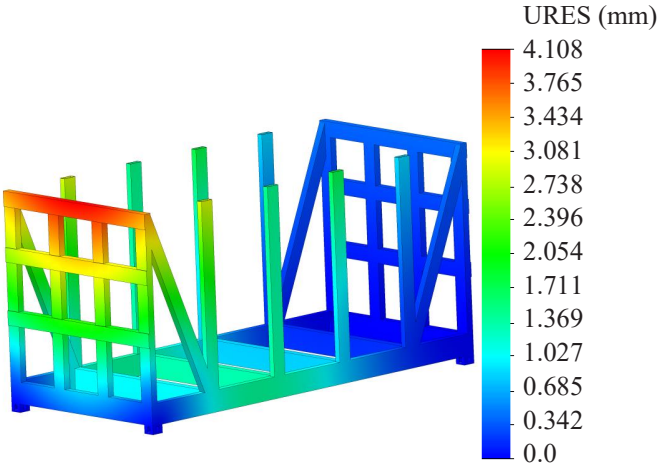

b)

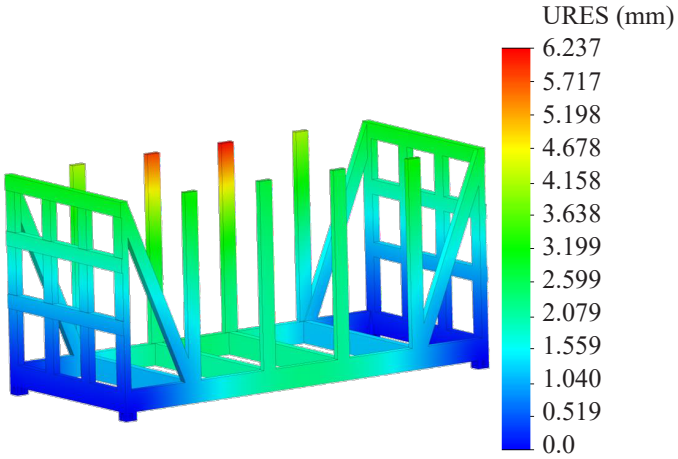

Figure 3.116 – The displacements in the detachable module units:
a) mode I; b) mode II

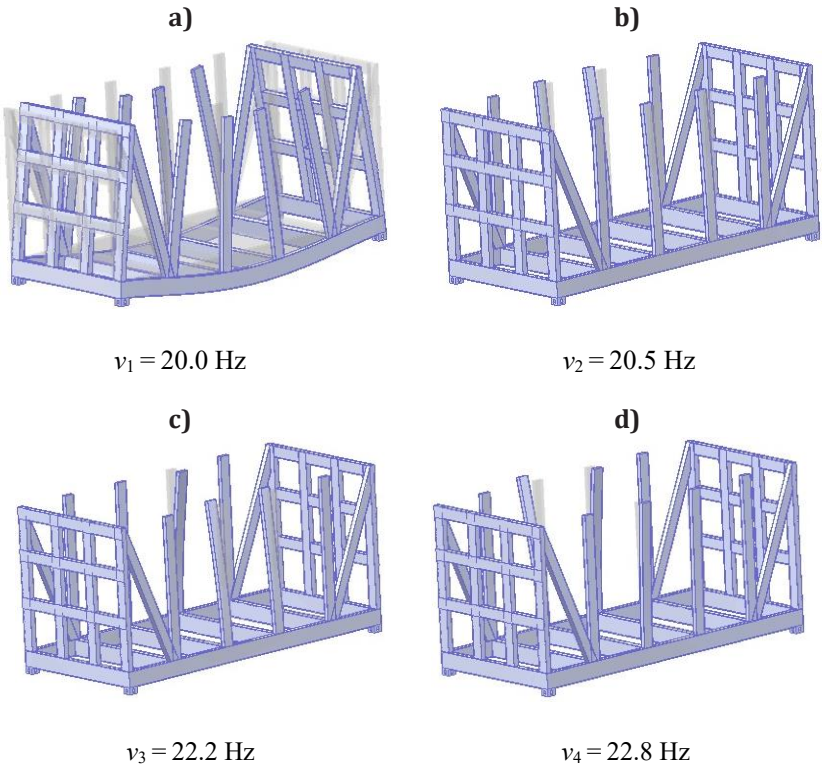

Figure 3.117 – The results of modal analysis of the detachable module (scale 15:1):
a) mode I; b) mode II; c) mode III; d) mode IV

The traffic safety was assessed by the first oscillation frequency, which, in accordance with [15], must have a value of at least 8 Hz. Therefore, it can be concluded that traffic safety in terms of modal analysis was ensured.

The peculiarities of the vertical dynamics of the flat wagon with detachable modules are highlighted in [40]. There can be some variations of detachable module designs, including FLAT RACK by type [3–5, 48–50, 61].

3.8 Load of the improved tank container transported by rail

The tank containers are used to increase the efficiency of bulk cargo transportation [82]. Currently, a large number of tank containers are in operation, varying in design features and processing technology. They can be transported by different vehicles at various load diagrams. The analysis of existing regulatory documents on the design and calculation of tank containers showed that their most unfavourable load mode is the shunting collision when transported by rail. The longitudinal forces caused by the inertia forces act on the tank container, as well as reactive forces in the areas of interaction of fittings with fitting stops. With the exceeding dynamic forces acting on the tank container over the vertical component of the gross weight, it moved in the longitudinal plane and the fittings bump into the fitting stops. Thus, they can be damaged, which will require unscheduled repairs of the vehicles. If such a tank container is part of the train, it can be quite destructive for the environment. Therefore, the issues of improving the design of tank containers to improve their strength in operation are quite relevant.

In order to improve the tank container, the strength of its load-bearing structure was calculated in order to identify the most loaded components [81, 82].

The TK25 tank container was chosen as a prototype. The spatial model was built in SolidWorks (Fig. 3.118).

The strength was calculated using the finite element method of the tank container in SolidWorks Simulation (Fig. 3.119). The optimal number of tetrahedra was calculated graphically and analytically. The model had 170.406 elements with a maximum size of 120 mm and a minimum size of 24 mm. The number of nodes was 56.409.

The design diagram included the following loads to the tank container (Fig. 3.120):

– vertical static load P_v;

– horizontal force acting on the tank bottom P_h;

– pressure from the bulk cargo to the tank P_p;

– reactions in fitting stops P_f to the action of horizontal loads that the tank container perceived.

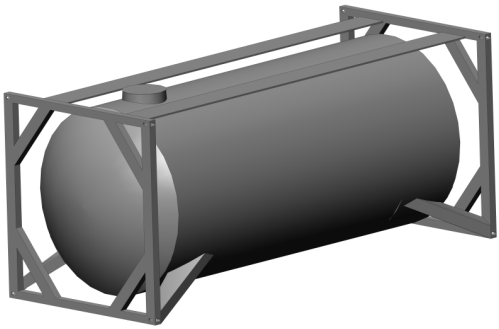

Figure 3.118 – The spatial model of the tank container

These loads are specified in the regulatory document DSTU ISO 1496-3:2013, which is a translation of the English ISO 1496-3:1995 + ISO 1496-3:1995/Amd 1:2006 Series 1 freight containers – Specification and testing – Part 3: Tank containers for liquids, gases and pressurized dry bulk.

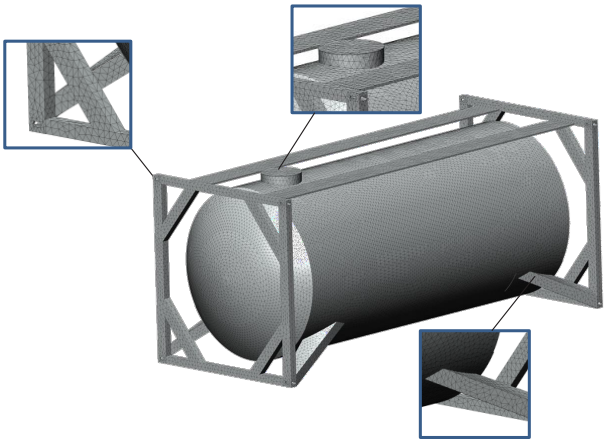

Figure 3.119 – The finite-element model of the tank container

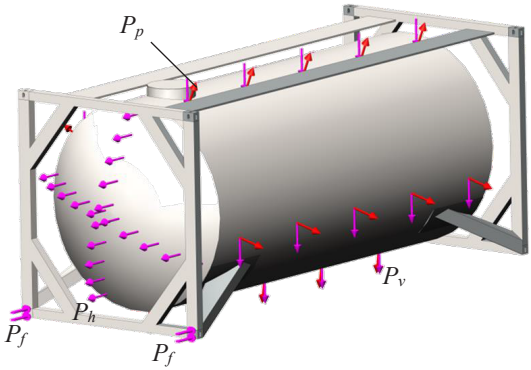

Figure 3.120 – The design diagram of the tank container

The dynamic load acting on the tank container was determined with mathematical modelling of its longitudinal load using the mathematical model built by the Institute of Technical Mechanics [2]. It was taken into account that the tank container was placed on the flat wagon model 13-401. The design diagram is shown in Fig. 3.121.

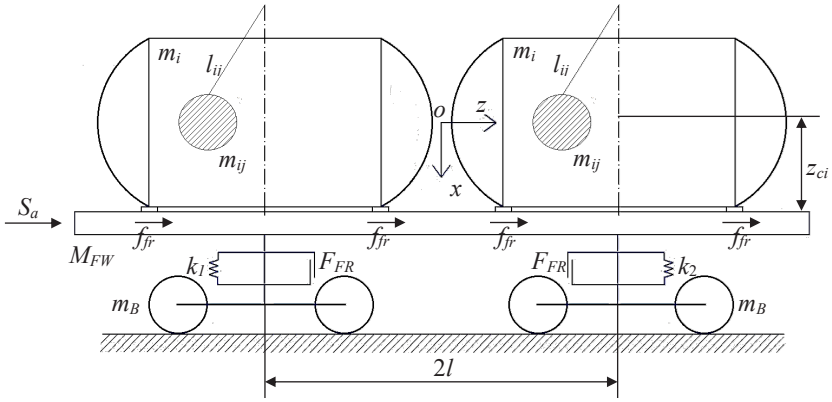

Figure 3.121 – The design diagram of the flat wagon loaded with tank containers

The vertical displacements of the tank container relative to the flat wagon frame were neglected. The flexibility of the bulk cargo relative to the tank walls was also included. The movement of bulk cargo was described by a set of mathematical pendulums. The longitudinal impact force acting on the flat wagon was assumed to be 3.5 MN.

The tank container was considered as an attached mass relative to the flat wagon frame with longitudinal flexibility due to gaps between fitting stops and fittings [82]. It was also taken into account that the tank containers were placed on the flat wagon, had the same amount of liquid cargo in the tank.

$$\left(M_{FW}+2\cdot m_B+\frac{n\cdot I}{r^2}\right)\cdot\ddot{x}_{FW}+M_{FW}\cdot h\cdot\ddot{\varphi}_{FW}= \\ =S_a-\sum_{i=1}^{2}\left(f_{fr}\cdot sign\cdot\left(x_{FW}-x_i\right)'\right), \tag{3.50}$$

$$I_{FW}\cdot\ddot{\varphi}_{FW}+M_{FW}\cdot h\cdot\ddot{x}_{FW}-g\cdot\varphi_{FW}\cdot M_{FW}\cdot h= \\ =l\cdot F_{FW}\left(sign\dot{\Delta}_1-sign\dot{\Delta}_2\right)+l\left(k_1\cdot\Delta_1-k_2\cdot\dot{\Delta}_2\right), \tag{3.51}$$

$$M_{FW}\cdot\ddot{z}_{FW}=k_1\cdot\Delta_1+k_2\cdot\Delta_2-F_{FR}\left(sign\dot{\Delta}_1-sign\dot{\Delta}_2\right), \tag{3.52}$$

$$\left(m_i+\sum_{j=1}^{k}m_{ij}\right)\cdot\ddot{x}_i+\left(m_i\cdot z_{ci}+\sum_{j=1}^{k}m_{ij}\cdot c_{ij}\right)\cdot\ddot{\varphi}_i-\sum_{j=1}^{k}m_{ij}\cdot l_{ij}\cdot\ddot{\xi}_{ij}= \\ =\left(f_{fr}\cdot sign\cdot\left(x_{FW}-x_i\right)'\right), \tag{3.53}$$

$$\left(I_{\theta i}+\sum_{j=1}^{k}m_{ij}\cdot c_{ij}^2\right)\cdot\ddot{\varphi}_i+\left(m_i\cdot z_{ci}+\sum_{j=1}^{k}m_{ij}\cdot c_{ij}\right)\cdot\ddot{x}_i+ \\ +\sum_{j=1}^{k}m_{ij}\cdot c_{ij}\cdot l_{ij}\cdot\ddot{\xi}_{ij}-g\cdot\left(m_i\cdot z_{ci}+\sum_{j=1}^{k}m_{ij}\cdot c_{ij}\right)\cdot\left(\varphi_{FW}-\varphi_i\right)=0, \tag{3.54}$$

$$\left(m_i+\sum_{j=1}^{k}m_{ij}\right)\cdot\ddot{z}_{FW}=0, \tag{3.55}$$

$$I_{ij} \cdot \ddot{\xi}_{ij} - m_{ij} \cdot l_{ij} \cdot \ddot{x}_{ij} - m_{ij} \cdot c_{ij} \cdot l_{ij} \cdot \ddot{\varphi}_i + g \cdot m_{ij} \cdot l_{ij} \cdot \ddot{\xi}_{ij} = 0 \qquad (3.56)$$

where

$$\Delta_1 = z_{FW} - l \cdot \varphi_{FW} \; ; \; \Delta_2 = z_{FW} + l \cdot \varphi_{FW} ;$$

M_{FW} is the mass of the load-bearing structure of the flat wagon; I_{FW} is the moment of inertia of the flat wagon relative to the longitudinal axis; f_{fr} is the amplitude value of the dry friction force; m_B is the bogie weight; I is the moment of inertia of a wheelset; r is the radius of a wheel with average wear; n is number of axles in the bogie; l is the half base of the flat wagon; F_{FR} is the absolute value of dry friction force in the spring group; k_1, k_2 are the stiffness of springs in the suspension of the flat wagon bogies; k is the number of tones of the bulk cargo fluctuations; m_i is the mass that is equivalent to the i-th tank container with a portion of the liquid cargo that does not move relative to the tank; m_{ij} is the mass of the j-th pendulum in the i-th tank container; z_{ci} is the height of the centre of gravity of the tank container; c_{ij} is the distance from the plane $z_i = 0$ to the fixation point of the j-th pendulum in the i-th tank container; l_{ij} is the length of the j-th pendulum; I_θ is the reduced moment of inertia of the i-th tank container and the bulk cargo that does not move relative to the tank; I_{ij} is the moment of inertia of the pendulum; x_{FW}, φ_{FW}, z_{FW} are the coordinates corresponding to the longitudinal, angular around the longitudinal axis, and vertical displacements of the flat wagon, respectively; x_i, φ_i are the coordinates corresponding to the longitudinal and angular displacements of the tank container around the longitudinal axis, respectively; ξ_{ij} is the angle of deviation of the j-th pendulum from the vertical.

The differential equations of motion were solved using the Runge-Kutta method in MathCad. The initial conditions were set to zero.

The results demonstrated that without gaps between fitting stops and fittings, the acceleration acting on the tank container was about 40 m/s^2. The maximum accelerations occurred when the gap between fitting stop and fitting was 30 mm. In this case, the acceleration was about 300 m/s^2.

This acceleration value was taken into account when calculating the strength of the tank container. The model was secured by the fittings. The construction material was Steel 09G2S [15]. The permissible stresses acting in the tank container were assumed to be equal to 310.5 MPa. Based on the calculations, the main strength indicators of the tank container were obtained (Figs. 3.122 and 3.123).

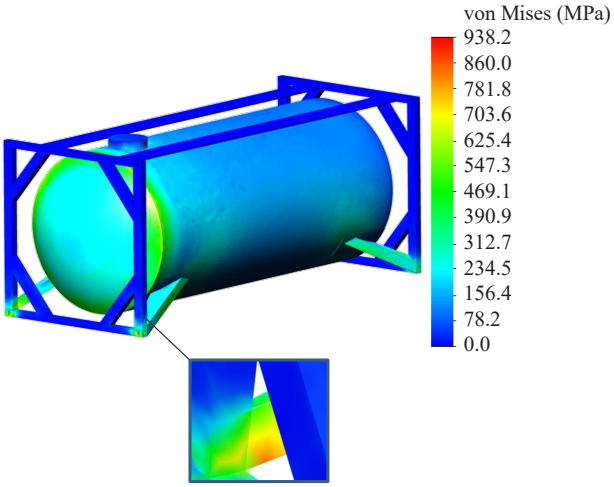

Figure 3.122 – The stress state of the tank container

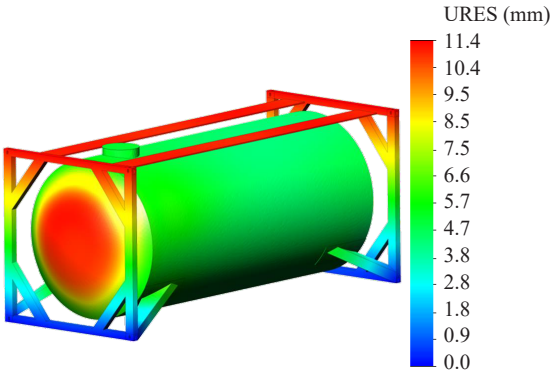

Figure 3.123 – The displacements in the tank container units

Thus, the maximum stresses occurred in the zone of interaction of the support with the vertical pole; they were 938.2 MPa (Fig. 3.122). The resulting stresses were higher than permissible. The maximum displacements were in the middle part of the tank bottom and were 11.4 mm (Fig. 3.123). This distribution of displacement fields can be explained by both the loads applied to the tank and its fastening.

In order to ensure the strength of the tank container, it was proposed to improve its frame by introducing reinforcing elements into the structure (Fig. 3.124).

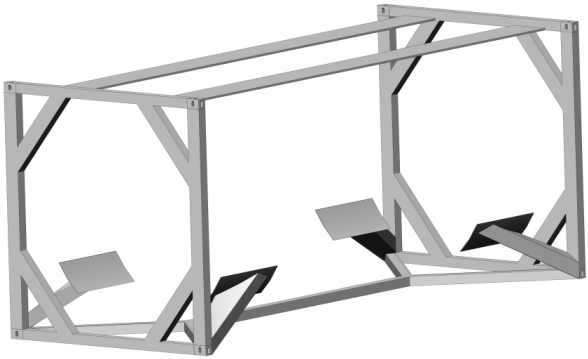

Figure 3.124 – The tank container frame

The reinforcing element was made in the form of a fork, the end parts of which (braces) were placed at the angle $\alpha = 45°$ to the horizontal (Fig. 3.125). The units of interaction of the braces with each other on the left and right sides of the tank container were connected by a longitudinal belt made of the same profile as the frame belts.

The spatial model of the tank container is shown in Fig. 3.126.

The improvements were substantiated by means of the strength calculation of the tank container and its modal analysis.

The finite-element model was built with tetrahedra, the number of which was 182.213, and nodes, the number of which was 60.189 (Fig. 3.127). The maximum element size was 120 mm, and the minimum element size was 24 mm.

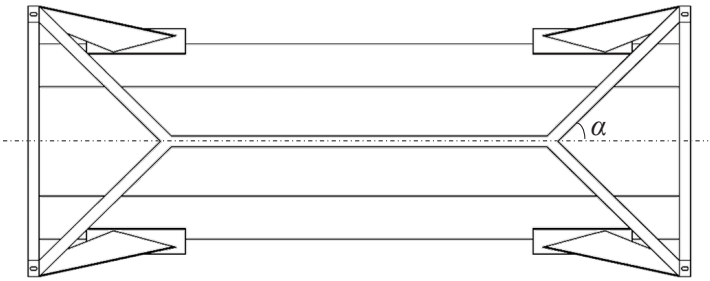

Figure 3.125 – The tank container frame (bottom view)

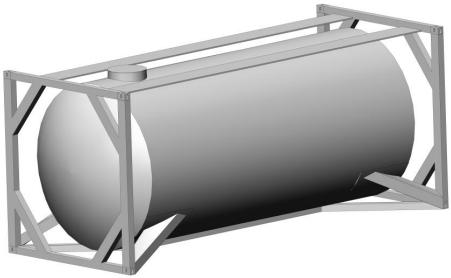

Figure 3.126 – The spatial model of the improved tank container

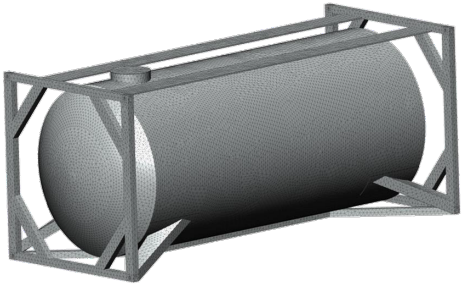

Figure 3.127 – The finite element model of the improved tank container

The design diagram of the tank container, its fastening diagram and the construction material were identical to those taken for the calculation of the typical tank container. The calculation results

are shown in Figs. 3.128 and 3.129. The maximum stresses were recorded in the manhole area – 215 MPa (Fig. 3.128), which was lower than permissible.

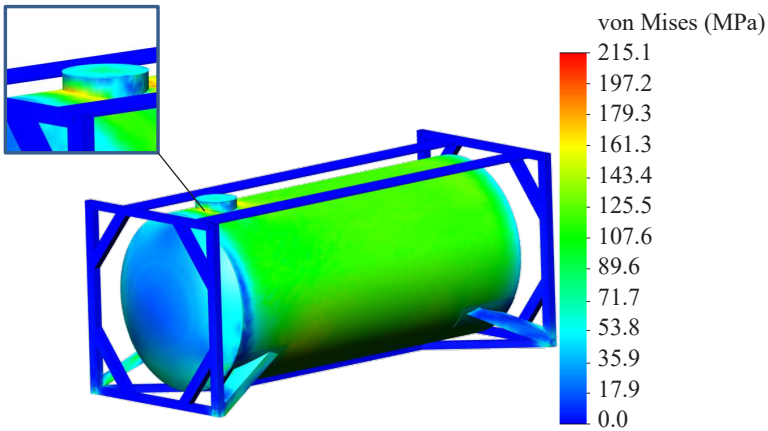

Figure 3.128 – The stress state of the improved tank container

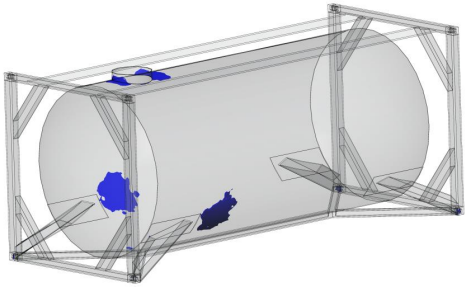

Figure 3.129 – The most loaded areas of the tank container

The maximum displacements occurred at the tank bottom and were 2.6 mm (Fig. 3.130). They were located closer to the end part of the tank on the side of the longitudinal force to the flat wagon (Fig. 3.131). The displacements were recorded along the horizontal axis running through the tank bottom.

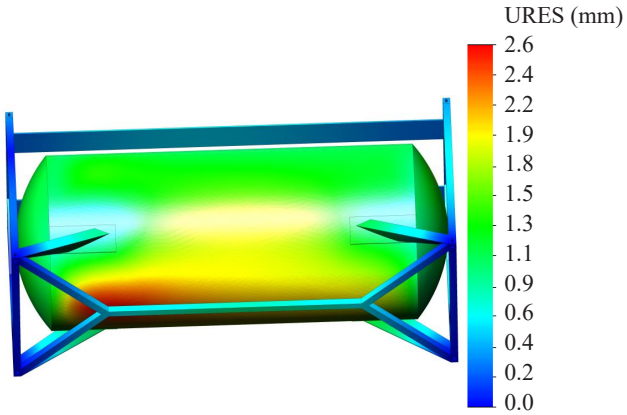

Figure 3.130 – The displacements in the units of the improved tank container

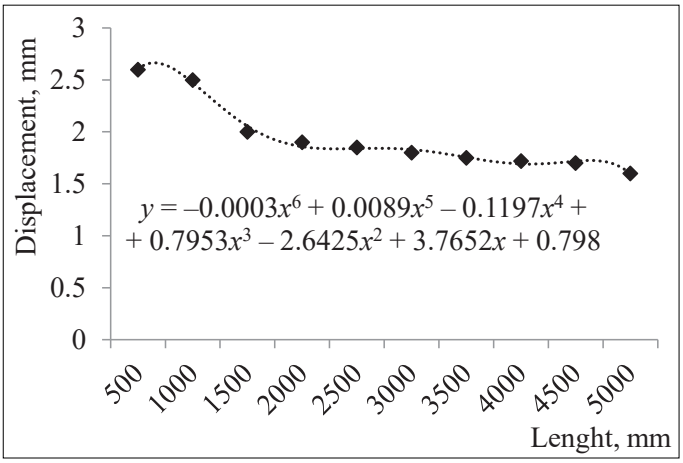

Figure 3.131 – The distribution of displacements along the tank length

The safety of tank container during transportation was determined using the modal analysis of its structure and the design diagram shown in Fig. 3.120. Based on this analysis, the frequencies and shapes of the natural oscillations of the tank container were obtained (Fig. 3.132).

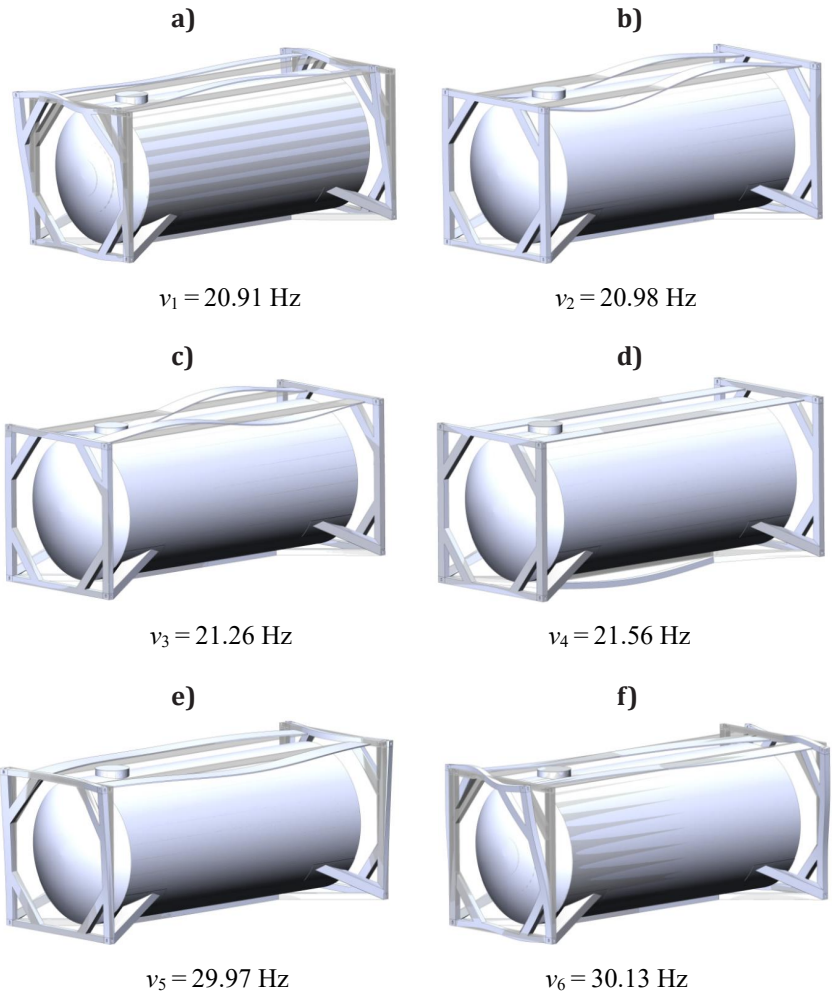

Figure 3.132 – The shapes and frequencies of tank container oscillations (in magnification scale 15:1):
a) mode I; b) mode II; c) mode III; d) mode IV;
e) mode V; f) mode VI

The safety of transportation of the tank container was assessed by the first natural frequency of oscillations; it amounted to 20.91 Hz (Fig. 3.137, a). Thus, the safety of transportation in terms of the modal analysis was observed, since this frequency was higher than permissible.

3.9 Load of the container for grain under operating modes

The 1CC container was chosen as a prototype for improvements [44, 85]. The spatial model of the container is shown in Fig. 3.133.

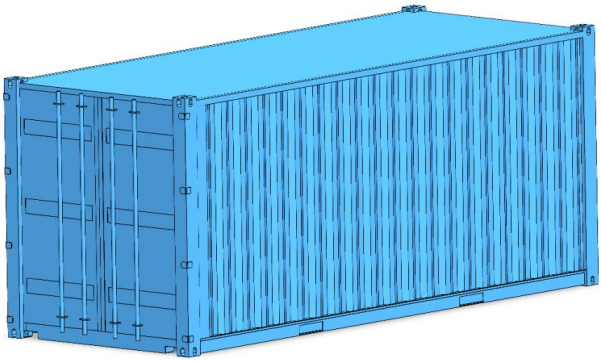

Figure 3.133 – The spatial model of the 1CC container

This container is loaded through the end doors, which form the end wall when closed. The container can be loaded/unloaded using mechanized machinery.

It was proposed to install three loading hatches of standard diameter on the roof so that to adapt this container to the transportation of grain. The discharge door can be installed in the end wall at a height of 1/3 from the bottom rail (Fig. 3.134).

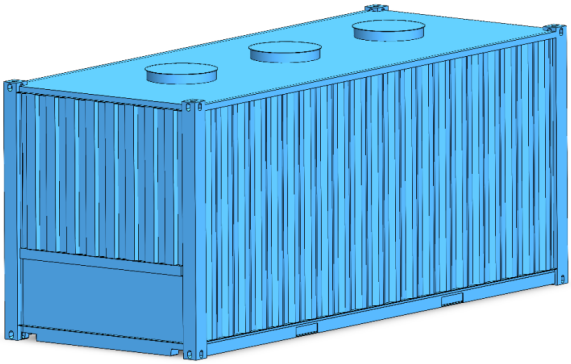

Figure 3.134 – The spatial model of the container

The proposed improvement was substantiated by calculating the strength of the container at the main load modes:

– transportation of the container as part of a rail train;
– lifting it by upper corner fittings; and
– unloading the container.

The strength of the container transported by rail was determined when it was transported as part of a rail train during a jerk. This mode included the longitudinal force of 2.5 MN on the front stops of the automatic coupling [15].

The calculation was done using the finite element method in SolidWorks Simulation. The design diagram of the container is shown in Fig. 3.135. It was taken into account that the container perceived the vertical load P_v, which included its load capacity. The own weight of the container was also included by means of the options of SolidWorks Simulation, provided that the structure was made of Steel 09G2S. The pressure force P_p was applied to the sidewalls of the container, and the force P_w was applied to the end walls. The inertia forces P_f were applied to the container fittings facing the engine of the flat wagon.

The active (static) pressure of the bulk cargo on the walls of the container was determined with the technique given in [15].

The inertia forces P_f acting on the fitting stops were determined with mathematical modelling of the longitudinal dynamics of the

flat wagon loaded with two containers in accordance with [45]. The results of the calculation show that the acceleration acting on the containers was about 27 m/s^2.

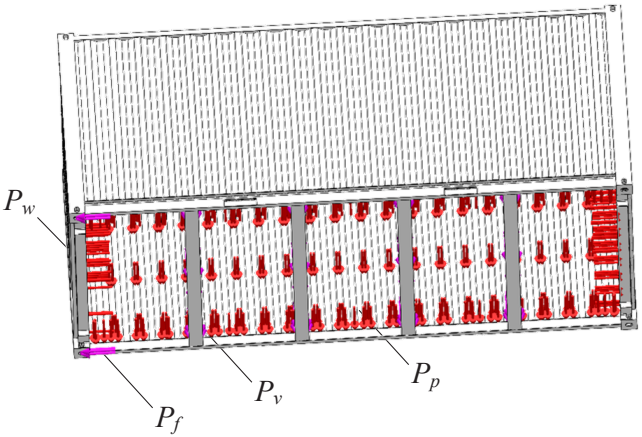

Figure 3.135 – The design diagram of the container

This acceleration was taken into account when calculating the strength of the container, namely, when taking into account the forces P_f and P_w in the calculation model shown in Fig. 3.135.

The load of the container when it moved as part of the train was determined using its finite element model. The model was built with tetrahedra. The mesh was formed on the basis of mixed curvature and had 1,027,293 elements and 1,838,877 nodes. The maximum element size was 60 mm, and the minimum was 3 mm. The number of Jacobian points for the high-quality mesh was 16.

The container was secured by the fittings. The results of its strength calculation when transported as part of a train are shown in Figs. 3.136 and 3.137. The maximum stresses were in the middle part of the horizontal beam for fastening the discharging door and were 121.4 MPa (Fig. 3.141). These stresses were lower than permissible, which for the specified mode were taken equal to 210 MPa. The maximum displacements were recorded in the sidewall and were 1.8 mm (Fig. 3.137).

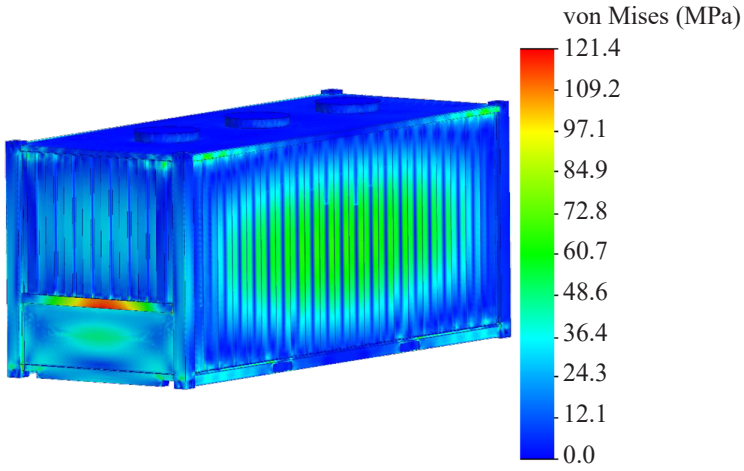

Figure 3.136 – The stress state of the container transported as part of a train

Thus, the strength of the container at a given load mode was observed.

The subsequent stage included the determination of the strength of the container lifted by the upper corner fittings. The design diagram of the container is shown in Fig. 3.135. It was taken into account that the container was lifted with slings placed at an angle of 45° to the horizontal. Therefore, the load transferred from the slings to the container was decomposed into vertical P_v and horizontal P_h. The design diagram included also the vertical load and the pressure of the bulk cargo on the container walls (not shown in Fig. 3.138). The calculation results are shown in Figs. 3.139 and 3.140.

Thus, when the container was lifted by the upper corner fittings, the maximum stresses occurred in the areas of interaction of the corner posts with the cross bearers; they were 108.6 MPa (Fig. 3.139). These stresses did not exceed permissible.

The maximum displacements were recorded in the sidewalls; they amounted to 1.6 mm, therefore, when the load was applied, the strength of the container was observed.

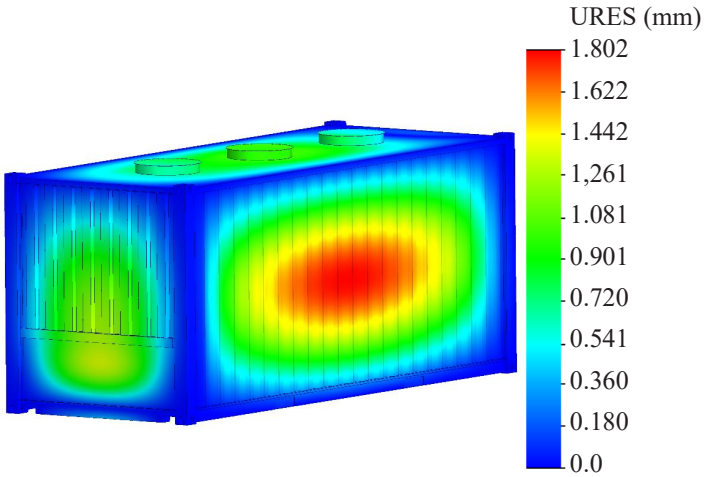

Figure 3.137 – The displacements in the units of the container transported as part of a train

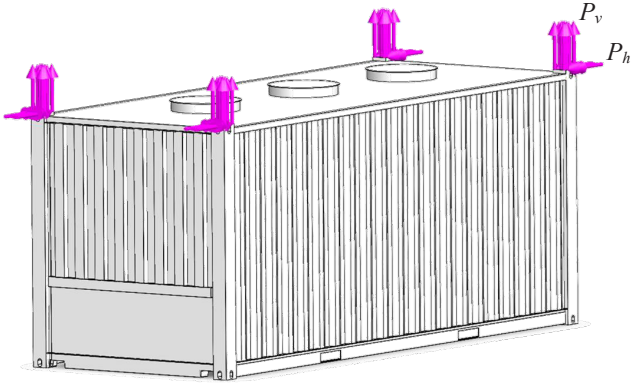

Figure 3.138 – The design diagram of the container lifted by the upper corner fittings

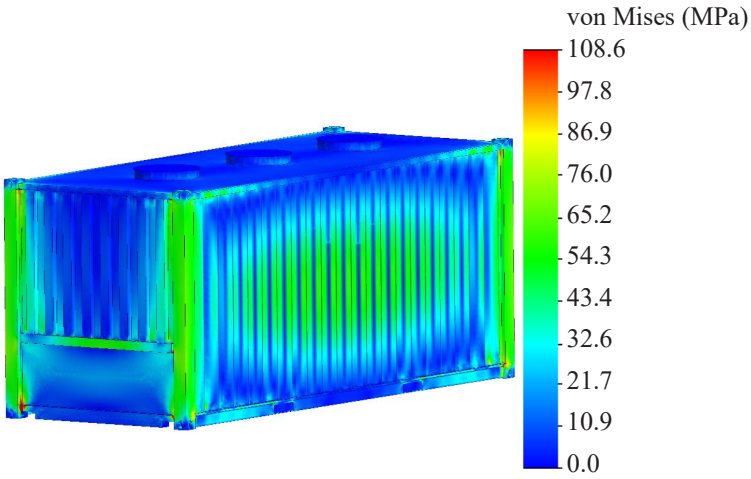

Figure 3.139 – The stress state of the container lifted by the upper corner fittings

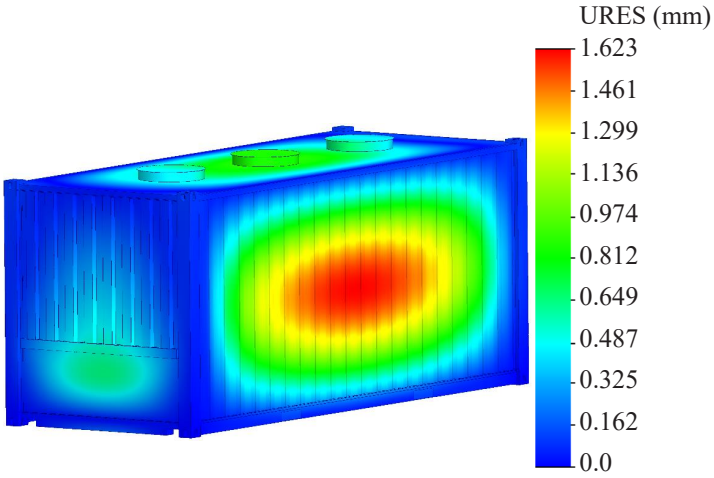

Figure 3.140 – The displacements in the units of the container lifted by the upper corner fittings

The load of the container during its unloading by weight was also studied (Fig. 3.141).

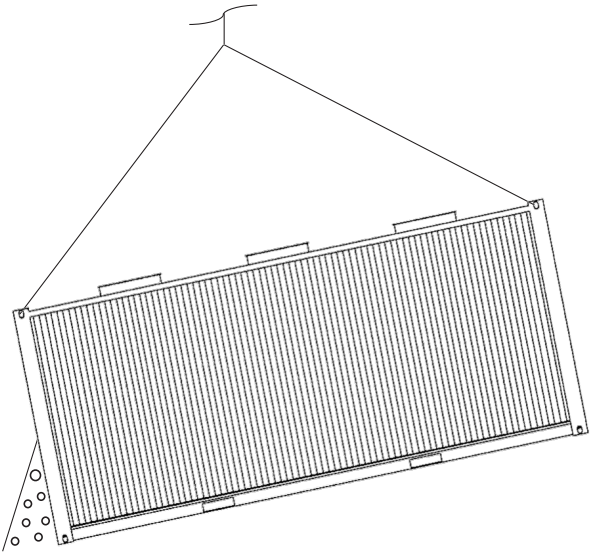

Figure 3.141 – The container unloading diagram

The strength of the container was calculated at the angle of its inclination to the horizontal $\alpha = 45°$. It was taken into account that the container was tilted to a specified angle, and after that its unloading began.

The design diagram of the container is shown in Fig. 3.142. The loads are marked similar to the marking in the diagram shown in Figs. 3.135 and 3.138.

The results of the calculation are shown in Figs. 3.143 and 3.144.

The maximum stresses occurred in the horizontal beam for fastening the discharge door and were 187.4 MPa (Fig. 3.143), which was lower than permissible. The maximum displacements were also recorded in the horizontal beam – 2.2 mm. Thus, the strength of the container was observed.

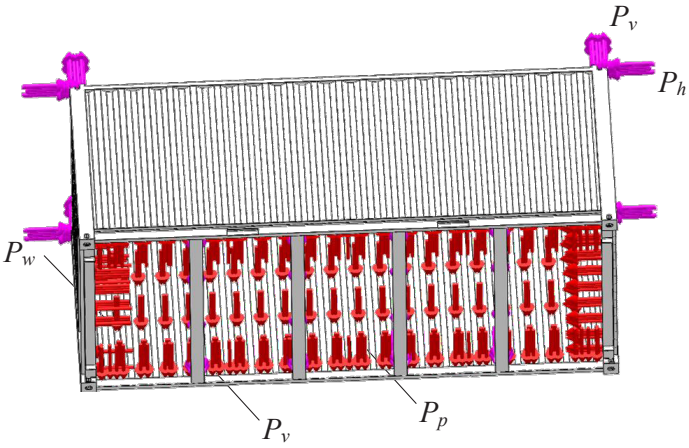

Figure 3.142 – The design diagram of the container during its unloading

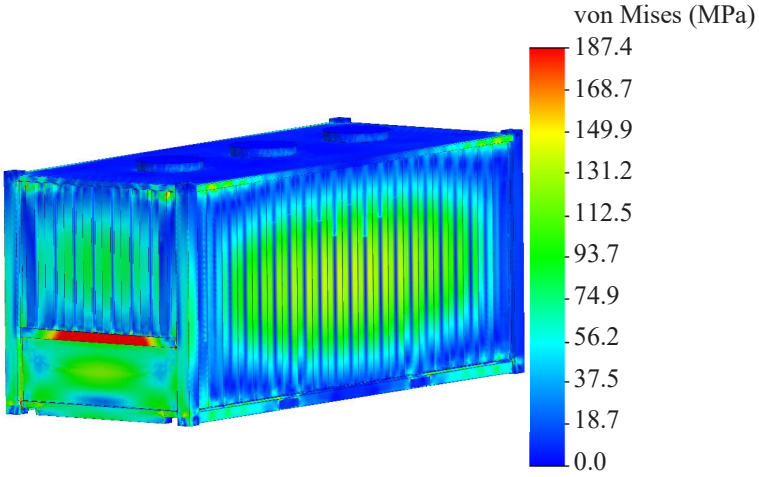

Figure 3.143 – The stress state of the container during its unloading

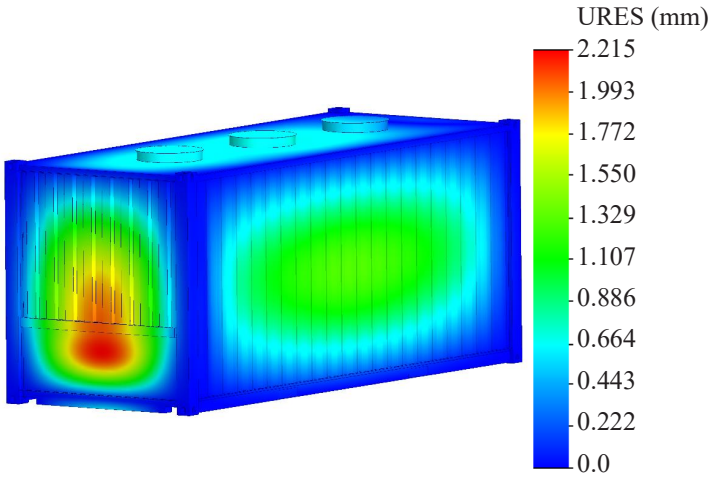

Figure 3.144 – The displacements in the units of the container during its unloading

Conclusions to Section 3

1. The force factors that take place in the structure of the container frame during operational loading modes are determined. At the same time, two schemes are taken into account: the effect of a vertical loading on the frame of the container when it is lifted by the upper corner fittings (I loading mode); the effect of longitudinal loading on the frame during transportation by rail transport (II loading mode). It was found that the maximum value of the longitudinal force in the I mode occurs in vertical struts and equals 31.6 kN. The maximum value of the lateral force is recorded in the intermediate vertical struts and equals 19.6 kN. The maximum value of the bending moment also occurs in the intermediate vertical struts and is equal to 13.6 kN · m.

To determine the longitudinal force acting on the frame of the container, mathematical modeling of its dynamic loading when

placed on a flat wagon was carried out. It was established that the longitudinal acceleration acting on the container is about 20 m/s^2. In view of this, the calculation of the container frame in the II mode was carried out. The maximum value of the longitudinal force occurs in the bottom part of the frame and equals 100 kN. The maximum value of the lateral force was recorded in the longitudinal beams and amounted to 21.1 kN. The maximum bending moment occurs in the bottom part of the frame and is equal to 11.5 kN · m.

The profile of the container frame execution was selected – a square pipe with parameters: H = B = 120 mm, S = 4 mm, W = 67.05 cm^3. Here, the mass of the container frame was about 500 kg. The strength of the container frame was calculated. The calculation results showed that the maximum stresses occur in the lateral beam and amount to 197.6 MPa. The maximum displacements occur in the middle part of the longitudinal beam and amount to 1.8 mm. Therefore, the strength of the container frame under the considered operational loadings is ensured..

The strength of the container was calculated taking into account the determined parameters of the panelling corrugations. It was also found that the maximum stresses under the most unfavourable load mode (shunting collision) occurred in the container fittings and were equal to 287 MPa. The resulting stresses were lower than permissible. The maximum displacements in the container units were recorded in the end wall and amounted to 3.5 mm.

3. The strength of the container with sandwich-panel walls under operating load conditions was determined.

3.1 The strength of the container with sandwich-panel walls under static loads was determined. The first stage of the study included the determination of the thickness of metal sandwich-panel sheets using the Bubnov-Galerkin method. The thickness of the side panelling sheet of the container walls was 1.6 mm, and the end panelling sheet was about 3.0 mm. By taking into account the rectangular corrugations, it was possible to reduce the thickness of the end wall sheet to 1.0 mm. The thickness of the sidewall sheet was the same.

The strength of the container with sandwich-panel walls under the longitudinal load was also determined. The maximum stresses occurred in the container fittings and were 268.3 MPa, which was lower than permissible by 13.6 %. In the zones of interaction of the end walls with the corner posts of the container, the stresses amounted to about 215 MPa. The resulting stresses were 24 % lower than those in a typical design. The maximum displacements were recorded at the bottom of the end wall of the container and amounted to 2.6 mm.

The strength of a container with sandwich-panel walls with the transverse load to its structure was determined. The maximum stresses in the container were recorded in the areas of interaction of the sidewall with the corner posts. The numerical values of these stresses were 178 MPa, which was 15.2 % lower than permissible. The maximum displacements were in the middle part of the sidewall and were 3.1 mm. Consequently, the strength of the container was ensured.

3.2 The strength of the container with sandwich-panel walls under dynamic loads was determined

The lateral dynamics of the container with sandwich-panel walls was investigated. The maximum accelerations acting on the container were 1.7 m/s^2. The resulting acceleration value was almost 5 % lower than that acting on a container of a typical design. The calculation was implemented at a stiffness coefficient of the energy-absorbing material of 1.5 kN/m and a coefficient of viscous resistance of 2.0 kN · s/m.

The strength of the container with sandwich-panel walls was calculated. The results of the calculation showed that the maximum stresses occurred in the zones of interaction of the bottom rails with the fitting stops and were equal to about 180 MPa. Importantly, the resulting stresses were 6 % lower than those in a typical container design.

4. In order to reduce the vertical load of the container, it was proposed to introduce the sandwich-panel floor. The vertical load of the container placed on the flat wagon was determined through mathematical modelling. It was assumed that the containers

had the same load at the full load capacity. It was found that the accelerations acting on the container were about 2 m/s^2. The resulting acceleration value was 5.7 % lower than that acting on a container of a typical design.

The strength of the container under operating load modes was determined. It was found that when the container perceived vertical loads, the maximum stresses occurred in its sidewalls and amounted to 118.4 MPa; that was much less than permissible. The maximum displacements occurred in the bottom sheet of the sandwich panel and were 1.13 mm.

With loading/unloading equipment placed in the container, the maximum stresses in its structure amounted to 84.3 MPa, which was also much lower than the permissible values. These stresses occurred in the interaction zone of the top sheet of the central sandwich panel with the longitudinal beam.

The maximum displacements were recorded in the middle part of the sandwich panel located in the centre of the floor and was less than 1 mm.

5. The dynamic load of the sandwich-panel wall container transported as part of a combined train by train ferry was determined through mathematical modelling. The highest values of accelerations occurred at the course angles of the wave relative to the hull of the train ferry $\chi = 60°$ and $\chi = 120°$. The maximum acceleration of the container relative to the regular place on the deck was about 2.3 m/s^2. The total value of acceleration acting on the container was 4.4 m/s^2 (0.45 g). The resulting acceleration value was 4.3 % lower than that acting on a container of a typical design.

The roll angle of the train ferry was taken as acceptable regarding the container stability. The results of the calculations showed that the container stability was ensured at roll angles up to 17°. The stability factor of the container was 1.

6. A concept for the hopper container design was proposed. The features of the load of the hopper container concept at operating modes were described.

6.1 The dynamic load of the hopper container placed on the flat wagon during shunting collision was determined. The calculations

were made for the technical characteristics of the flat wagon model 13-401M on bogies 18-100. It was found that the maximum acceleration acting on the container in the longitudinal direction was 36.7 m/s^2 (3.7g).

The strength of the hopper container placed on the flat wagon during shunting collision, as well as during its stacking, was studied. The maximum equivalent stresses of the container, taking into account its placement on the flat wagon during shunting collision, were recorded in the zones of interaction of the bottom rail with the fittings and they were 315.1 MPa; thus, they did not exceed the permissible values. During stacking, the maximum equivalent stresses were in the corner post and amounted to 245.3 MPa, which were lower than permissible.

The design of the detachable roof of the container was proposed and its strength was also calculated. By taking into account the structural solutions, the weight of the roof was determined as about 300 kg. The results of the calculation for the strength of the roof at its longitudinal load demonstrated that the maximum equivalent stresses occurred in the areas of its interaction with the upper fittings and were 50.2 MPa, which is much lower than the permissible values.

6.2 The strength of the hopper-type container placed on the flat wagon during transportation by train ferry was determined. The maximum equivalent stresses in the container were recorded in its bottom rail and amounted to 294.2 MPa, which is lower than permissible. Consequently, the strength of the container when transported by sea as part of a combined train was ensured.

The stability of the hopper-type container relative to the frame of the flat wagon transported by train ferry was determined. It was found that at a typical diagram of interaction of the container with the frame of the flat wagon, the stability of its equilibrium was ensured at the roll angles up to 26°.

6.3 The mathematical modelling of the vertical dynamics of the flat wagon loaded with hopper-type containers was carried out by taking into account their elastic interaction. The calculation

included the wagon moved along an elastic track, and the containers had the identical load.

The main indicators of the dynamics of the flat wagon loaded with hopper-type containers were determined by taking into account their elastic interaction. The maximum acceleration acting in the centre of mass of the bearing structure of the flat wagon was 1.51 m/s^2, which did not exceed the permissible value. The acceleration of the bogies was 24.5 m/s^2. The acceleration acting on the containers was 1.6 m/s^2. The forces arising in the spring suspension were equal to 68.1 kN. The vertical dynamics coefficient was 0.12. The movement of the flat wagon was accessed as excellent.

The computer modelling of the dynamic load of the load-bearing structure of a long-base flat wagon loaded with hopper containers was carried out. The maximum acceleration was concentrated in the middle part of the bearing structure of the flat wagon and was 1.47 m/s^2. The obtained value of vertical acceleration corresponded to the excellent motion.

The built model of the dynamic load of the load-bearing structure of the long-base flat wagon loaded with hopper-type containers was verified. It was found that the calculated value of the *F*-criterion was F_c = 1.45, which was lower than the tabular value F_t = 3.87. Thus, the hypothesis on the adequacy of the built model was not denied.

7. The design of the detachable module for transporting long cargoes was proposed. The special feature of it was its framed design. The cargo area is represented by the frame. The profiles of the detachable module were determined by the moments of resistance of its components.

The dynamic load of the detachable module was determined by mathematical modelling. It was found that the maximum acceleration acting on the flat wagon loaded with two detachable modules was about 37 m/s^2. The obtained acceleration was taken into account for further calculation of the detachable module. Channel No. 27, reinforced with a 4-mm vertical sheet was chosen

as the frame profile, for end superstructures and vertical poles – channel No. 20, reinforced with a 3.5-mm sheet.

The strength of the detachable module was calculated at longitudinal loads. The maximum stresses in the detachable module were 286.5 MPa; they occurred in the cross bearers in the areas of their interaction with the fittings. These stresses were 7.7 % lower than the permissible stresses. The maximum displacements in the design of the detachable module occurred in the upper belt of the end superstructure and were 4.1 mm.

The strength of the detachable module at transverse loads was calculated. The maximum stresses in the design of the detachable module were 292.4 MPa. These stresses were concentrated in the areas of interaction of the main longitudinal beam with the fitting stops. However, these stresses did not exceed the permissible ones and were 5.8 % lower. The maximum displacements were recorded in the central poles on the tilted side of the detachable module and amounted to 6.2 mm.

The modal analysis conducted made it possible to determine the natural frequencies and shapes of oscillation of the detachable module. It was found that the first natural oscillation frequency of the detachable module was 20 Hz. That is, the traffic safety of the detachable module regarding the frequency analysis was ensured.

8. In order to enhance the efficiency of bulk cargo transportation, the tank container design was improved. The most loaded areas of the tank container, which was chosen as a prototype, were identified by means of its strength calculation. Thus, the longitudinal load of a typical tank container design during shunting collision was investigated. The dynamic load of the tank container placed on the flat wagon during the shunting collision was determined through mathematical modelling. It was found that without gaps between fitting stops and fittings, the acceleration acting on the tank container was about 40 m/s^2. The maximum accelerations were obtained when the gap between fitting stop and fitting was 30 mm. In this case, the acceleration was about 300 m/s^2. The results of the tank container strength

calculation showed that the maximum stresses occurred in the zone of interaction of the tank support with the vertical pole and were 938.2 MPa. These stresses were higher than permissible. The maximum displacements occurred in the middle part of the tank container bottom and were 11.4 mm.

The strength of the tank container frame can be ensured by introducing reinforcing elements into its structure. These elements were made in the form of a fork, the braces of which were placed at an angle of $\alpha = 45°$ to the horizontal. The units of interaction of the braces with each other on the left and right sides of the tank container were connected by a longitudinal belt.

The longitudinal load of the improved tank container design during shunting collision was investigated. The maximum stresses were recorded in the manhole area and amounted to 215 MPa. The resulting stresses were lower than permissible. The maximum displacements occurred at the tank bottom and amounted to 2.6 mm. The modal analysis of the tank container demonstrated that traffic safety was ensured, since the first natural oscillation frequency exceeded 8 Hz.

9. The strength calculation for the container transported as part of a train was carried out. Mathematical modelling was used to determine the dynamic load acting on the container. It was found that the acceleration acting on the containers placed on the flat wagon was about 27 m/s^2. By taking this into account, the maximum stresses that occurred in the container amounted to 121.4 MPa; they were lower than permissible. These stresses were concentrated in the middle part of the horizontal beam for fastening the discharge door. The maximum displacements were fixed in the sidewall of the container and amounted to 1.8 mm.

The strength of the container lifted by the upper corner fittings was also calculated. It was found that the maximum stresses occurred in the interaction areas between the corner posts of the container and cross bearers; they were 108.6 MPa. The resulting stresses did not exceed the permissible ones. The maximum displacements were recorded in the sidewalls and were equal to 1.6 mm.

The strength of the container during its unloading was also calculated. At this mode, the maximum stresses occurred in the horizontal beam for fastening the discharge door. The stresses were 187.4 MPa, which was lower than permissible. The maximum displacements were also recorded in the horizontal beam for fastening the discharge door and were equal to 2.2 mm.

Consequently, under the considered load diagrams, the strength of the improved container was observed.

The proposed concepts of modular vehicles are economically feasible. For example, according to preliminary calculations, the use of a detachable module for transporting long cargoes can give an economic effect by reducing manufacturing costs compared to that for typical modular vehicles. The economic effect for the first year of the calculation period can be UAH 6,886,000. The economic effect of the cumulative total in the last year of the calculation period (10 years) can be UAH 26,579,960.